

DOE/MC/26052--3337

DE93 000273

**Advanced Turbine Design for Coal-Fueled Engines
Phase I - Erosion of Turbine Hot Gas Path Blading**

Final Report

**J.H. Wagner
B.V. Johnson**

April 1993

Work Performed Under Contract No.: DE-AC21-89MC26052

For
U.S. Department of Energy
Office of Fossil Energy
Morgantown Energy Technology Center
Morgantown, West Virginia

By
United Technologies Corporation
United Technologies Research Center
East Hartford, Connecticut

MASTER

DISTRIBUTION OF THIS DOCUMENT IS UNLIMITED

DISCLAIMER

This report was prepared as an account of work sponsored by an agency of the United States Government. Neither the United States Government nor any agency thereof, nor any of their employees makes any warranty, express or implied, or assumes any legal liability or responsibility for the accuracy, completeness or usefulness of any information, apparatus, product, or process disclosed, or represents that its use would not infringe privately owned rights. Reference herein to any specific commercial product, process, or service by trade name, trademark, manufacturer, or otherwise, does not necessarily constitute or imply its endorsement, recommendation, or favoring by the United States Government or any agency thereof. The views and opinions of authors expressed herein do not necessarily state or reflect those of the United States Government or any agency thereof.

This report has been reproduced directly from the best available copy.

Available to DOE and DOE contractors from the Office of Scientific and Technical Information, P.O. Box 62, Oak Ridge, TN 37831; prices available from (615)576-8401, FTS 626-8401.

Available to the public from the National Technical Information Service, U.S. Department of Commerce, 5285 Port Royal Rd., Springfield, VA 22161.

**Advanced Turbine Design for Coal-Fueled Engines
Phase I - Erosion of Turbine Hot Gas Path Blading**

Final Report

**J.H. Wagner
B.V. Johnson**

Work Performed Under Contract No.: DE-AC21-89MC26052

**For
U.S. Department of Energy
Office of Fossil Energy
Morgantown Energy Technology Center
P.O. Box 880
Morgantown, West Virginia 26507-0880**

**By
United Technologies Corporation
United Technologies Research Center
400 Main Street
East Hartford, Connecticut 06108**

April 1993

Advanced Turbine Design for Coal-Fueled Engines

TABLE OF CONTENTS

<u>SECTION</u>		<u>Page</u>
	LIST OF TABLES	vi
	LIST OF FIGURES	vi
	LIST OF SYMBOLS	ix
	EXECUTIVE SUMMARY	1
1	INTRODUCTION	3
	Overview	3
	Deposition Concerns	3
	Corrosion Concerns	4
	Project Focus	4
	Turbine Particle Loading Limitations	4
	Previous Blade Erosion Studies	5
	UTRC	5
	University of Cincinnati and Others	6
	Objective	6
	Approach	6
2	TURBINE OPERATING CONDITIONS	8
	Baseload Operating Conditions	8
	Gas Products of Combustion	8
3	TURBINE MEANLINE AND AIRFOIL DESIGNS	11
	Baseline Turbine Characteristics	11
	Alternate Turbine Characteristics	12
4	PARTICLE TRAJECTORY PROCEDURES AND MODELS ..	22
	Flowfields	22
	2-D Cascade Flow Code	22
	3-D Flow Code	22
	Particle Trajectory Analysis	23
	Particle Dynamics	23
	Particle Aerodynamic Drag Model	24
	Particle Rebound Model	25
	Trajectory Calculation Procedure	25

<u>SECTION</u>	<u>Page</u>
2-D Trajectories	26
3-D Trajectories	26
Particle Monitoring	27
Typical Particle Trajectories	27
5 EROSION PREDICTION PROCEDURES AND MODELS ...	32
Background	32
Erosion Model	33
Particle Diameter Scaling	34
Ductile Material Scaling	34
Temperature	34
Velocity	35
Angle	35
Brittle Material Scaling	35
Normalization of Erosion Results	36
Additional Experimental Data Requirements	37
6 PARTICLE TRAJECTORY AND EROSION CHARACTERISTICS FOR BASELINE TURBINE DESIGN ..	40
Particle Definition Parameters	40
Particle Trajectories	41
Particle Impact Characteristics	42
Erosion Characteristics	42
Ductile Material	42
Brittle Material	43
7 EFFECTS OF TURBINE DESIGN ON EROSION CHARACTERISTICS	50
Particle Impact Speed and Angle	50
Erosion Rates	50
Effect of Number of Stages	51
Effect of Mean Radius	51
Effect of Airfoil Pitch	51
Effect of Airfoil Inlet Incidence	52
Effect of Airfoil Shape	52
Summary	52
8 PARTICLE TRAJECTORY AND EROSION CHARACTERISTICS FOR 3-D BASELINE TURBINE	60
Particle Trajectories	60

<u>SECTION</u>	<u>Page</u>
Erosion Characteristics	60
Vane Results	61
Blade Results	61
Vane Shroud and Blade Outer Air Seal Results	62
Comparison Between 3-D and 2-D Erosion Results	63
9 ANALYSIS	75
Prediction of Turbine Life	75
Sample Calculation (10 Micron Particle, 2-D Baseline Blade)	75
Consequences of Hot Gas Filter Failure	76
Utilization of Results for Larger or Smaller Turbines	77
10 CONCLUSIONS	82
REFERENCES	83
APPENDIX	89
Derivation of Particle Trajectory Equations	89

LIST OF TABLES

<u>Table</u>	<u>Page</u>
2-1 Turbine Baseload Operating Conditions	10
2-2 Coal Analysis	10
2-3 Ultimate Analysis of CWS (Mole %)	10
2-4 Gas Products of Combustion of CWS and DF2	10
3-1 Design Parameters for Baseline First Stage	15
3-2 Turbine Stage Characteristics	15
3-3 Geometric and Flow Conditions for First-Stage Meanline Designs ...	16
3-4 Comparison of Geometric Parameters With LSRR Turbine	16
3-5 Overall Turbine Performance Parameters	16
4-1 Particle Trajectory Parameters	28
4-2 Trajectory Code Control Flag Status Definitions	28
6-1 Dimensionless and Dimensional Particle Variables for Baseline Vane and Blade	44
9-1 Simulated Particle Diameters and Densities for Three Turbines for Selected Stokes Numbers, St	78
9-2 Simulated Particle Diameters and Densities for Three Turbines for Selected Particle Density Reynolds Numbers, σ	78

LIST OF FIGURES

<u>Figure</u>	<u>Page</u>
3-1 Interactive P&W Turbine Design System Allows Rapid Flowpath Definition/Parametric Optimization	17
3-2 Turbine Cross Sections	18
3-3 Airfoil Coordinate System and Nomenclature, Baseline Turbine Blade	19
3-4 Vane Meanline Airfoil Profiles	20
3-5 Blade Meanline Airfoil Profiles	20
3-6 Vane Meanline Airfoil Pressure Distributions	21
3-7 Blade Meanline Airfoil Pressure Distribution	21
4-1 Baseline Turbine Aerodynamic Computation Grids and Airfoil Surface Nomenclature	29
4-2 Particle Aerodynamic Drag Model	30
4-3 Particle Rebound Model	30
4-4 2-D Particle Trajectories Through Baseline Meanline Vane Airfoil Row	31

Figure		Page
4-5	2-D Particle Trajectories Through Baseline Meanline Blade Airfoil Row	31
5-1	Erosion Rate as a Function of Particle Size	38
5-2	Erosion Model for Nickel-Based Super Alloy Airfoils	39
5-3	Erosion Model for Airfoils with Thermal Barrier Coatings	39
6-1	2-D Particle Trajectories Through Baseline Meanline Vane Airfoil Row	45
6-2	2-D Particle Trajectories Through Baseline Meanline Blade Airfoil Row	45
6-3	Effect of Particle Diameter and Density on Percent of Particles Hitting Vane and Blade	46
6-4	Effect of Stokes Number and Particle Reynolds Number on Percent of Particles Hitting Vane and Blade	46
6-5	Effects of Particle Size and Density on Particle Impact Speed for Baseline Meanline Airfoils	47
6-6	Effect of Particle Size and Density on Particle Impact Angle for Baseline Meanline Airfoils	48
6-7	Effect of Particle Size and Density on Erosion Rate for Baseline Meanline Meanline Airfoils of Ductile Material	49
6-8	Effect of Surface Material on Erosion Rate for Baseline Meanline Airfoils. Open Symbols – Brittle Material (Thermal Barrier Coating); Symbols – Ductile Material	49
7-1	Comparison of Particle Impact Speeds and Angle Distributions on All Airfoils for 25 Micron, 2.5 gm/cc Particle	53
7-2	Comparison of Erosion Distribution on All Airfoils for 25 Micron, 2.5 gm/cc Particles	54
7-3	Effect of Particle Size and Density on Erosion Distribution From Four Stage, Increased Radius and Increased Pitch Airfoils	55
7-4	Effect of Particle Size and Density on Peak Erosion Rate From Baseline, Four Stage Increased Radius and Increased Pitch Airfoils ..	56
7-5	Effect of Particle Size and Density on Average Erosion Rate From Baseline, Four Stage, Increased Radius and Increased Pitch Airfoils ..	57
7-6	Effect of Blade Shape and Particle Size on Erosion Distribution From Airfoil Open Symbols: MOD-1; Shaded Symbols – Baseline ...	58
7-7	Effect of Blade Shape, Particle Size and Particle Density on Average and Peak Erosion Rates. Open Symbols MOD-1; Shaded Symbols – Baseline	59
8-1	Typical 3-D Particle Trajectories in Baseline Blade Passage	64
8-2	Contours of Particle Impact Speeds, V/U_1 , in 3-D Baseline Vane Airfoil Row	65
8-3	Contours of Particle Impact Angles, β_p , in 3-D Baseline Vane Airfoil Row	66
8-4	Effect of Particle Diameter on the Erosion Distribution, $e(\text{in./lbm})$, From Vane Airfoils	67

Figure	Page
8-5 Contours of Particle Impact Speeds, V/U_1 , in 3-D Baseline Blade Airfoil Row	68
8-6 Contours of Particle Impact Angles, β_p , in 3-D Baseline Blade Airfoil Row	69
8-7 Effect of Particle Diameter on the Erosion Distribution, $e(\text{in./lbm})$, From Blade Airfoils	70
8-8 Effect of Particle Diameter on the Erosion Distribution, $e(\text{in./lbm})$, From Vane and Blade Outer Case	71
8-9 Streamwise Distribution of Erosion on Outer Airseal for Baseline Airfoils and Sphere Particle Diameters: 0-5; \square -25; Δ -100 microns ...	72
8-10 Erosion Distribution, $e(\text{in./lbm})$, Due to 25 Micron Particles on Baseline Airfoils	73
8-11 Effects of Particle Diameter on Peak and Average Erosion Rates From 2-D and 3-D Baseline Airfoils	74
9-1 Particle Size Distributions From Selected Coal-Figured Combustion Tests	79
9-2 Dust Loading and Size Distribution at Turbine Inlet of Second-Generation PFB Baseline Plant (Fig. D-4 of Ref. 54)	80
9-3 Effect of Particle Loading and Peak Erosion Rates on Estimated Turbine Life (Westinghouse & GE Life Estimates From [54])	81

LIST OF SYMBOLS

a	Projected area of particle
A_a	Total inlet annulus
A_i	Area of surface element for 3-D flow
A_u	Inlet frontal area of unit airfoil passage
b_x	Airfoil axial chord
C	Velocity of air
C_d	Particle drag coefficient
D_p	Particle diameter, micron
E	Erosion rate, cm^3/gm
e_i	Material recession rate of surface element i (i.e. inches of recession per pound of erodent at the turbine inlet)
g_c	Gravitational constant, $32.17 \text{ ft lbm/lb}_f \text{ sec}^2$
h	Airfoil height, in.
H	Specific work for stage, BTU/lb_m
IE	Partice impact efficiency based on "First" and "Second" passes
J	Conversion factor, 778 ft-lbf/BTU
k	Moles of air/mole gas product
K_1	Constant for erosion model (Eqns. 5-1, 5-2)
K_2	Constant for erosion model (Eqns. 5-1, 5-2)
m	Exponent for velocity effects of erosion model (Eqns. 5-1, 5-2)
n	Parameter for erosion model (Eqns. 5-1, 5-2), $90/\beta_0$
N	Number of airfoils
NP	Total number of particles started at inlet of 3-D turbine passage
NPS	Total number of particles started at inlet of 2-D turbine passage
P	Pressure, psi
ppm	Parts per million by weight
q	Moles of CH_2 /mole gas product
q_e	Dynamic pressure of turbine exit flow
R_m	Radius of meanline, in.
Re_{bx}	Reynolds number based on airfoil axial chord and relative airfoil conditions at row inlet
Re_p	Particle Reynolds number based on particle and fluid relative motion
s	Airfoil surface arc length from leading edge
S	Airfoil surface arc length from edge (Fig. 3-3)

S_i	Surface arc length of element
St	Stokes number
t	Dimensionless time
T	Airfoil pitch, in.
T	Time
u	Normalize relative flow velocity
U	Velocity, ft/sec
V	Velocity of particle relative to local fluid velocity
V_m	Turbine work parameter, $[U_m^2/(2g_c JH)]^{0.5}$
v	Volume of particle
x	Normalized axial distance
X	Particle position
y	Normalized tangential distance
y_0	Dimensionless angular speed of rotating coordinate system (Section 4)
z	Normalized radial distance
α	Absolute flow angle (Fig. 4-1), deg
β	Relative flow angle (Fig. 4-1), deg
β_0	Constant to set β_{max} , deg (Eqns. 5-1, 5-2)
β_p	Particle impact angle (Fig. 4-1), deg
μ	Absolute viscosity
σ	Particle density Reynolds number, $Re_{bx}/(\rho_p/\rho_1)$
ρ	Density, lb/ft ³
%First	Percent of particles which hit airfoil from the "First Pass"
%Second	Percent of particles which hit airfoil from the "Second Pass" defined by the "First Pass"

Subscripts

1	Vane inlet location
1	Average property for inlet plane of flowfield
1	Before impact
1	Axial coordinate direction
2	Blade inlet location
2	After impact
2	Tangential coordinate direction
3	Blade exit location

3	Radial coordinate direction
amb	Ambient
b	Relative to blade airfoil inlet flow properties
b_x	Relative to airfoil axial chord
c	Coal
cws	Coal water slurry
f	Fluid property
i	Surface element
in	Turbine inlet
le	Leading edge (Fig. 3-3)
m	Blade speed at midspan
max	Maximum value
n	Normal component relative to airfoil surface
p	Particle property
s	Static property
t	Tangential component relative to airfoil surface
t	Total property
te	Trailing edge (Fig. 3-3)
v	Relative to vane airfoil inlet flow properties
x	Axial component

EXECUTIVE SUMMARY

The U.S. Department of Energy (DOE) Morgantown Energy Technology Center (METC) awarded a 2-phase contract to United Technologies Research Center. This project began in December of 1988 with the title "Advanced Turbine Design for Coal-Fueled Engines." The objective of Phase I, "Erosion of Turbine Hot Gas Path Blading," was to identify turbine airfoil shapes and aerodynamic characteristics which would result in improved turbine blade and vane life for coal-fuel systems. The objective of Phase II is to determine the suitability of state-of-the-art hot gas-path turbine blade materials and coating systems for advanced PFBC conditions with regard to corrosion/deposition aspects. The subject of the present report is the results from the Phase I effort.

An analytic study was conducted to determine the effects of turbine design, airfoil shape and material on particulate erosion of turbine airfoils in coal-fueled, direct-fired gas turbines used for electric power generation. First-stage, mean-line airfoil sections were designed for 80 MW output turbines with 3 and 4 stages. Two-dimensional particle trajectory calculations and erosion rate analyses were performed for a range of particle diameters and densities and for ductile and ceramic airfoil materials. Results indicate that the surface erosion rates can vary by a factor of 5 and that erosion on rotating blades is not well correlated with particle diameter. The results quantify the cause/effect turbine design relationships expected and assist in the selection of turbine design characteristics for use downstream of a coal-fueled combustion process. Three-dimensional particle trajectory calculations and erosion rate analysis were performed for the baseline turbine airfoil design. The results showed the effects of secondary flow and the radial transport of particulates on the erosion rates from the vanes, blades, blade platform and the turbine outer airseal. Results from both the two-dimensional and three-dimensional erosion rate studies indicate the importance of filtering the gas entering the turbine from direct-fired combustion processes. The results also quantify the consequences of breaks in or by passes of that filtering system and can be used to estimate the response times for shift to an alternate system required to prevent serious damage to a turbine.

The approach of the present program was to conduct a parametric study to determine the effects of turbine design and airfoil shape on particulate erosion. Erosion was predicted using flowfield information, particle trajectory surface interaction statistics and surface erosion models. Particle erosion and rebound information from previous METC sponsored projects was utilized in the formulation of the surface interaction and erosion models for the evaluation of the turbine stage designs. Guidelines for the design of the airfoil shapes and the aerodynamic operating conditions were consistent with the large axial flow turbines being evaluated in current METC programs.

Predicted erosion results for the airfoils of each turbine stage were compared to the results of the baseline stage. Criteria for the comparison of the results included local peak values of erosion as well as integrated surface averages. In this manner each turbine stage design was rated for erosion resistance. The predicted erosion rates for the meanline section of the baseline turbine with 2-D flow and particle calculations, indicated that the maximum local erosion rate with no filters and all the particulates from coal with 3 percent ash entering the turbine would be 0.001 inches per minute. The predicted erosion rates from 3-D flows

and particle calculations indicated a peak erosion rate of 0.004 inch per minute and a turbine life of 25 minutes, based on a maximum allowable surface recession of 0.1 inch.

Predicted turbine erosion rates were decreased by a factor of 5 by varying the turbine design. Increasing the number of stages and increasing the mean radius of the gas path significantly reduced the predicted erosion rates for the 2-D flows. The predicted peak erosion rates on blades with these design changes were comparable to the peak erosion rates for the vane airfoils with all gas path designs. Reduction in the predicted erosion rate for the various turbines analyzed was a strong function of particle diameter. Particles with other diameters resulted in smaller erosion reductions. Additionally, the results indicate that airfoil erosion is strongly affected by airfoil aerodynamics as well as turbine operating condition (i.e. decreasing the required turning within an airfoil row). These results indicate that substantial gains in erosion resistance can be achieved by changes in the turbine operating condition depending on particle diameter.

Three dimensional secondary flows caused increases in the peak and average erosion on both the vane and blade airfoils. The peak erosion rate from the 3-D calculations for the baseline blade was approximately three to five times the peak erosion from the 2-D calculations for the mean line of the baseline blade. Additionally, the 3-D interblade secondary flows and the addition of a stationary outer case wall caused erosion patterns which were different than or not obtainable with the 2-D analyses. Although the 3-D erosion patterns for the baseline turbine stage were different than that for the baseline 2-D streamwise distribution, the same aerodynamic factors which reduced erosion for the 2-D designs, i.e., increased radius and increased number of stages, are expected to reduce the 3-D erosion distribution on blades.

The investigators conclude that:

1. Turbine erosion resistance was shown to be improved by a factor of 5 by varying the turbine design. Increasing the number of stages and increasing the mean radius reduces the peak predicted erosion rates for 2-D flows on the blade airfoil from values which are 6 times those of the vane to values of erosion which are comparable to those of the vane airfoils.
2. Turbine erosion was a strong function of airfoil shape depending on particle diameter. Different airfoil shapes for the same turbine operating condition resulted in a factor of 7 change in airfoil erosion for the smallest particles studied (5 micron).
3. Predicted erosion for the various turbines analyzed was a strong function of particle diameter and weaker function of particle density.
4. Three dimensional secondary flows were shown to cause increases in peak and average erosion on the vane and blade airfoils. Additionally, the interblade secondary flows and stationary outer case caused unique erosion patterns which were not obtainable with 2-D analyses.
5. Analysis of the results indicate that hot gas cleanup systems are necessary to achieve acceptable turbine life in direct-fired, coal-fueled systems. In addition, serious consequences arise when hot gas filter systems fail for even short time periods. For a complete failure of the filter system, a 0.030 in. thick corrosion-resistant protective coating on a turbine blade would be eroded at some locations within eight minutes.

SECTION 1

INTRODUCTION

Overview

The use of direct-fired, coal-fueled gas turbines in combined-cycle power generation systems will allow the effective utilization of the vast coal reserves in the United States, thereby, reducing dependence on foreign oil. However, direct combustion of coal produces significant amounts of particulates and can release high levels of alkali. Filters and cyclone separators can reduce particulates and particulate-bound alkali, but hot gas path components of a coal-fueled gas turbine will be subject to the deleterious effects of some particulates passing through these devices.

Since the early 1980s, the United States Department of Energy (DOE) has funded projects to develop gas turbines which can burn coal directly. DOE sponsored three proof-of-concept Direct Coal-Fired Gas Turbine (DCFGT) projects to demonstrate the feasibility of clean energy production using coal [50]. The goal of these projects was to make industrial or utility coal-fired gas turbine systems commercially available by the mid- to late 1990s. The contractors identified three significant barriers to turbine durability early in the development of DCFGTs: 1) deposition – accumulation of small particulates on airfoil surfaces; 2) erosion – rapid wear of turbine airfoils and hot gas path components due to particulates; and 3) corrosion – rapid chemical attack of airfoil materials after breakdown of surface coatings. These barriers also exist for gas turbines used with pressurized fluidized bed combustor (PFBC) systems.

Deposition Concerns

Deposition of particulates from the combustion of pulverized coal and coal water slurries is complex. The mechanisms of the deposition process are discussed by a number of investigators [3, 4, 26, 48, 53]. The process is dependent on many factors such as combustion chemistry, gas path history, particle size, particle composition, surface impact speed, impact angle, local fluid temperature and surface temperature. Deposition is potentially the most severe limitation of coal use for direct-fired power generation [48]. Deposition is characterized by the sticking and accumulation of particles to a surface by an unsteady process which is influenced by the local surface chemistry. The process is governed by the method of particle arrival (i.e. vapor condensing, diffusion, thermophoresis or inertia). Partial vapor condensation, diffusion and thermophoresis are generally associated with submicron particulates. The work documented in this report only addressed the effects of particles with diameters between 5 and 100 microns. The deposition process associated with this range of particles is dominated by inertia and in general cannot be specified through physical arguments alone. Currently, the prediction of inertial deposition relies upon experimental results where deposition has been found to be linearly dependent on a stickiness coefficient. The stickiness coefficient is an indication of the amount of glues which are present to promote adhesion of the particles to a surface.

The deposition results discussed in the literature indicate that deposition is likely for the baseload operating conditions selected, i.e. a turbine inlet temperature of 2100 F and a

maximum turbine airfoil surface temperature of 1400 F [2, 6, 47, 57, 58, 61, 73]. Deposition is most likely to occur at surface locations with particle impingement angles near 90 degrees. For the specified gas temperature (2100 F) silicates and aluminosilicates are glues and at the specified maximum airfoil surface temperature (1400 F) sulfates are glues [48]. Stickiness coefficients for the baseload operating conditions are estimated [3] to be between 0.02–0.1 indicating a 2–10 percent adhesion efficiency. Although there is considerable sophistication in the prediction of diffusion and vapor deposition [48, 53], the prediction of inertial deposition is still in an infant state of development [26]. The deposition characteristics for inertial particle arrival methods have not been fully explored [48].

Ideally, no inertial deposition is acceptable. Once deposition is initiated, the deposition either leads to “catastrophic fouling” or at best “asymptotic fouling” where deposition is offset by deposit removal. Deposition and erosion are not mutually exclusive [6, 59, 73]. The deposition process may occur after an initial period of erosion. The control of deposition may require specifying low ash fuels, fuel treatment, new blade designs and lower metal temperatures [3, 47]. Fuel additives can be used to trap condensible alkalis to minimize deposition [48]. However, calcium sulfur–sorbents have been shown to increase deposition by a factor of 20 compared to the deposition from the combustion of coal water slurries alone [29]. Deposition may also be minimized with complete combustion (100 percent burnout) which yield lower amounts of volatiles known to increase deposition [47]. The deposition associated with the combustion of coal water slurries is significantly less than that for residual oils [29].

Although there is a significant amount of deposition behavior documented for various test conditions and materials, there is a limited amount of inertial deposition data in the form of sticking coefficients which can be used to predict deposition for inertially dominated particles. The lack of sticking coefficient data for the anticipated combination of particulate composition, impact speeds and angles suggests that it is premature to develop a deposition model with the available data and, therefore, that the prediction of airfoil surface deposition is currently intractable. Therefore, the focus of the program is directed to the evaluation of turbine designs based on predicted erosion results only.

Corrosion Concerns

Corrosion from alkali, chlorine and other trace elements from the combustion products of coal potentially limit the life of turbine. The cause/effect relationships and proposed solutions for minimizing corrosion from the products of Pressurized Fluidized Bed Combustion (PFBC) will be addressed in the second topical report under this contract.

Project Focus

The work described in this report supports the DCFGT effort by addressing the problems of erosion and presenting turbine design modifications which can reduce erosion rates.

Turbine Particle Loading Limitations

Turbine manufacturers and researchers [54, 60] have concluded from studies of coal–fueled systems [27] that little erosion is attributed to particles with diameters less than 5

microns. Stringer and Drenker concluded that one-half of one percent of total erosion damage is due to particles which have diameters below 5 microns. Therefore, they concluded to prevent the derating of turbine life, the turbine inlet particulate loading for diameters greater than 5 micron (and especially greater than 10 micron) must be limited.

Each gas turbine manufacturer has application guidelines limiting the size and quantity of particulates entering the turbine hot gas path. When many larger particles are allowed to enter the turbine, erosion will be heavy, requiring the manufacturer to lower estimated airfoil life. When the total number of particles is too high, deposition will be a problem, requiring more frequent turbine cleaning. In addition, high particulate loadings into the turbine will result in exhaust concentrations which exceed the Environmental Protection Agency (EPA) New Source Performance Standards (NSPS) regulations for particulates.

Solar Turbines is developing DCFGF technology through proof-of-concept [17]. Solar estimates that the turbine can be operated with up to 100 ppm total particulates provided 99.5 percent are less than 10 micron and 99 percent are less than 5 micron. Solar considers these limits necessary to maintain a 30,000 hour blade life and prevent unacceptable deposition. The EPA NSPS regulations specify maximum amounts of all particulates (regardless of size). Application of the NSPS rules for small boilers [24] to the solar's DCFGF project requires Solar to limit particulates to about 20 ppm, even though the turbine could tolerate higher levels with acceptable erosion and deposition.

The DOE DCFGF contractors plan to limit particulate loadings was previously described [5]. Several contractors of DCFGF and PFBC systems propose barrier filters for pre-turbine cleanup of particulates. If these filters are successful, the systems will meet EPA NSPS requirements for total particulates because of the 99.9+ percent overall capture efficiency of these filters. Since barrier filters have collection efficiencies approaching 99.99 percent for particles over one micron, erosion will be negligible. However, significant erosion could occur if there were a partial or complete failure of the barrier filters, or if a less efficient particle removal device (such as a cyclone separator) is used.

Previous Blade Erosion Studies

UTRC

United Technologies Corporation has maintained interest in the utilization of coal as a fuel for gas turbines since the early 1970s when the long-term need for improved utilization of our coal resources became a national focus. At that time, a United Technologies Research Center program directed toward identifying the problems associated with erosion of particulates was initiated. This program produced a fundamental understanding for the nondimensional modeling of particulate flow in airfoil cascades [18, 20, 21] and insight into the effects of film cooling jets upon particulates impacting the leading edge region of airfoils [62]. During the early 1980s, the corporate interests were diverted from coal fuel applications and our particle trajectory/erosion modeling technology was focused on damage in aircraft gas turbines due to sand ingestion.

The UTC recent initiatives to develop the FT8, FT4000 and the KWU 84.4 land-based turbines has caused the Research Center to reexamine the durability problems associated

with coal-fueled turbines. During 1988, UTRC, under the present contract with DOE/METC, initiated the present program to determine the effects of particulates upon turbine life and to determine aerodynamic and operating conditions which would improve turbine life. At the same time, UTRC extended its capability, under a corporate research project, to include the prediction of particle trajectories in the complex 3-D flows between stationary vanes and rotating blades. UTRC used this capability for predicting trajectories in 3-D flows.

University of Cincinnati and Others

The prediction of turbine vane and blade airfoil erosion has been studied by a number of investigators [8, 9, 23, 28, 32, 44, 45, 72, 76]. These investigators have predicted airfoil surface erosion using 2-D and 3-D flowfields, developed particle trajectory calculations and airfoil surface-particle rebound and erosion analytical models. The work listed above was related to the analysis of existing turbine designs. The predicted erosion results of a number of these investigators were in nominal correspondence with the erosion experience for the specific turbine designs analyzed. The work of Weinglarz and Menguturk [76] is particularly noteworthy relative to the present work in that they investigated the parametric effects of turbine scale and rotational speed (i.e. turbine design parameters) on the predicted airfoil erosion. The present study complements this earlier work by investigating the effects of aerodynamic design on predicted turbine airfoil erosion for a fixed gas turbine size and rotational speed suitable for a large utility, power generation turbine.

Objective

The objective of DOE/METC's present contract with UTRC was to identify airfoil shapes and turbine aerodynamics which reduce the effects of particulate erosion, without sacrificing turbine efficiency. The results of this study will assist in selecting turbine characteristics when developing a new turbine system, designed for acceptable life utilizing hot gases containing the products of coal combustion. Although certain turbine designs can reduce particle erosion, using turbines downstream of a coal combustor will require reliable and efficient removal of particulates to maintain turbine life.

The emphasis of the present work is on the use of flowfield contouring to reduce particle impact and erosion. The alteration of turbine aerodynamic flowfield contours is accomplished by changing the turbine operating conditions and airfoil shapes. Different operating conditions typically require airfoil design changes to maintain certain fixed design parameters (i.e. flow incidence, stage pressure ratios, etc.). However, airfoil shape may be altered for a particular turbine design requirement with a corresponding change in aerodynamic efficiency (i.e. total pressure loss). This paper discusses situations where both turbine operating condition and airfoil shape were changed and where only the airfoil shape was changed. Results of this project will be applicable to turbine airfoils downstream of both pressurized fluidized combustors and direct coal-fired combustors.

Approach

The approach of the present program was to conduct an analytic parametric study of the effects of turbine design and airfoil shape on particulate erosion. Alternate turbine design

concepts included increasing the number of stages, increasing the mean radius and increasing the airfoil circumferential spacing. It was anticipated that these changes may increase the erosion resistance of direct-fired, coal-fueled gas turbines. In addition, the effects of airfoil and coating materials were investigated.

Baseload operating conditions for the turbine simulation were specified to be compatible with a utility-sized turbine burning Coal Water Slurry (CWS). Gas products of combustion of CWS fuel were estimated for meanline, flow path and trajectory calculations. Meanline designs were completed for the first stage of a baseline turbine and for three additional turbine configurations. Turbine airfoils were designed for these meanline designs using the Pratt and Whitney Turbine Design System. A literature survey of surface/particle interaction studies yielded particle rebound and surface erosion models. 2-D and 3-D particle trajectory calculation codes were used to calculate particle trajectories and surface impacts.

The effects of particle diameter were determined for particle diameters between 5 and 100 microns. The range of particle diameters studied was based on test results of the Westinghouse subscale coal-fired slagging combustor [5]. The effects of the airfoil design on erosion were determined from the aerodynamic, particle trajectory and surface interaction calculations. The particle trajectory analysis was performed for many particle initial locations for ranges of Stokes and particle density Reynolds numbers to obtain a statistical distribution of particle impact parameters on the airfoil surfaces. These surface interaction parameters were used as input to a post processing trajectory analysis code which yielded surface distributions of erosion rate based on the particle loading at the turbine inlet. Thus, the effects of airfoil loading and relative flow velocities on erosion from the 2-D meanline airfoil surfaces were determined.

The effects of 3-D flow fields can be significant for certain classes of particles. Accordingly, 3-D particle trajectories and erosion distributions were determined for the airfoils, the vane outer shroud and the blade outer air seal of the baseline turbine stage. The flow field used for the baseline turbine stage was available from previous studies at the Pratt & Whitney/Commercial Engine Division of United Technologies Corporation.

SECTION 2

TURBINE OPERATING CONDITIONS

Baseload Operating Conditions

For of this study, the turbine inlet temperature and pressure were selected to be 2100 F and 180 psia (12.2 atmospheres), respectively. These conditions are consistent with a likely operating point for a coal-fueled gas turbine which would be commercially available in the mid-1990s. These conditions are also consistent with the design envelope for the turbine used in an advanced PFBC system. The specified turbine baseload operating conditions are listed in Table 2-1a.

Unit specific parameters (Table 2-1b) were chosen after an analysis of specifications of existing turbine engine power plants. From the wide range in unit power ratings of the DOE/METC demonstration programs (2 to 200+ MW systems), the 80 to 100 MW power rating range was chosen for the gas turbine simulation. Turbine engines of this size typically have 3 to 4 turbine stages. A three stage turbine was chosen as the baseline with the idea that one of the new turbine designs may have decreased stage loading, thereby, requiring an additional stage to maintain a fixed power rating. The mass flowrate was chosen to reflect turbine engine flows of power plants currently in operation and was maintained at 670 lbm/sec for all turbine designs. The goal for the meanline designs of the different turbines was to design a turbine which would produce a net power in the range of 80 to 100 MW.

The unit power rating was determined by subtracting the required compressor shaft power from the total turbine shaft output. The power required for compression was estimated by assuming a six (6) percent drop in pressure between the compressor exit and the turbine inlet, an 85 percent compressor efficiency, a 15 percent flow bypass for turbine component cooling and a compressor inlet temperature of 59 F. To simplify the turbine simulations and subsequent meanline designs, the bypass coolant air was not reinjected into the turbine gas stream flow.

Gas Products Of Combustion

The turbine meanline and airfoil shape design codes required information about the gas products of combustion to calculate flow properties. Current DOE-sponsored coal utilization programs focus on the combustion of CWS as the most likely fuel for the next generation of coal-burning, direct-fired gas turbines. Therefore, gas products of combustion of CWS were estimated for the meanline, flow path and trajectory calculations.

The products of combustion were determined using the coal properties of a typical coal [55] mixed to a 50 percent solids loading. The formulation for the resulting composition, neglecting the sulphur and the ash, is shown in Tables 2-2 and 2-3. The coal formulation [55], minus the water, was then combined with an equal amount of water by weight to form the resultant CWS mixture shown below. This CWS was subsequently treated as a hydrocarbon fuel with the following molecular structure.

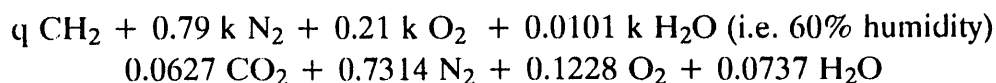


or after normalizing on a per mole of mixture basis,



The stoichiometric fuel/air ratio for the combustion (i.e. no excess oxygen in products) of this fuel was determined to be 0.1751 lbm CWS/lbm AIR. A combustion analysis of this CWS mixture was conducted to determine the fuel/air ratio for fuel-lean combustion to obtain a firing temperature of 2580 R (assuming a 1 percent enthalpy loss between the combustor exit and the turbine inlet, the temperature of the hot gas stream decreases about 20 R to the specified 2560 R inlet temperature). This analysis resulted in a fuel-lean, fuel/air ratio of 0.065 lbm CWS/lbm AIR (or an equivalence ratio of 0.37). The resultant fuel-lean gas products of combustion are shown in Table 2-4.

Pratt & Whitney turbine aerodynamics codes do not contain gas product information from the combustion of CWS. Therefore, a fuel/air ratio for Diesel Fuel No. 2 (DF2) was found to simulate the products of combustion of CWS. This was completed by determining what amount of DF2 (simulated by the molecular structure CH₂) would be required to obtain similar amounts of gas products. The analysis consisted of balancing the moles of carbon, then nitrogen, oxygen and water.



where k = moles of air/mole gas product

q = moles of CH₂/mole gas product

For the balance of 1) Carbon, q = 0.0627

2) Nitrogen, k = 0.926

3) Oxygen, k = 1.034

4) Water, k = 1.089

This balance resulted in three molar coefficients (k, shown above) which were averaged by weighting the relative importance of each coefficient with the percent molar composition of the products. Using the mole percent of each of the gas products of the combustion of CWS as weighting factors, k was estimated to be 0.949. This analysis resulted in a fuel/air ratio (F/A = (M_{CH₂} q)/(M_{AIR} k)) for the DF2 simulated fuel of 0.032 lbmCH₂/lbmAIR (or an equivalence ratio of 0.47).

Table 2-1 Turbine Baseload Operating Conditions

a) METC Specified Parameters:

Rotation Rate	3600 RPM
Turbine Pressure Ratio (basis: inlet/atm.)	12.2
Turbine Inlet Pressure	180 psia
Turbine Inlet Temperature	2100 F
Maximum Turbine Blade Surface Temperature	1400 F

b) Unit Specific Parameters:

Unit Total Power Rating	80 MW
Number of Turbine Stages	3
Turbine Inlet Flowrate	670 lbm/sec

Table 2-2 Coal Analysis

	Wt%	moles/100 _{lbmCWS}	moles/mole _C	lbm/mole _C
C	50.74	4.23	0.5348	6.4176
H	3.34	3.34	0.4223	0.4223
N	1.03	0.07	0.0088	0.1232
O	4.37	0.27	0.0341	0.5456
H ₂ O	<u>40.51</u>	-----	-----	-----
	100.00	7.91	1.0000	7.5087

Table 2-3 Ultimate Analysis of CWS (Mole %)

Carbon	23.75
Hydrogen	55.81
Oxygen	20.04
Nitrogen	0.39

Heat of Fusion, $h_{f,cws} = -3384.4$ Btu/lbm

Molar Weight, $M_{cws} = 6.6691$

Table 2-4 Gas Products of Combustion of CWS and DF2

	CWS mole%	DF2 mole%
O ₂	12.28	10.63
N ₂	73.14	75.73
H ₂ O	7.37	7.30
CO ₂	6.27	6.33
Trace Gases	< 1	Neglected

SECTION 3

TURBINE MEANLINE AND AIRFOIL DESIGNS

Four midspan turbine first stages were designed using the Pratt and Whitney Turbine Design System. The primary goal of this portion of the program was to design turbine stages which were resistant to erosion in coal-fueled engines. Each turbine first stage included one stationary vane row followed by one rotating blade row. The midspan airfoils were designed using correlations for profile loss, secondary loss, blade tip leakage and incidence loss. Each turbine design was selected to be significantly different to provide a wide aerodynamic operating range for effective comparisons of predicted erosion resistance. A pictorial representation of the relationships obtainable with the P&W Turbine Design System is shown in Fig. 3-1.

Three new meanline turbines were designed in addition to the baseline design. In all cases, the overall total turbine pressure ratio ($P_{in}/P_{atm} = 12.2$) was maintained. Total turbine power for each turbine was allowed to vary in accordance with changes in the calculated turbine efficiency. Several concepts were identified for improving the erosion resistance of coal-fueled gas turbines blades:

- Increase mean radius to reduce the aerodynamic and particle velocities.
- Increase the number of stages from three to four to decrease the loading on each stage.
- Increase airfoil pitch for reduced particle impact.
- Adjust airfoil shapes for aerodynamic control of particle turning using baseline turbine meanline design.

Turbine operating conditions were chosen for electrical baseload conditions as described in a previous section. The selected operating conditions were used for input parameters for the particle trajectory and surface interaction analysis as well as the criteria for the design of the turbine stages. Each of the three meanline designs will be discussed below.

Baseline Turbine Characteristics

The baseline turbine first stage has characteristics, which are typical of those used in large stationary and aircraft gas turbines, and is one of the best documented turbine stages available. This configuration is the first vane and first blade in the Large Scale Rotating Rig (LSRR) at UTRC. Documentation includes results of benchmark experimental studies measuring the time-averaged and unsteady flow effects, heat transfer from the airfoils, effect of airfoil spacing and secondary flows at selected locations [12, 15, 19]. Analytical studies at UTRC, NASA/Ames [52] and elsewhere have been conducted to assess computational procedures for predicting these effects. This design served as a suitable baseline for determining the erosion resistant benefits from the new turbine designs.

The goal for the baseline meanline design was to design a first stage with velocity triangles similar to the LSRR first stage and produce a net power in the range of 80 to 100

MW. Additional design parameters were chosen for the first stage of the meanline design (Table 3-1). These parameters were selected based on typical gas turbine power plant values (e.g. Velocity Ratio, V_m) and the operating characteristics of the baseline first stage (i.e. C_x/U). A thorough description of the mechanics of gas turbine meanline analysis is described by Oates [49].

The cross section of the baseline turbine design is shown in Fig. 3-2 with the turbine cross sections of the Westinghouse 501D [56] and the GE MS7001F [13] turbines. The cross sections are shown for comparison only. The operating parameters for each of the units are also shown on Fig. 3-2. The baseline turbine cross section is representative of current engines on the market and is therefore viable for analysis.

A summary of the baseline turbine meanline design is shown in Table 3-2a. The second and third stages are shown to substantiate the validity of the first stage baseline design. The baseline vane and blade airfoils had meanline design characteristics which were similar to those of the LSRR design (Table 3-4). The baseline vane design was compatible with both the LSRR design and conventional design practice. However, the baseline blade design, scaled directly from the LSRR blade design, resulted in a relatively large flow overspeed (noted by the * in Fig. 3-7a) on the pressure side of the blade near the leading edge. The relative incidence angle for the baseline blade (i.e. scaled LSRR blade) was approximately -18 degrees. This high negative incidence angle for the baseline blade was due to the direct application of an aggressively designed aircraft turbine to a more conventional, stationary, baseload power plant application. Therefore, a modified baseline blade was designed by adjusting the leading edge geometric parameters of the baseline blade to obtain a more conventional relative flow incidence of -5 degrees. The erosion characteristics of the modified baseline blade were also obtained for comparison to the results from the baseline blade to determine the effect of incidence on blade surface erosion.

Airfoils were designed for the first stage of each of the meanline designs. The airfoils were designed using the Pratt & Whitney Turbine Design System (Fig. 3-1) and conventional practices. The airfoil surface pressure distributions were used to evaluate the acceptability of these airfoil designs. A number of dimensionless geometric parameters were kept equal to values which define the existing geometry in the UTRC LSRR (i.e. pitch/chord, height/chord ratios). These dimensionless parameters, plus additional dimensions, are shown in Tables 3-3 and 3-4. The airfoil coordinate system is shown in Fig. 3-3 with the baseline blade meanline shape.

Alternate Turbine Characteristics

Three additional turbine meanline design studies were conducted. The purpose of the additional designs was to significantly change the aerodynamic operating condition to reduce airfoil erosion. The goal of the alternate designs was to adjust several fundamental design parameters from the baseline turbine values separately to determine the effect on erosion. Several meanline designs were completed with the following changes from the baseline turbine.

1. Increased the number of stages from three to four.
2. Increased the mean radius from 35.2 to 42.2 inches.
3. Increased the airfoil spacing approximately 10 percent.

The results of making these changes are discussed briefly below and summarized in Tables 3-2 through 3-4. Adding the fourth stage and increasing the mean radius resulted in decreased Mach numbers through both new stages after the vane inlet plane. Although increasing the radius caused a 17 percent decrease in incident Mach number on the vane and 27 percent decrease in incident Mach number on the blade, the relative Mach numbers exiting each blade row were relatively unchanged. However, adding the fourth stage resulted in substantial reductions in Mach number (12 to 16 percent) at the exit plane of both airfoil rows and the inlet plane of the blade. Increasing the airfoil spacing 10 percent resulted in essentially identical aerodynamic parameters compared to the baseline turbine with a corresponding 10 percent increase in the airfoil loading coefficients. Increasing mean radius and adding a fourth stage were expected to reduce relative Mach numbers through the first stage to levels which may effectively reduce airfoil surface erosion. The overall Turbine Performance Parameters for the four turbines are shown in Table 3-5.

The airfoils for the three alternate meanline turbine designs were obtained by adjusting the leading and trailing edge metal angles of the baseline airfoils to obtain the velocity triangles defined by the meanline designs. All of these airfoil shape designs were derivatives of the baseline vane and blade airfoils with relatively small changes. Flow angles exiting each airfoil row were calculated by using empirical deviation angle correlations. In addition, careful attention was given to the airfoil surface pressure distributions. Airfoil shapes were chosen to (1) minimize leading edge diffusion (i.e. leading edge overspeeds), (2) obtain a smooth acceleration on the suction surface with minimal diffusion near the trailing edge and (3) place the location of minimum pressure on the suction surface at or aft of the airfoil throat location. These criteria and a subjective analysis of the airfoil shapes and pressure distributions were used to obtain realistic turbine airfoil shapes for the alternate meanline designs.

One of the major goals of the program was to determine the effect of airfoil shape on the erosion due to particulates. Airfoils were designed consistent with the baseline meanline turbine design with a significantly different shape compared to more customary airfoil designs. The primary goal of the new airfoil designs (MOD-1) was to increase the radius-of-curvature of the particles turning in the airfoil passage, thereby, conceptually decreasing the centrifugal force which causes particles to deviate from the fluid streamlines. The ultimate result of this philosophy was that (1) the pressure surfaces of the baseline airfoils were "filled-in" and (2) the leading edge metal parameters were changed to accommodate the thicker airfoils.

Cross sections of the vane and blade airfoils designed for this program plus the baseline vane and blade airfoils are shown in Figs. 3-4 and 3-5, respectively. The solid lines in the figures show the baseline airfoil shapes. In general, the adjustments to the vane airfoils (Fig. 3-4a) were minimal while the major changes to the blade airfoils were increases in the leading edge metal angles (Fig. 3-5a). The modified baseline blade section is also shown in Fig. 3-5a with short dashed lines. (Note the modified leading edge compared to the baseline blade.)

The MOD 1 airfoils are shown in Figs. 3-4b and 3-5b. As discussed above, the major difference between these airfoils and the baseline airfoils is the relatively larger radius of curvature on the pressure sides of the airfoil sections.

The distributions of airfoil surface pressure normalized with the inlet total pressure for the vane and blade airfoils are shown in Figs. 3-6 and 3-7, respectively. Loading on the vane and blade airfoils was significantly reduced for the four-stage and increased radius turbine designs (Figs. 3-6a and 3-7a) because of the decrease in the required turning. Loading was increased for the increased pitch turbine stage because of the reduction in the number of airfoils. In general, the pressure distributions are typical of those for turbine vane and blade airfoils.

Table 3-1 Design Parameters for Baseline First Stage

• Vane Aspect Ratio (h/b_x)	1.010
• Blade Aspect Ratio (h/b_x)	0.946
• Vane Gap/Chord Ratio (T/b_x)	1.300
• Blade Gap/Chord Ratio (T/b_x)	0.956
• α_1	90.0 deg.
• α_2	22.0 deg.
• β_2	26.0 deg.
• C_x/U_m	0.63
• Exit pressure	14.7-0.6 q_e
• V_m	0.52

Table 3-2 Turbine Stage Characteristics

Stage	a) Baseline Turbine			b) Four-Stage Turbine			
	First	Second	Third	First	Second	Third	Fourth
Pressure Reaction (%)	50.0	50.0	50.0	50.0	50.0	50.0	50.0
Temperature Reaction (%)	54.7	61.9	63.5	53.5	58.1	58.5	60.0
Percent Work Split	26.9	36.6	36.5	20.2	25.0	27.4	27.4
Inlet Radius Tip, in.	37.89	38.08	43.37	37.89	39.73	43.18	46.87
Inlet Radius Root, in.	32.51	32.17	28.98	32.51	32.28	30.17	27.91
α_2	21.5	---	---	23.3	---	---	---
β_3	25.2	---	---	25.9	---	---	---
$P_{t,1}/P_{s,3}$	1.73	---	---	1.60	---	---	---
Delta Eff. from Baseline	0.0	---	---	+0.8	---	---	---
Stage Power, Btu/sec	54265.4	---	---	41864.5	---	---	---
C_x/U_m	0.58	---	---	0.53	---	---	---
Stage	c) Increased-Radius Turbine			d) Increased-Pitch Turbine			
	First	Second	Third	First	Second	Third	
Pressure Reaction (%)	50.0	50.0	50.0	50.0	50.0	50.0	
Temperature Reaction (%)	54.8	61.1	62.6	54.9	61.9	63.5	
Percent Work Split	26.9	36.6	36.5	26.9	36.6	36.5	
Inlet Radius Tip, in.	44.89	47.72	53.00	37.89	38.08	43.37	
Inlet Radius Root, in.	39.51	36.44	33.02	32.51	32.17	28.98	
α_2	18.1	---	---	21.6	---	---	
β_3	21.1	---	---	25.3	---	---	
$P_{t,1}/P_{s,3}$	1.83	---	---	1.73	---	---	
Delta Eff. from Baseline	+1.8	---	---	-0.5	---	---	
Stage Power, Btu/sec	55849.8	---	---	54214.2	---	---	
C_x/U_m	0.39	---	---	0.58	---	---	

Table 3-3 Geometric and Flow Conditions for First-Stage Meanline Designs

Name of Quantity	Baseline		Four-Stage		Inc.-Rad		Inc.-Pitch		MOD-1	
	Vane	Blade	Vane	Blade	Vane	Blade	Vane	Blade	Vane	Blade
b_x (in.)	5.317	5.686	5.317	5.686	5.317	5.686	5.317	5.686	5.317	5.686
U_1 (ft/sec)	454.0	638.3	454.0	545.1	376.9	465.0	454.0	637.6	454.0	638.3
U_m (ft/s)	---	1105.8	---	1105.8	---	1325.8	---	1105.8	---	1105.8
R_m	35.2	35.2	35.2	35.2	42.2	42.2	35.2	35.2	35.2	35.2
N	32	41	32	41	38	49	29	37	32	41
S_{te}/b_x	1.8406	1.6033	1.8174	1.5258	1.8881	1.5934	1.8803	1.6292	1.8756	1.6445
S_{te}/b_x	3.4009	2.9146	3.3730	2.8290	3.4580	2.9391	3.4391	2.9263	3.4133	2.8862
S_{max}/b_x	3.4278	2.9581	3.3993	2.8731	3.4856	2.9831	3.4662	2.9690	3.4403	2.9299
T/b_x	1.2999	0.9557	1.2999	0.9487	1.2999	0.9487	1.4348	1.0513	1.2999	0.9487
h/b_x	1.0118	0.9462	1.0118	0.9462	1.0118	0.9462	1.0118	0.9462	1.0118	0.9462

Table 3-4 Comparison of Geometric Parameters With LSRR Turbine

Turbine	Airfoil	b_x (inches)	R_m (inches)	N	h/b_x	T/b_x
LSRR	vane	5.932	27	22	1.0115	1.2999
	blade	6.341	27	28	0.9462	0.9555
Baseline	vane	5.317	35.2	32	1.0118	1.2999
	blade	5.686	35.2	41	0.9462	0.9487
Modified Baseline Four Stage, MOD-1	vane	5.317	35.2	32	1.0118	1.2999
	blade	5.686	35.2	41	0.9462	0.9487
Increased Radius	vane	5.317	42.2	38	1.0118	1.3123
	blade	5.686	42.2	49	0.9462	0.9517
Increased Pitch	vane	5.317	35.2	29	1.0118	1.4344
	blade	5.686	35.2	37	0.9462	1.0513

Table 3-5 Overall Turbine Performance Parameters

Turbine	Baseline	4-Stage	Inc. Radius	Inc. Pitch
$P_{t,in}/P_{t,amb}$	11.27	11.56	11.68	11.27
$P_{t,in}/P_{s,amb}$	14.08	13.43	13.21	14.07
Turbine Power, Btu/s	201730.0	207250.0	207620.0	201540.0
Net Power Unit Rating, MW =	78.7	84.5	84.9	78.5

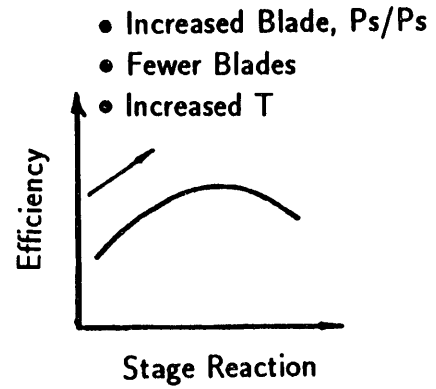
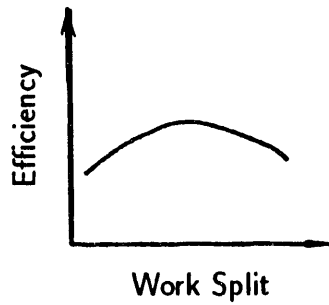
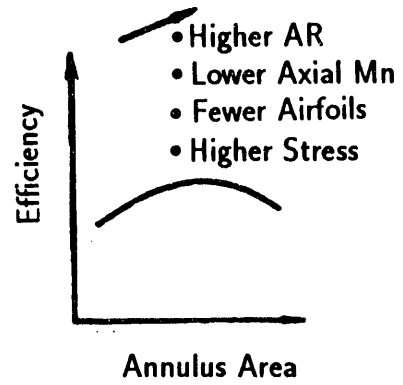
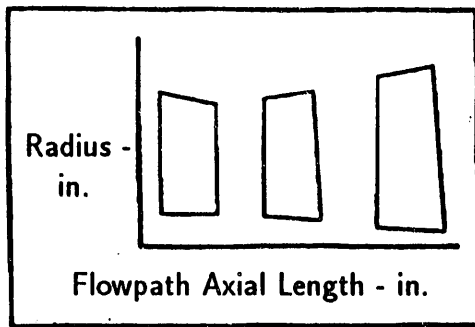


Figure 3-1 Interactive P&W Turbine Design System Allows Rapid Flowpath Definition/Parametric Optimization

GE MS7001F
136 MW 898#/s
PR=13.5 $T_T=2300^{\circ}\text{F}$

Baseline
79 MW 670#/s
PR=12.2 $T_T=2100^{\circ}\text{F}$

Westinghouse 501D
98 MW 814#/s
PR=14.5 $T_T=1,350^{\circ}\text{F}$

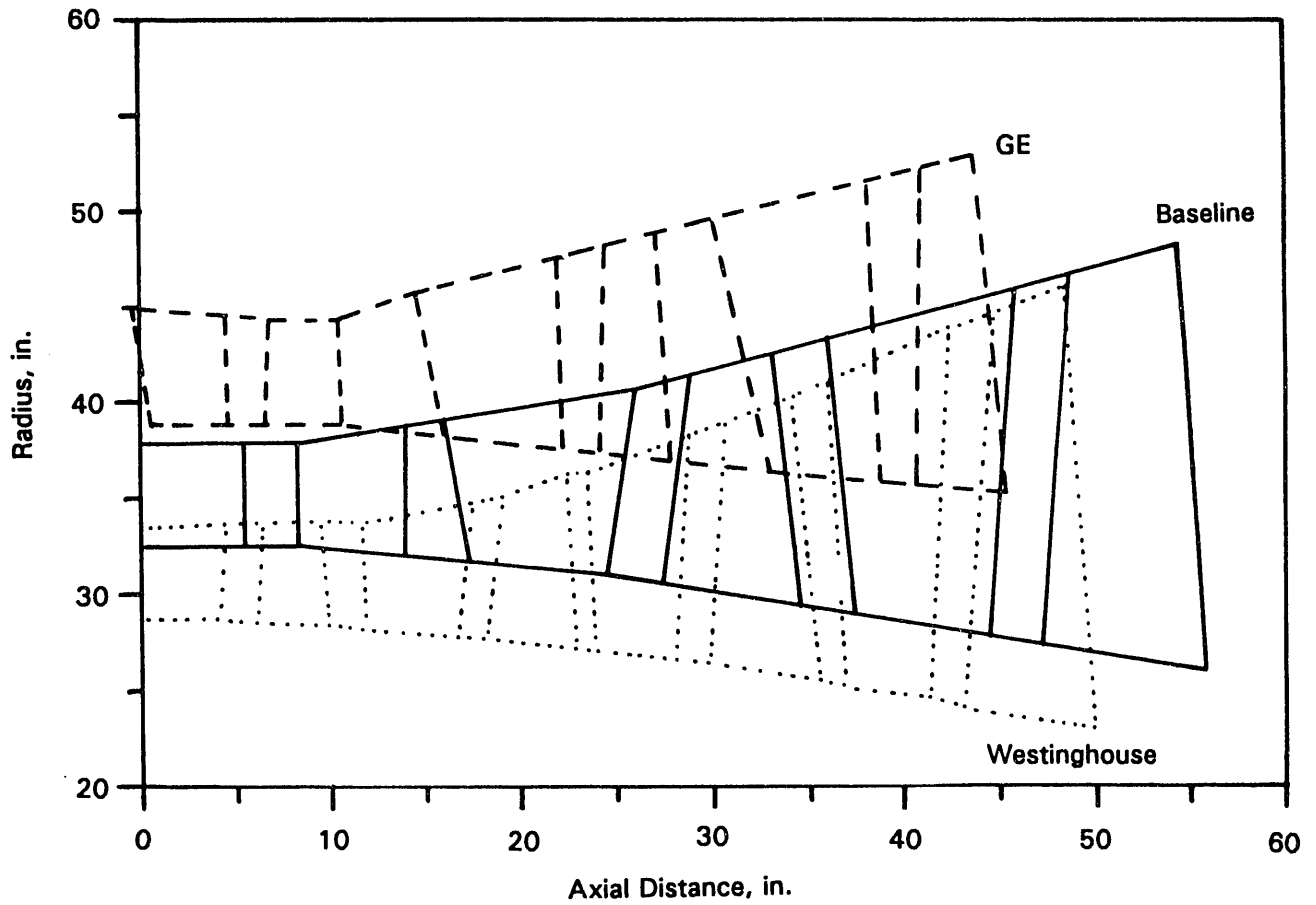


Figure 3-2 Turbine Cross Sections

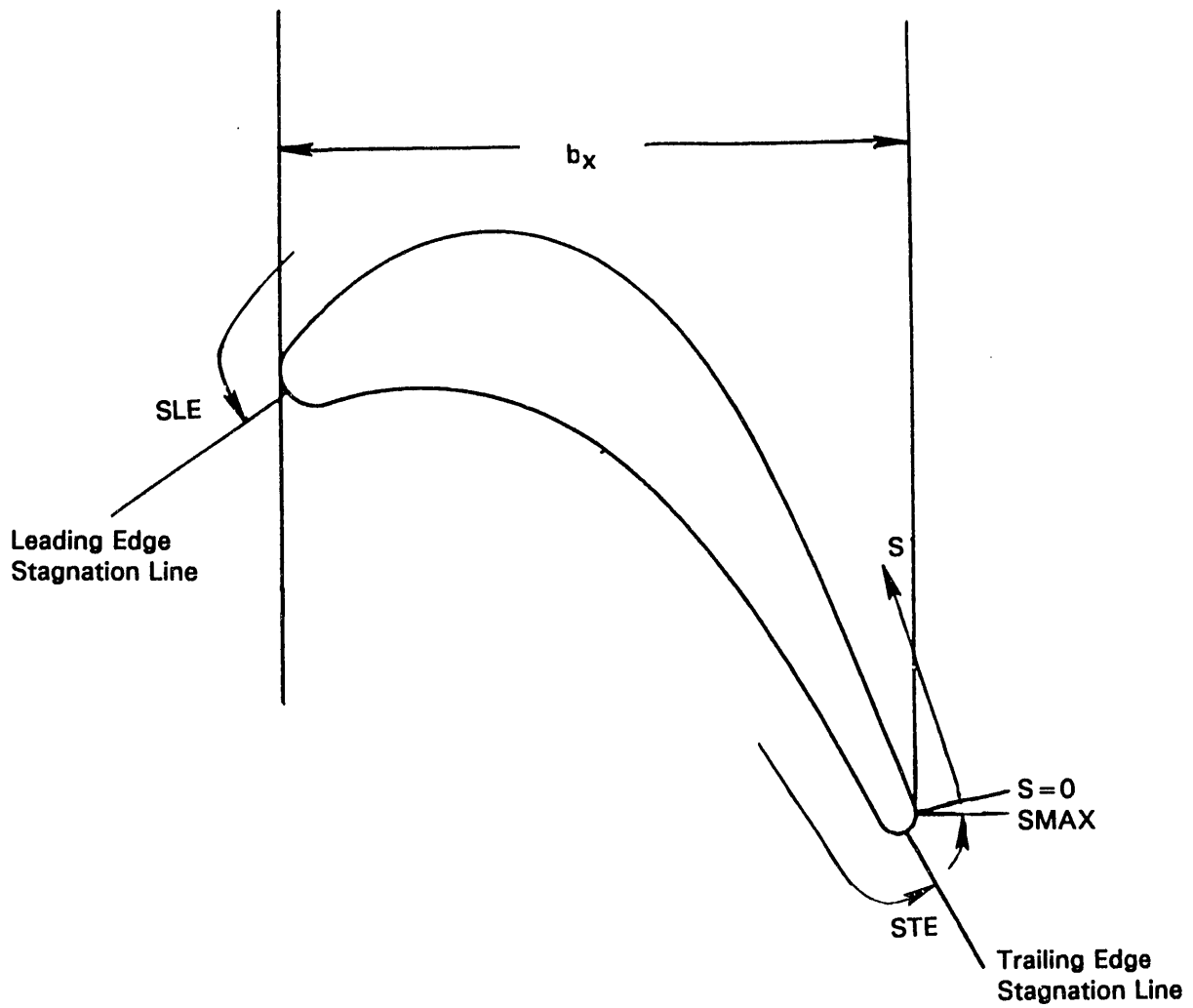


Figure 3-3 Airfoil Coordinate System and Nomenclature, Baseline Turbine Blade

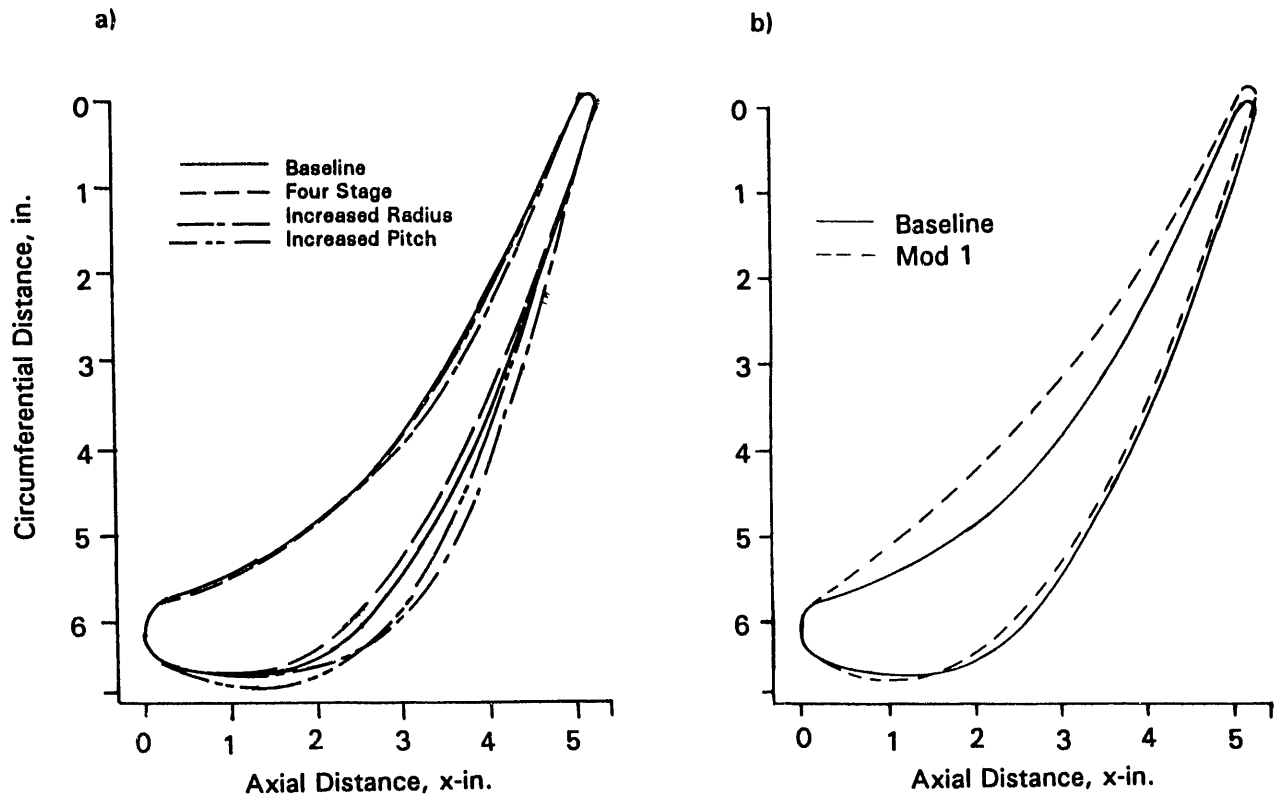


Figure 3-4 Vane Meanline Airfoil Profiles

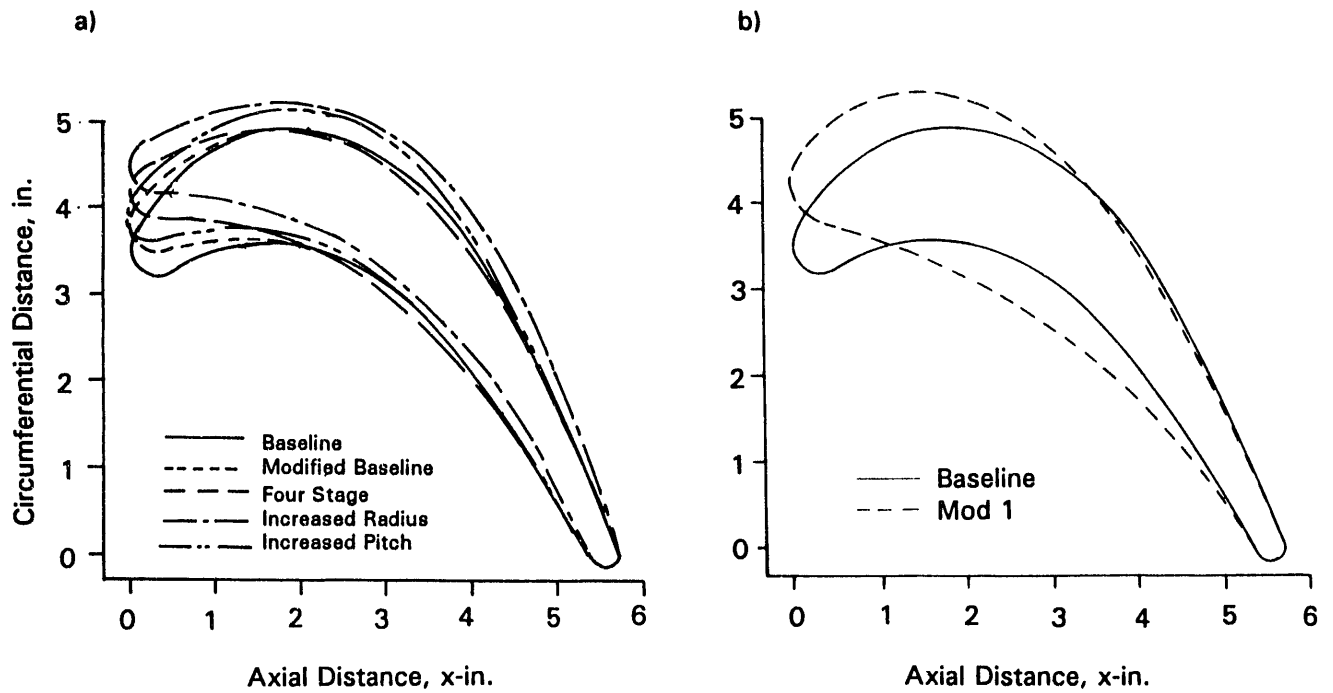


Figure 3-5 Blade Meanline Airfoil Profiles

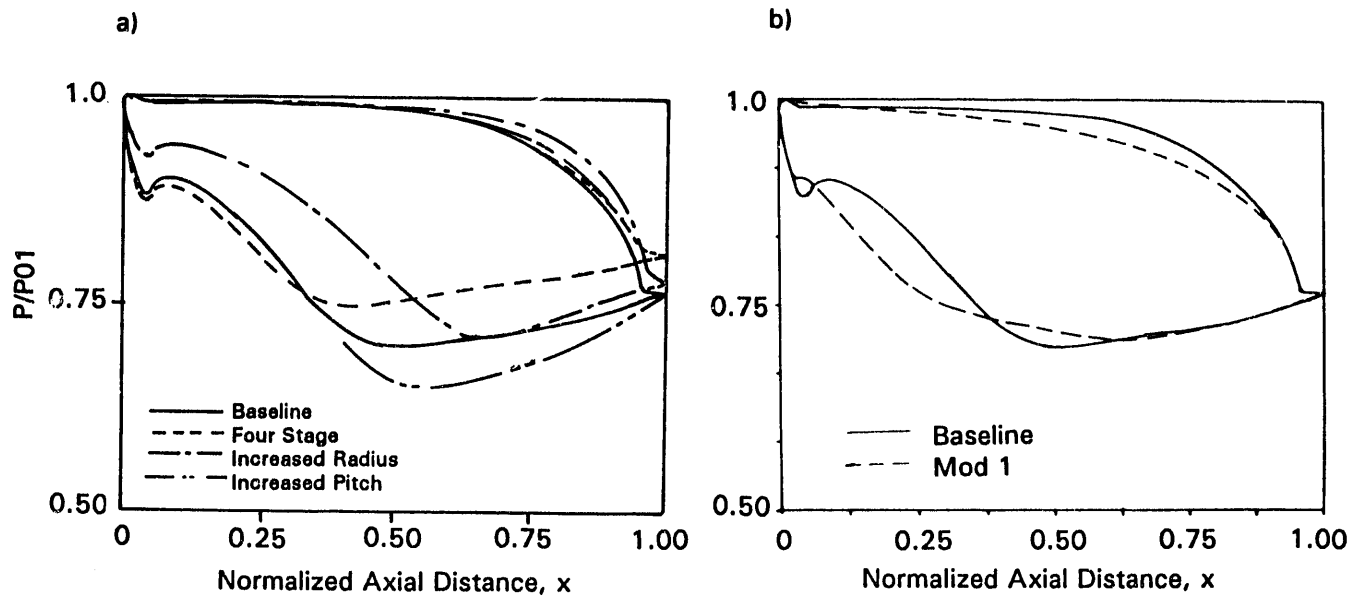


Figure 3-6 Vane Meanline Airfoil Pressure Distribution

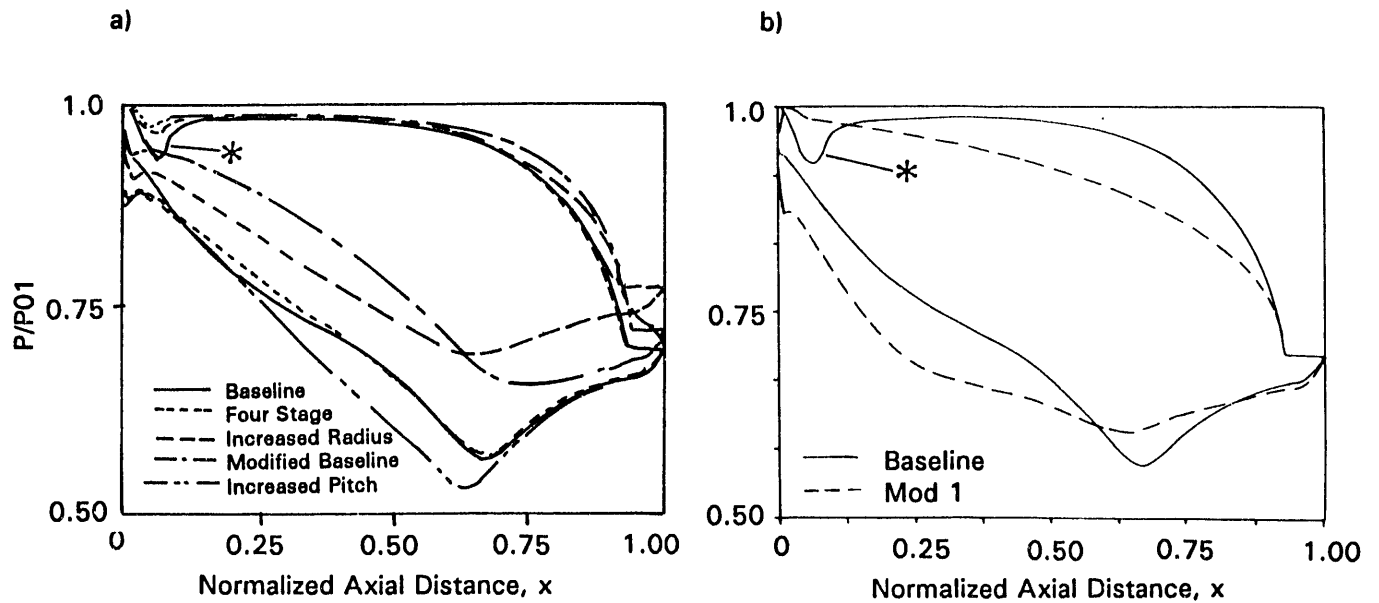


Figure 3-7 Blade Meanline Airfoil Pressure Distribution

SECTION 4

PARTICLE TRAJECTORY PROCEDURES AND MODELS

The Aerodynamic and Particle Trajectory Codes used in the performance of this study were developed under United Technologies Corporation (UTC) sponsorship prior to use on the DOE METC project. Although the methodology was not developed under the contract, it is important that the details be available for the reader. Therefore, the models and equations used in the particle trajectory codes are described in this section.

Flowfields

2-D Cascade Flow Code

Computational fluid dynamic codes were used to generate 2 and 3-D flowfields. The majority of the trajectories were calculated through 2-D flowfields to assess the effects of airfoil and turbine design on the resulting erosion. Flowfields for all of the 2-D turbine designs were calculated using a potential flow code developed at UTRC called CASPOF. The aerodynamic parameters from the meanline code were used as input to the potential flow code.

The CASPOF code [16] was used to calculate the velocity field in a 2-D cascade with the meanline airfoil shapes. Airfoil pressure distributions obtained with the code compare well with experimental turbine results [33]. The code utilizes a multiple gridding method (Fig. 4-1). A coarse, semi-rectangular (11 nodes between airfoils and 120 nodes from the inlet plane to the exit plane) was used to calculate the blade-to-blade aerodynamics. A fine, O-grid (200 nodes around the perimeter of the airfoil and 11 nodes linearly located normal to the airfoil surface) was used to calculate the detailed aerodynamics in the vicinity of the airfoil. Local fluid velocity and density were used as the particle moves through the flowfield. A bilinear interpolation scheme was used to interpolate within the mesh nodes and switches between the coarse and fine mesh depending on location to improve the accuracy of the trajectory calculation procedure. Accuracy of the trajectory calculation was further enhanced by allowing the particle step size to vary in accordance with changes in direction of the particle or when approaching or leaving a surface. For large changes in particle direction, step size was decreased until the change in direction is below a specified maximum. For small changes in particle direction, step size was increased to a preset maximum step size of 4% of the axial chord.

3-D Flow Code

Flowfields for the 3-D baseline vane and blade airfoils were calculated from the restart file of a full 3-D Euler analysis of the UTRC Large Scale Rotating Rig facility. The geometry of the passage was adjusted to the scale of the baseline turbine of the present analysis. The restart files that were used were for a low Mach number case and adjusted to simulate the compressible flowfield of the baseline design. The adjustments were made with axially dependent, linear multiplier functions within the airfoil row so as to match the exit velocities and densities of the simulated baseline turbine. The flow velocity information for the 3-D

flowfields were normalized with the inlet flow conditions. Normalizing the flowfields facilitated the calculation of subsequent trajectories using the dimensionless forms of the governing particle trajectory equations described below.

Particle Trajectory Analysis

The most critical aspect of this program was the calculation of many particle trajectories through 2-D and 3-D flowfields. The trajectory calculations produced surface impact statistics which were used to estimate erosion and also airfoil row exit statistics which were used to restart the particles in the next airfoil row. The equations used to calculate particle motion and the calculation procedure are discussed in this section. The derivation of the equations [20] is reiterated in the Appendix and discussed in the following paragraphs.

Particle Dynamics

Particle dynamics in gas turbine flow fields is extremely complex. The complexities arise from a number of phenomena including, but not limited to, flow turbulence, particle rotation, changing particle and surface conditions and high shear flows. A recent review paper [31] discusses many aspects of calculating particle behavior with these complicating effects. As noted by Humphrey, practical solutions to real problems can result in improved understanding of erosion phenomena. Therefore, idealizations of the real complexities of calculating particle dynamics were made. Specifically, due to the anticipated low particle loadings at the turbine inlet (i.e., approximately 5 to 200 ppm) particle-particle interactions were ignored (loadings noted above correspond to average particle separation distances of 150 to 500 particle diameters) and discrete particle analysis in an unperturbed flowfield was assumed valid. In addition, due to the assumed high particle-to-fluid density ratios, all forces on the particle other than those due to aerodynamic drag (i.e., Magnus, Basset and Saffman forces) were neglected [31, 32].

Flowfield turbulence and the statistical nature of rebounding particles (e.g. [65]) were also not considered in this analysis. Although the flowfield turbulence and statistical rebound effects could be modelled and included in the analysis either directly or indirectly [31] based on random perturbations and/or viscous calculations, the added complexity was not warranted for meeting the objectives of the present calculations.

As shown in the APPENDIX, the fundamental dimensional equation for particle motion is [Eqn. A1].

$$\ddot{\vec{X}} = \frac{\rho_f a}{2\rho_p v} C_d \frac{\vec{V}}{|\vec{V}|} \vec{V} \quad (4-1)$$

and the dimensionless equation for particle motion becomes [Eqn. A4]

$$\ddot{\vec{x}} = \frac{3}{4} \sqrt{\frac{\sigma}{18 St}} \left(\frac{\rho_f}{\rho_{f,1}} \right) C_d |\vec{u} - \dot{\vec{x}}| (\vec{u} - \dot{\vec{x}}) \quad (4-2)$$

The formulation derived was used to calculate trajectories in 2-D and 3-D flowfields. In the case of 2-D flowfields, the formulation yielded two equations in the form of $\ddot{x}(= \ddot{x}_1)$ and $\ddot{y}(= \ddot{x}_2)$ for the coordinate system shown in Figure 4-1. For 3-D flowfields, the acceleration term on the left side of the equation was replaced with terms which allowed for radial variations.

i.e. $\ddot{x}_1 = \ddot{x}$

$$\ddot{x}_2 = \ddot{y} - 2 * \dot{z} * (\dot{y}/z + y_0)$$

$$\ddot{x}_3 = \ddot{z} - z * (\dot{y}/z + y_0)^2$$

where x is the axial direction,

y is the tangential direction,

z is the radial direction and

y₀ is the dimensionless angular speed of the whole flowfield (i.e. flowfield of blade is specified in relative frame of reference)

The equations were solved using a standard, fourth order Runge-Kutta solving routine to integrate through a given flowfield [1].

Particle Aerodynamic Drag Model

The physical parameters which describe particles in the combustion gases of coal-fueled, direct-fired gas turbines are strongly dependent on the combustion chemistry, gas path history and the gas path temperature. The particle shape can range from smooth and spheroidal to angular, depending on firing temperature. Additionally, large particles can be formed during the combustion phase due to agglomeration of fine particles. Such particles may be larger than the top size of the micronized coal used to make the slurry. These particles are many times left with voids (from the gasification of the imbedded carbon) which make the particles friable. Therefore, particles are not limited by the top size of the original coal grind and can have very smooth, glassy surfaces or very rough, angular surfaces.

The drag coefficients are expected to vary significantly over the anticipated range of particle surface roughness. The particles in the present program are assumed to be smooth

and spherical. This assumption is valid for particles which are not smooth and spherical when effective particle diameters are used in lieu of the actual measured diameters. The effective particle diameter is defined as the diameter of an idealized smooth, spherical particle with the same drag characteristics as the modeled particle. In addition, the effective particle density is determined by dividing the modeled particle mass by the effective particle volume.

The mechanics of calculating particle trajectories within airfoil rows is documented by Dring et al. [20] and is briefly described in another section. Particle trajectories are governed by the resultant forces on the particle due to the aerodynamics of the flow surrounding the particle. The forces on the particles were calculated based on the relative velocity between the particle and the fluid. The difference in fluid and particle speed and direction imparts an accelerating force on the particle due to aerodynamic drag. All other forces on the particle were neglected as described by Hussein and Tabakoff [32]. The aerodynamic drag coefficients for ranges of particle Reynolds number used by Dring and in the present program are shown algebraically and graphically in Figure 4-2. These drag coefficients are consistent with those used by other investigators, e.g. [23].

Particle Rebound Model

Particles which impact the airfoil surface generally lose some kinetic energy due to combinations of erosion and imperfect (i.e. inelastic) surface rebound. Prediction of this behavior is difficult [34] and rebound models are best constructed from experimental results. Numerous experimental studies of rebound parameters for use in trajectory calculations, mostly by Tabakoff and his coworkers, have been completed for many surface materials, particle compositions and experimental test conditions [64, 65, 68, 69, 74, 75]. These studies document the restitution ratios of the normal and tangential velocities for impact angles relative to the surface.

The rebound model is used to determine the resultant velocity after a particle impacts the surface of the airfoil. The use of the rebound models can have significant effects on predicted erosion [41]. Particle composition and size has been shown to have large effects on rebound parameters [68]. However, rebound parameters are relatively insensitive to surface material and surface temperature [74]. Therefore, to provide the most general analysis as possible, restitution coefficients for fly-ash have been developed from the results of Tabakoff [64, 65] for coal ash particles for application with a variety of potential airfoil materials. This generic rebound model reflects the general response of several different particles and surface materials. The tangential and normal velocity rebound parameters developed for this program are presented in Eqs. 4-3 and 4-4 and in Figure 4-3.

$$V_{n2}/V_{n1} = 1.0127 - 1.3458 \beta_p + 0.9569 \beta_p^2 - 0.2263 \beta_p^3 \quad (4-3)$$

$$V_{t2}/V_{t1} = 0.9813 + 0.0907 \beta_p - 2.7278 \beta_p^2 + 3.5867 \beta_p^3 - 1.1964 \beta_p^4 \quad (4-4)$$

Trajectory Calculation Procedure

The procedure for calculating particle trajectories was essentially identical for the 2-D and 3-D trajectory calculations. In both cases the initial speed and direction of particles for the stationary vane were coincident with the inlet flow. The number and spacing of the

particle initial locations were chosen to obtain statistically consistent and significant surface interaction results. However, the initial speed and direction of particles for the rotating blade row were determined with a vector transformation process using results from a statistical analysis of the particles which exit the stationary blade row. In this manner the particle parameters were transferred from the stationary reference frame at the exit of the stationary vane to the relative reference frame at the inlet of the rotating blade.

The initial, surface interaction and final parameters which describe the particle response in blade rows were used as input to a surface interaction analysis code to estimate local erosion rates. Intermediate data files were used to transfer the required information from the 2-D trajectory calculations to the surface analysis routines. This procedure allowed erosion predictions using different erosion models for the same set of trajectory and surface interaction results. To avoid handling extremely large data files, the surface impact information from the individual 3-D trajectory calculations was sent to the surface analysis routines directly.

The parameters shown in Table 4-1 were transferred to the surface analysis routines for each particle trajectory. The impact information (noted with an “**”) was used to calculate surface impact erosion statistics for each designated surface element as described in the section on Erosion Models.

2-D Trajectories. For the 2-D, meanline trajectory calculations, two sets of particles were started at the inlet of each blade row. The initial locations upstream of the stationary vane for first pass consisted of 200 evenly spaced points across a total vane pitch (i.e. spacing). The trajectory results from the first pass were used to 1) define the region of the vane pitch to concentrate the initial locations for the second pass and 2) determine the initial speed and direction for the particles which didn't hit the vane for the subsequent rotating blade. The second pass consisted of another 200 particles which were started in the region of the vane pitch where most of the particles were expected to impact the vane. The trajectory results from the second pass were used to 1) calculate the erosion on the vane surface and 2) determine the initial speed and direction for the particles which hit the vane for the rotating blade.

The speed and direction of the particles exiting the stationary vane were averaged for the two passes discussed above. Consequently, trajectories were calculated through the downstream rotating blade for two cases; for the particles which hit the vane and for those particles which didn't hit the vane. Therefore, for each subsequent airfoil row, the required number of particle trajectories doubled, depending on the history of each grouping of particles. For the present analysis, all particle trajectory calculations were stopped at the exit of the rotating blade row. Therefore, only 1200 particle trajectory calculations were required for each particle diameter/density combination for each turbine (i.e. typically 18,000 trajectories).

3-D Trajectories. Ten thousand particles were started at the inlet of the vane airfoil in a matrix of 100 by 100 evenly spaced points. Since there was little radial migration of particles in the vane, the average exit speed and direction of each set of 100 particles in the tangential direction was determined to start the particles at the inlet of the rotating blade row. As with the particles in the 2-D flowfield, the particle velocity vectors exiting the vane were

transformed to the rotating coordinate system. Subsequently, 100 evenly spaced locations in the tangential direction (to account for blade motion relative to the vane) were calculated over a blade pitch for each set of the averaged particle parameters from the exit of the vane. Therefore, for each particle diameter/density combination, 20000 particle trajectories were determined (for the present analysis with three particle diameters, 60000 trajectories).

Particle Monitoring

The trajectory calculation computer code monitors particle status along each step of the calculation is tailored to address special situations which occur. The problems which frequently occurred were related to the steady flowfield which was used to determine the particle's movement and the rebound models which allowed the particle to impact the surface a number of times. Physical limits were placed on the particle to stop or control the calculation when it approached a surface boundary or left the region of interest. Therefore, flags in the code were used to monitor the status of a trajectory calculation. The flags were used to either suspend the calculation or modify the step size so that (1) the particle wouldn't turn too sharply at a large step size (which decreased spatial accuracy) or (2) the particle position would be known more precisely when approaching a surface or flow boundary limit. The flags shown in Table 4-2 were used by the code to control the particle trajectory calculation process. The flag number, the cause and the code response are listed in the Table.

The two most commonly used flags (other than 0) were flags 1 and 2 which were used to control step size at surface boundaries and the exit plane. However, for the smallest particles (i.e. 5 micron), a number of trajectories would abort because of extremely shallow impact angles relative to the airfoil surface or because of having reached the maximum number of impacts. Under these conditions the impact angles were often on the order of 0.02 degrees which approached the curvature of the airfoil at the impact location and the trajectory calculation was stopped. The authors believe that this action models real particles in that a particle impacting at such shallow angles is not impacting at all but merely rolling along the surface, thereby, causing negligible amounts of erosion. It is likely that such particles would deposit on the surface as a fine powder as has been observed in practice.

Typical Particle Trajectories

Particles with smaller Stokes numbers tend to accelerate with the fluid and to follow the fluid streamlines more closely, as shown in Figs. 4-4 and 4-5. Particle/surface impact angles tend to increase with increasing Stokes number. (Note, for particles with infinite Stokes numbers, the impact angle is a function only of the airfoil geometry.) Surface impact data show that particle velocities through the airfoil rows are increased a lesser amount for particles with large Stokes numbers compared to those with smaller Stokes numbers. This is due to the increased mass of those particles. Particles with smaller Stokes number tend to follow the fluid streamlines more closely and, for those particles which do impact the airfoil, impact at shallow angles. Increases in either the particle size (i.e. Stokes number), particle density and/or impact speed is expected to yield increased levels of predicted erosion rate. Comparison of particle trajectories by Dring et al. (1979) showed that the agreement of predicted and photographed experimental results was excellent for a wide range of particle diameters.

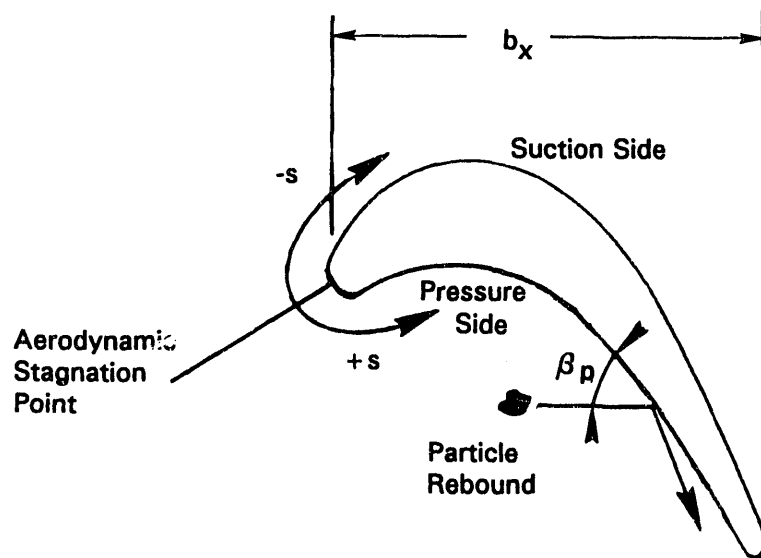
Table 4-1 Particle Trajectory Parameters

XPI	Initial X location of Particle
YPI	Initial Y location of Particle
ZPI	Initial Z location of Particle
VXPI	Initial Velocity of Particle in X Direction
VYPI	Initial Velocity of Particle in Y Direction
VZPI	Initial Velocity of Particle in Z Direction
SPIMPi*	Particle Speed at Surface Impact
APIMPi*	Particle Direction at Surface Impact
ASIMPi*	Airfoil Surface Angle at Impact Location
XPF	Final X location of Particle
YPF	Final Y location of Particle
ZPF	Final Z location of Particle
VXPF	Final Velocity of Particle in X Direction
VYPF	Final Velocity of Particle in Y Direction
VZPF	Final Velocity of Particle in Z Direction

Table 4-2 Trajectory Code Control Flag Status Definitions

Flag	Cause	Code Response
0	Normal Code	No action required
1	Hit Surface	After reducing step size 10 times, 1. Perform rebound calculation 2. Write impact information
2	Passed flow boundary	After reducing step size 10 times, write final particle information
3	Max iterations in Runge Kutta solver	Stop calculation, write final status solver
4	Couldn't make turn with minimum step within set range	Reduce step size up to 10 times
5	Max number of steps	Stop calculation, write final status
6	Particle not moving	After 10 tries, stop calculation, write final status
7	Max number of impacts	Stop calculation, write final status
8	Impact location not changing	After 10 hits at same location, stop calculation, write final status

a) Nomenclature



b) Grids

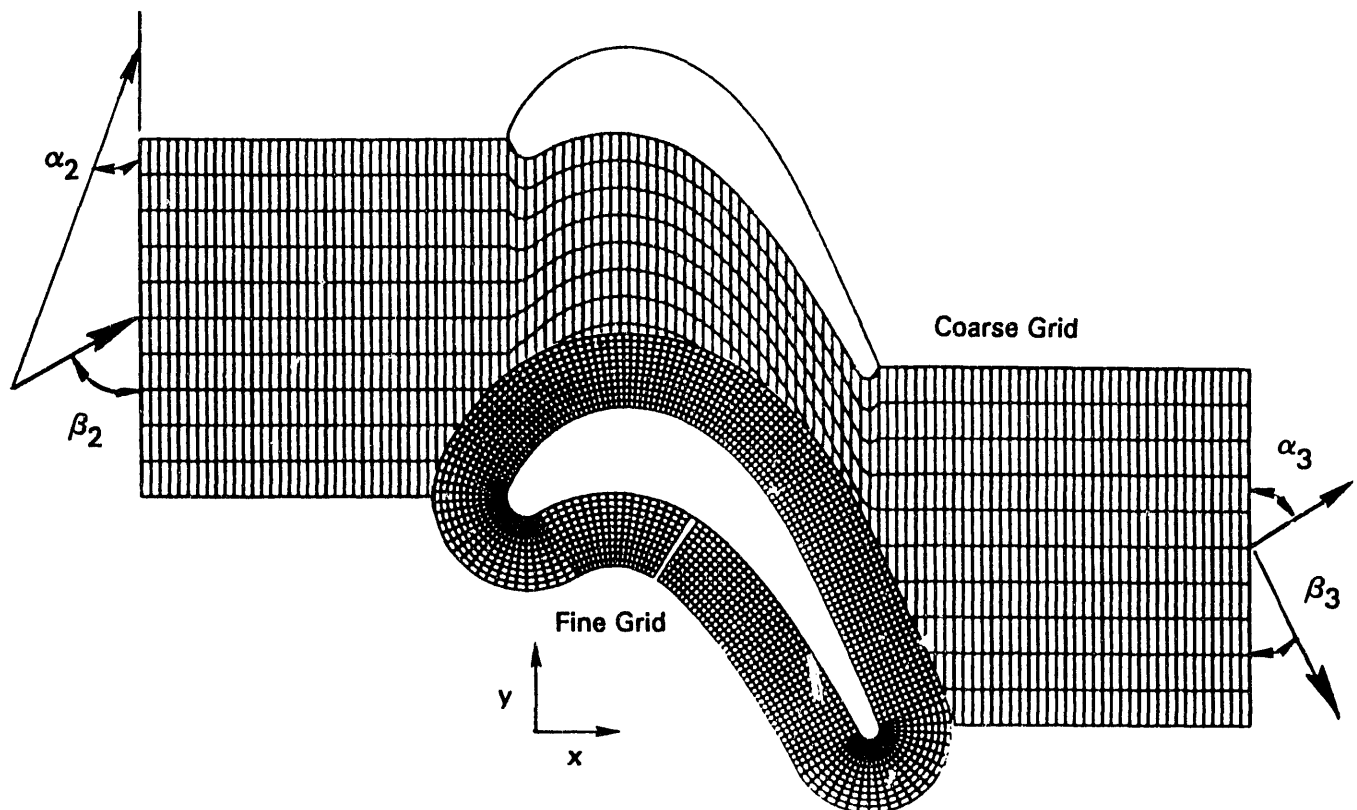


Figure 4-1 Baseline Turbine Aerodynamic Computation Grids and Airfoil Surface Nomenclature

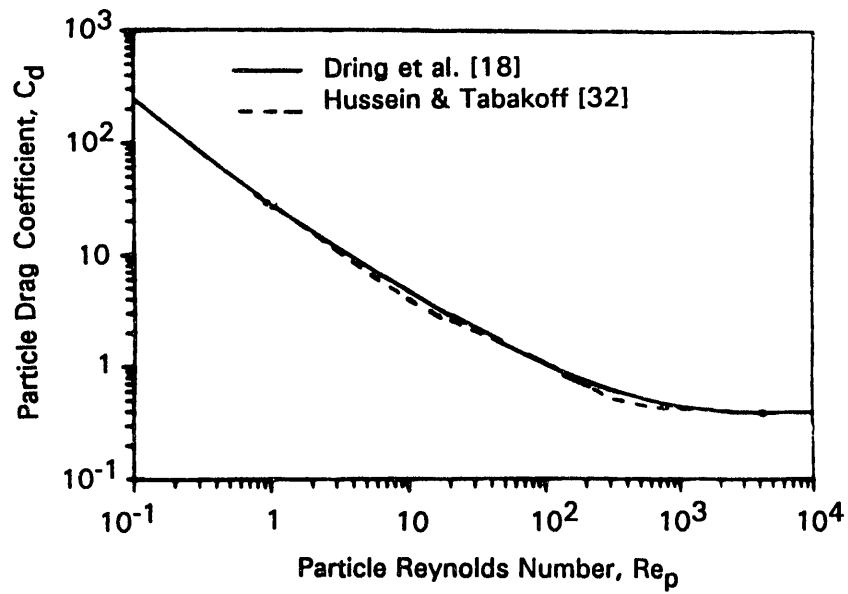


Figure 4-2 Particle Aerodynamic Drag Model

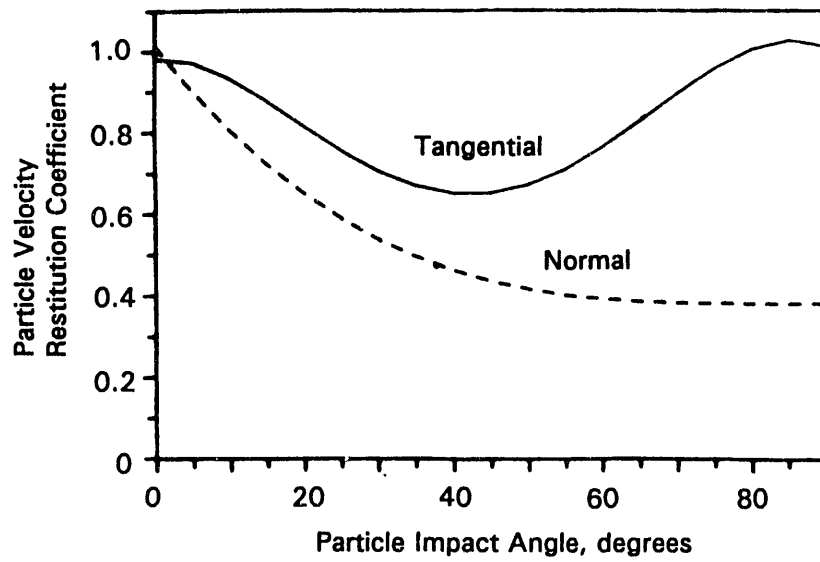


Figure 4-3 Particle Rebound Model

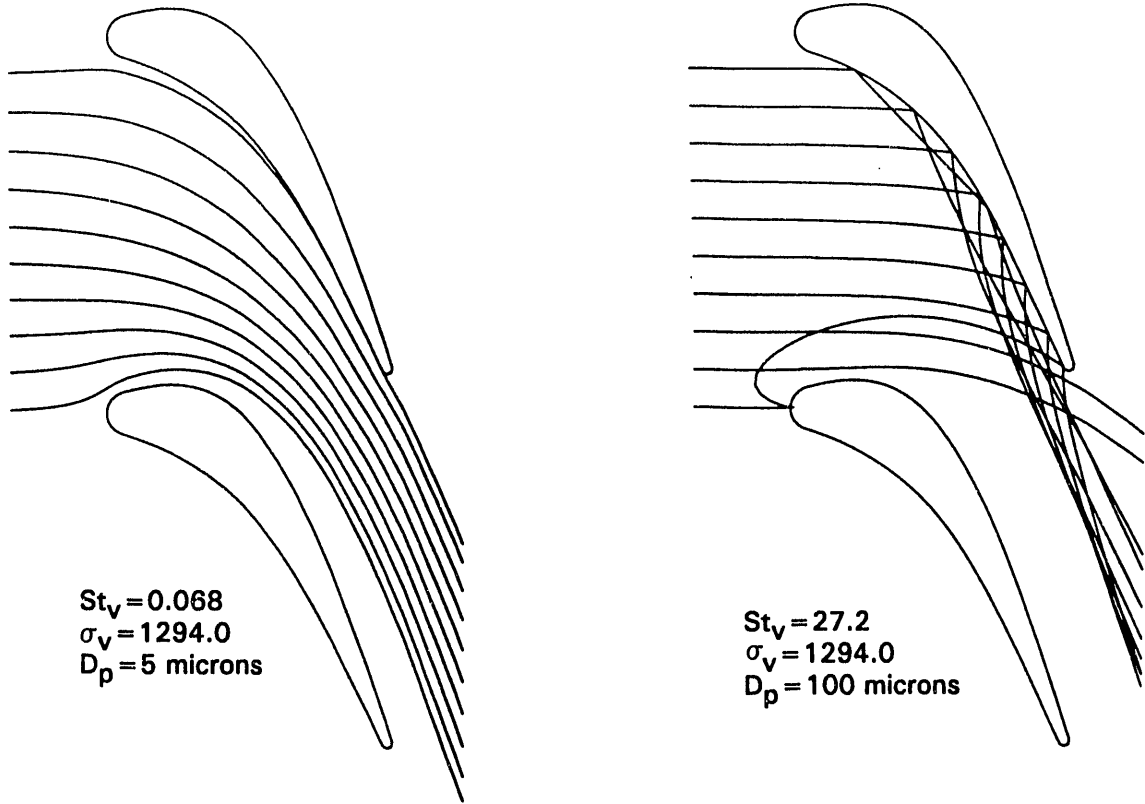


Figure 4-4 2-D Particle Trajectories Through Baseline Meanline Vane Airfoil Row

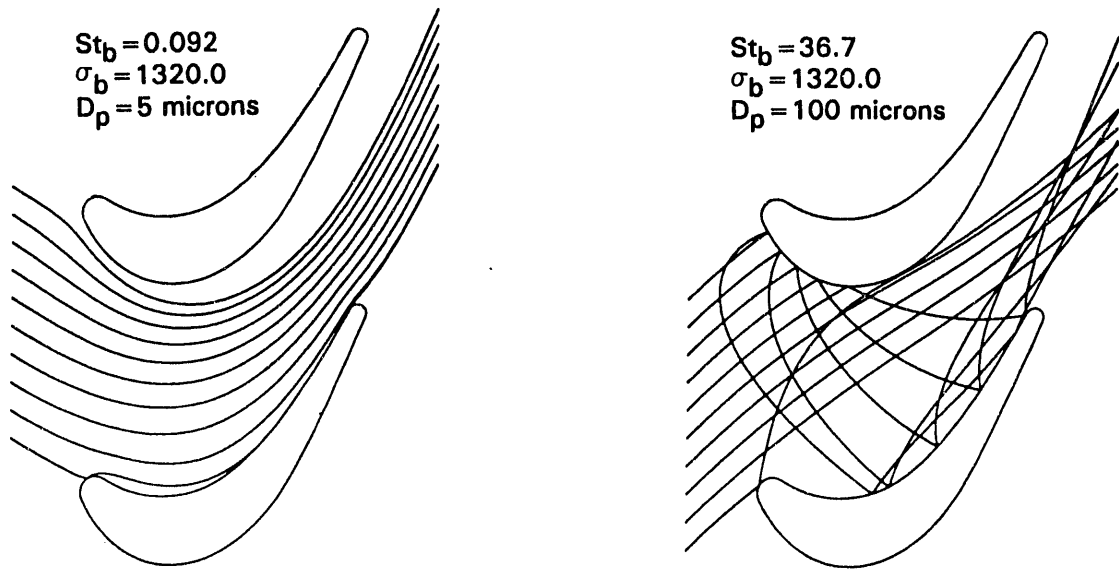


Figure 4-5 2-D Particle Trajectories Through Baseline Meanline Blade Airfoil Row

SECTION 5

EROSION PREDICTION PROCEDURES AND MODELS

Mathematical models were employed to characterize the physical and aerodynamic properties of the particulate material and to assess the erosion on the surfaces of the airfoils. These models are based on previously published studies and ongoing coal-fired combustion and turbine research. Particle aerodynamic drag, rebound and erosion models were required to accurately calculate particle trajectories and estimate local erosion rates. Two erosion models were formulated. One for turbine airfoils made with nickel-based, super-alloys (i.e. ductile) and one for turbine airfoils with thermal barrier coatings (i.e. brittle). The brittle erosion model was developed and used to assess the resultant erosion because of the current market trends toward higher turbine inlet temperatures. Following is a brief discussion of previous erosion studies, followed by the descriptions of the erosion models used to characterize ductile and brittle erosion.

Background

Erosion has been the study of many investigators and a comprehensive review of the earliest work is beyond the scope of this program. However, good overviews of previous erosion studies and the basic structures of current erosion models can be found in the literature [14, 25, 30, 37, 42]. Much of the early erosion work was focussed on improving the physical understanding of the mechanisms of erosion. Although, this was important for the development of the structure of erosion predictions, the data base wasn't broad enough to develop models for high temperature systems designers. To help satisfy this need, a number of high temperature erosion facilities have been developed to produce erosion data over ranges of typical turbine operating parameters.

There are numerous studies of material erosion and corrosion in high temperature simulators with particle laden flows [6, 7, 11, 43, 58, 59]. These results are useful for material comparisons but are difficult to utilize for the prediction of surface impact erosion. The study of erosion for this program focussed on the works by Levy [37, 38, 39, 40], Tabakoff and coworkers [35, 63, 64, 65, 66, 67, 70, 71, 73, 74] and Beacher [10] because of their direct application to the utilization of coal combustion in energy producing systems. Typical data show that all of the items listed below can have significant effects on the erosion rate.

- Turbine airfoil material
- Surface coating
- Surface temperature
- Gas path and particulate temperatures
- Particle material
- Particle relative velocity
- Particle diameter and shape

- Surface impact angle
- Corrosion environment of blades

Erosion results for conditions similar to that expected for a high temperature turbine environment were given special attention. For intermediate temperatures between room temperature and a material's melting temperature, erosion has been shown to decrease [10, 25, 40]. However, erosion sharply increases at high temperatures typical of turbine operating conditions [37, 40, 63, 70, 71]. The parameters listed below have been implicitly or explicitly selected from the baseload turbine operating conditions.

- Surface temperature of blade – 1400 F
- Gas path temperature – 2100 F (turbine inlet)
- Particulate temperature – local gas path temperature
- Particulate material – fly ash

The airfoil surface temperature for this study has been fixed at 1400 degrees F to simulate a relatively high performance, cooled turbine. Existing erosion data was used to obtain surface erosion models for this surface temperature.

The particle impact velocity and impact angles are determined for each particle as part of the parametric trajectory calculation study for ranges of particle diameter and density. The particle impact information was used to estimate the local airfoil surface erosion for a variety of turbine designs using a ductile erosion model. The baseline turbine design was also evaluated using the brittle model to simulate airfoils with thermal barrier coatings.

Erosion Model

Particulate erosion is also strongly affected by impact angle. Ductile alloys typically experience maximum erosion at impact angles near 30 degrees relative to the surface. Brittle alloys generally have higher erosion rates near impact angles close to 90 degrees. This phenomena is related to the differing modes of erosion for these materials (see references listed above for more complete discussions). Typical turbine airfoils are made from many different superalloys designed to withstand the high load, high temperature environment. However, most of the materials used in the manufacture of turbine airfoils are in the ductile family of metals. When turbine inlet temperatures are increased beyond customary levels, thermal barrier coatings are used to protect turbine airfoils. Therefore, the surface interaction erosion models were developed for nickel-based superalloys, which are typical of cooled, high performance turbines, and for airfoils with brittle, ceramic coatings.

The erosion model developed by Menguturk and Sverdrup [45] was used to predict the erosion of the turbine airfoils. Menguturk's erosion model has the desirable features that (1) it can be configured to have a single erosion maxima within the impact angle range of 0 to 90 degrees (i.e. for ductile and brittle erosion modes), (2) allows for finite erosion at 90 degrees in the ductile mode and (3) requires relatively simple coding to reproduce the characteristic shapes of erosion vs. impact angle for ranges of impact speeds.

$$E = K_1 ((V \cos(\beta_p))^m) \sin(n \beta_p) + K_2 (V \sin(\beta_p))^m \text{ for } \beta_p < \beta_0 \quad (5-1)$$

$$E = K_1 (V \cos(\beta_p))^m + K_2 (V \sin(\beta_p))^m \text{ for } \beta_p > \beta_0 \quad (5-2)$$

Note that K_1 , K_2 , β_0 and m are the only parameters which need to be adjusted to vary the mode of erosion. As discussed in subsequent paragraphs, the erosion model was adjusted to reflect ductile, as well as, brittle modes of erosion.

Particle Diameter Scaling

The effect of particle size on erosion is presented in Fig. 5-1 of [35] for Inconel 718 at 900 degrees F, a particle velocity of 1000 fps and an impact angle of 30 degrees. The erosion rates presented in the literature are strongly affected by particle size for particle diameters less than 40 microns. However, material erosion rates by alumina and silica particle impact are relatively insensitive to particle diameter for particle diameters greater than 40 microns. The large sensitivity of particle size on experimentally measured erosion rates for particle diameters less than 40 microns may be attributed to the aerodynamic deflection of the small particles around the test pieces. Deflections of particles in erosion experiments which are not accounted for will result in erosion rates which are lower than actual. The calibration of the ductile erosion model was based on erosion results from nickel-based and stainless steels produced by a mixture of fly-ash particles (4-38.4 micron) which is representative of the selected particle size range (5-100 micron). Therefore, for this study, the surface erosion rates (inches of erosion per lb of particles) in the erosion model are independent of particle size and a function of airfoil surface material, particle impact velocity, and particle impact angle only.

Ductile Material Scaling

The model was adjusted to reflect the erosive characteristics of ash on nickel-based superalloys, typical of high performance, cooled turbine airfoils. The constants used are based on previously published studies and ongoing coal-fired combustion and turbine research. The erosion results used to adjust the model for this program were drawn primarily from the works by Levy, Tabakoff and coworkers and Beacher and Mansour because of their direct application to the utilization of coal combustion in energy producing systems.

The review of the previous work indicated that complete sets of erosion data are not available for the materials which are likely to be used for vanes and blades of a coal-fired turbine. However, some data is available for nickel-based and stainless steel alloys with high particle velocities at metal temperatures close to 1400 degrees F. Consequently, Inconel 718 was selected for the blade and vane material, representative of the high-nickel-content super alloys used for airfoils in gas turbines. The modest amount of data available for Inconel 718 and other high-nickel super alloys was utilized to estimate the coefficients necessary for the Menguturk erosion model.

Temperature. The Hutchings model (presented in [65]) was used to calibrate the erosion model for the baseload airfoil operating temperature based on erosion results obtained at lower temperatures. The Hutchings model, based on the yield strengths of the airfoil material at the ambient and operating temperatures, was used to extend existing erosion data obtained at temperatures below the specified airfoil temperature.

Velocity. Erosion has been shown to increase with impact velocity to an exponent, m . The value of the exponent has generated considerable discussion. The general consensus, through physical arguments and experiments, is that the exponent is between 2 and 3 for ductile materials. These values of the exponent consider the kinetic energy of the particle and the energy transfer between the particle and the substrate. Additionally, other mechanisms are probably involved such as partitioning of the transferred energy. Velocity exponents between 2.2 and 2.4 are quite typical [42] and, based on current in-house experience, the velocity exponent of 2.25 was chosen for the ductile erosion model.

Angle. The parameters for K_1 , K_2 and B_0 were chosen to produce an erosion distribution with a peak at impact angles of approximately 30 degrees from the surface tangential plane. The values for these parameters are listed below.

$$\begin{aligned}K_1 &= 2.1 \text{ E-9} \\K_2 &= 1.8 \text{ E-10} \\\beta_0 &= 45 \text{ degrees} \\m &= 2.25\end{aligned}$$

Predictions of erosion for a range of impact velocities and a range of impact angles using this model are shown in Figure 5-2. The shapes of the curves are typical of those for a ductile metal. The erosion predictions shown are for a generalized nickel-based turbine airfoil material operated at 1400 degrees F based on erosion results obtained with fly-ash. Although the model was calibrated with high temperature, high velocity erosion results with fly-ash, the prediction is in good agreement (within 50 percent) with low velocity erosion results by Levy for much larger particles [40].

Brittle Material Scaling

An erosion model has been formulated to reflect the erosive characteristics of a brittle airfoil coating. Although the model was developed from erosion data for plasma sprayed zirconia, this class of model is applicable to the following materials:

- NiCrAlY and NiCoCrAlY alloys at low temperatures
- Titanium nitrides and Titanium diborides
- Ceramic coatings

Following are short discussions of their applications.

Some practical coatings which have been used for oxidation resistance on turbine airfoils are NiCrAlY and NiCoCrAlY alloys. However, these oxidation resistant coatings, as well as others, which exhibit brittle characteristics at room temperature are typically ductile at turbine airfoil operating temperatures.

“Hard-face”, erosion resistant coatings, such as titanium nitrides and titanium diborides, are useful in low pressure compressors for controlling erosion but are not likely to be used in the hot, turbine environment because of low oxidation resistance and low thermal fatigue life. However, in particle laden turbine inlet flows, it may be effective to accept these problems for improved erosion resistance.

Ceramic coatings are occasionally used to provide a thermal protective coating on turbine airfoils and combustor liners. These thermal barrier coatings are brittle at turbine operating temperatures, offer superior oxidation resistance but suffer from the same thermal fatigue, life-limiting problems associated with the titanium coatings. They offer the possibility of increased cycle performance with increased turbine inlet temperatures. However, a significant deficiency of the thermal coatings is their low erosion resistance which can result in erosion rates two orders of magnitude greater than nickel-based superalloys for the same particulate loading.

The erosion model for plasma sprayed zirconia (material used for thermal barrier coatings) was developed from results presented by Eaton and Novak [22]. The data presented was relatively independent of material temperature in the range of room temperature to 1600 F, therefore, no temperature adjustments were necessary. The constants in the generalized erosion model were adjusted for an erosion distribution for this brittle material. The data in the reference noted [22] was decreased to one-fifth of the reported values to reflect the author's expected improvements in erosion resistance when the material is used as a thermal barrier coating. Differences in erosion resistance were expected based on the differences in the coating application techniques on an airfoil compared to the application technique used in the study.

The parameters for K_1 , K_2 and B_0 were chosen to produce an erosion distribution with a peak at impact angles of approximately 90 degrees from the surface tangential plane. The values for these parameters are listed below.

$$\begin{aligned} K_1 &= 5.8 \text{ E-}8 \\ K_2 &= 3.3 \text{ E-}8 \\ B_0 &= 90 \text{ degrees} \\ m &= 2.5 \end{aligned}$$

The predicted erosion output from the brittle erosion model vs. impact angle for several impact velocities is shown in Figure 5-3. The adjusted data (data/5) for 1600 F from the reference is also shown.

Normalization of Erosion Results

The predicted erosion rates (volume removed/mass of impacting particles) were normalized with annular impact exposure based on airfoil height, number of airfoils and airfoil surface arc length. Assuming a uniformly distributed particle loading at the turbine inlet, the normalized surface erosion predictions consist of surface recession rates which are dependent on particulate loading level at the turbine inlet. The equations used to normalize the erosion rate (surface recession/mass of particles in the turbine inlet) are shown below.

$$e_i = \frac{\Sigma E_i / NPS \cdot A_u \cdot IE}{A_u \cdot S_i \cdot (\text{unit height})}$$

which reduces to

$$e_i = \frac{\Sigma E_i \cdot (\%First) \cdot (\%Second)}{NPS \cdot h \cdot N \cdot S_i} \quad \text{for 2-D flowfields}$$

$$e_i = \frac{(\Sigma E_i)}{NP \cdot A_i} \quad \text{for 3-D flowfields}$$

The formulations shown above were used to calculate the airfoil surface recession rate based on the particle loading at the turbine inlet. These results may be used with the particle loading factor (i.e. $lb_{m,particles}/lb_{m,turbine,inlet}$) and the total turbine inlet flowrate to estimate the recession rate per unit time. In this manner turbine airfoil life can be estimated for the configurations analyzed in this program.

The results presented in this report can be used for turbines of other scale as discussed in Section 9.

Additional Experimental Data Requirements

Although suitable erosion models were formulated from the literature, the applicability of the models to the wide variety of coatings used for gas turbine airfoils is questionable and an expanded data base for coating and material combinations is required for accurate erosion estimates. However, the ductile erosion model developed for this program is useful for comparing the erosive characteristics of the turbines designed to reduce erosion. The review of the literature has been enlightening, in that, there are few parametric erosion studies available for the turbine designer. The studies which vary more than one parameter are limited in scope and it is generally difficult to compare results from different facilities. Thus, there is a need for a comprehensive experimental study of erosion from turbine airfoil materials with particulates from coal combustion at the temperatures and velocities anticipated for coal-fueled turbines.

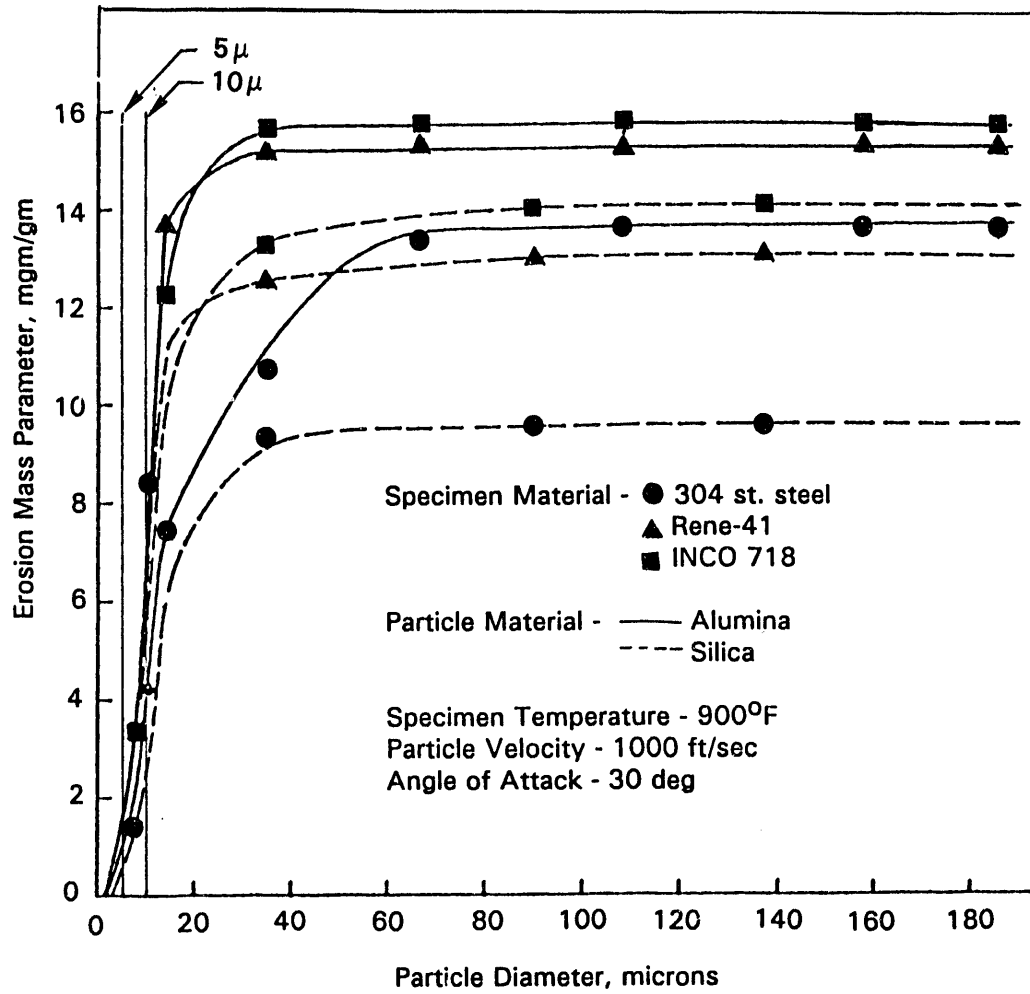


Figure 5-1 Erosion Rate as a Function of Particle Size (Figure 6 from Kotwal & Tabakoff [35])

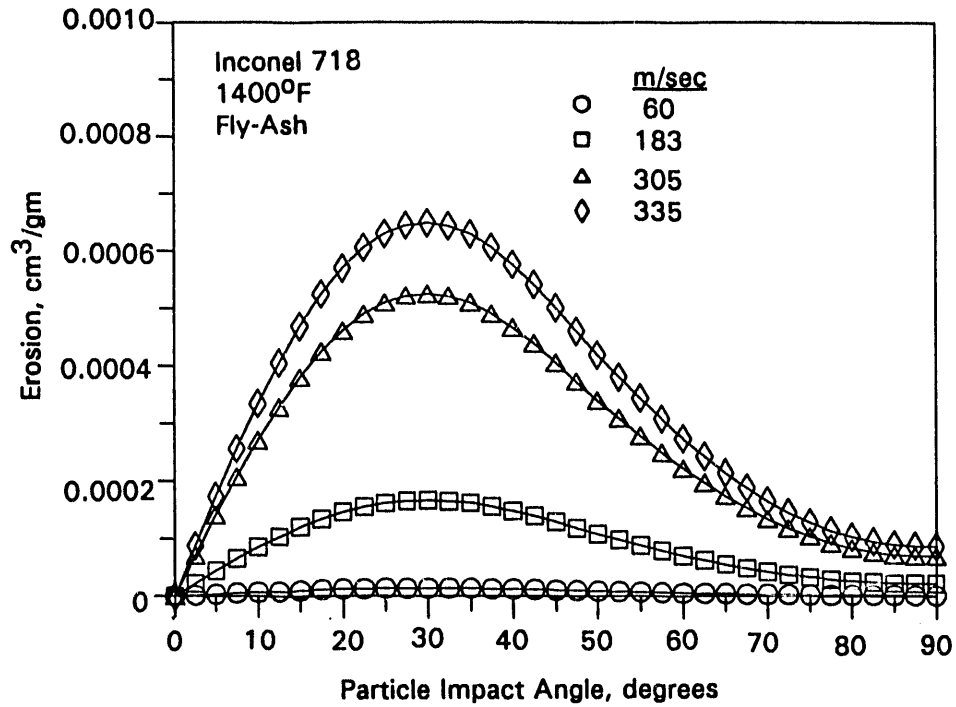


Figure 5-2 Erosion Model for Nickel-Based Super Alloy Airfoils

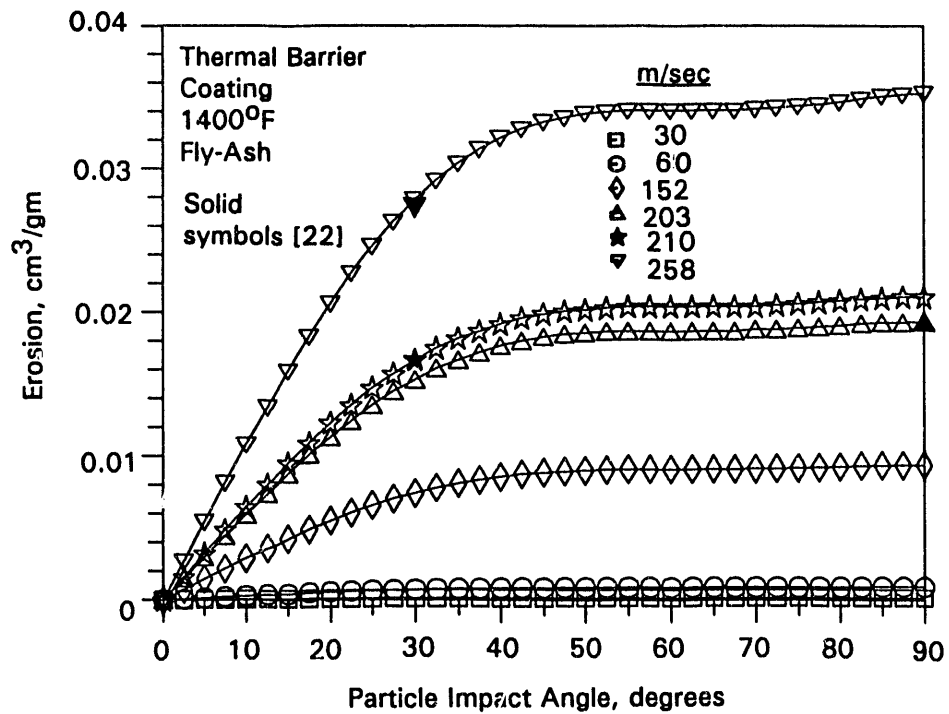


Figure 5-3 Erosion Model for Airfoils with Thermal Barrier Coatings
Note: See test for discussion on adjustments of data [22]

SECTION 6

PARTICLE TRAJECTORY AND EROSION CHARACTERISTICS FOR BASELINE TURBINE DESIGN

Discussion regarding the selection of particle sizes and densities, presented in this section, is also applicable to the next two sections. Results from the parametric study for the baseline first stage meanline will also show cause effect relationships applicable to the other meanline turbine designs and the 3-D baseline turbine stage design.

Particle Definition Parameters

The effects of the airfoil design on erosion were determined from aerodynamic, particle trajectory and surface interaction analyses. Particle diameters and densities were selected based on current and ongoing DOE funded programs. The particle parameters chosen are applicable to direct-fired systems of slagging combustor type and also for pressurized fluidized-bed combustors (PFBC). Turbine inlet conditions (described in another section) combined with the selected particle parameters assures applicability to next generation PFBC systems. Coal burning gas turbines with direct-fired combustion systems will experience increased levels of erosion in the hot section due to particulates. The particulates from the combustion process primarily comes from the coal ash and unburned carbon. Combustion systems designed for coal-burning systems are currently projecting carbon burnout in excess of 99 percent. Therefore, the erosion analysis of the present program is focused on erosion due to ash.

Of particular interest is the allowable projected particle loading for acceptable turbine life. The results of this study are presented in such a manner to facilitate the calculation of the allowable particle loading for a specified particle diameter and airfoil material removal or the anticipated airfoil life for a given particulate loading at the turbine inlet. Estimates of the airfoil life and allowable particulate loading at the turbine inlet will be presented in the section discussing the analysis of the results.

The range of particle diameters for analysis has been established from review of the open literature and the characteristics of particles leaving slagging combustors being operated under DOE contracts. Particles with diameters less than 5 micron pose little threat to turbine durability [26, 43] except for damage to corrosion protection coatings. However, particles leaving the combustor before any hot gas clean up can be as large as 100 micron [65]. It is anticipated that changing the aerodynamics of a turbine stage will have little effect on the erosion caused by such particles. Although the erosion from small particles (i.e. those less than 5 micron) is likely to affect coatings, the principal erosion effects are expected to occur from particles with diameters greater than 5 microns. This expectation is based on results from previous studies and will be shown by trends in the present study. Therefore, particle diameters of 5, 10, 25, 50 and 100 microns for the baseline particle density have been chosen for the turbine erosion analysis.

Particle densities were chosen based on the composition of ash. Coal ash is primarily composed of silicon dioxide (i.e., typically around 50 percent) which has a density of

approximately 2.6 gm/cc. The densities of particles analyzed for the present program were chosen to reflect the different forms of ash particles based on gas path history (i.e. solid and/or porous particles). Three particle densities of 1.25, 2.5 and 5 gm/cc were used in the analysis to simulate the possible range of fly-ash density for a wide range of turbine scales with the 2.5 gm/cc defined as the baseline density [46]. The 1.25 and 2.5 gm/cc densities are typical of those for friable and glassy ash particles, respectively. The largest density was included in this analysis to extend the applicability of the results to turbines of smaller scale as described in Section 9.

In these parametric studies, the primary parameters which were varied were the Stokes number, St , and the particle density Reynolds number, σ . Five values of Stokes number were used for each of the three values of particle density Reynolds number. The three values of σ represent the three levels of particle densities chosen for analysis. However, due to the nature of the definition of Stokes number (i.e. $St \propto \rho_p D^2$), fixed values of St represent various particle diameters depending on the particle density. Consequently as σ was varied for each value of St , the representative particle diameter varied by the square root of the particle density from the diameters represented by the baseline density. Results for the baseline first stage airfoils will be discussed in terms of both the dimensional (particle diameter, D_p and density, ρ_p) and the dimensionless (Stokes, St , and particle density Reynolds number, σ) variables. The combinations of dimensionless variables, for which particle trajectories and erosion calculations were made, and their associated dimensional quantities, for the three particle densities cited, are presented in Table 6-1.

Particle Trajectories

Particle trajectories were calculated for the conditions shown in Table 6-1. Trajectories through the vane and blade cascades for two particle diameters are shown in Figs. 6-1 and 6-2, respectively. Note that for the vane, the 5 micron particles follow the flow reasonably well and that only 1 of the 10 particles shown hit the vane. However, 8 of the 10 particle trajectories for the 100 micron particles and the same starting locations hit the vanes and one hit both vanes.

The trajectories for the 5 micron particles passing through the blade (Fig. 6-2 in a rotating coordinate system) are similar to those through the vane with 1 of 10 particles hitting the blade. The trajectories of the 100 micron particles through the blade are complex due to several factors. First, note that the 100 micron particles do not enter the blade cascade at the same angle as the 5 micron particles. This change of flow direction in the rotating coordinate system is caused by the 100 micron particles not being accelerated to gas path speed as they pass through the vane. Six of the ten particles hit both blades due to rebounds (13 hits for the 10 particles). Particle trajectory calculations are required for each airfoil stage and operating condition to obtain local erosion characteristics because of the complex rebounds and multiple-hit possibilities for each particle diameter and density. However, several generalized relationships will evolve as the results for these airfoils are discussed.

The percentage of particles hitting the baseline vane and blade are shown in Figs. 6-3 and 6-4 for all the particle diameter and density conditions identified in Table 6-1. The effects of particle diameter and density ratio on percent of particles hitting the blades and

vanes is shown in Fig. 6-3. For the 10 micron particles, the estimated number of particles hitting the vane varies from about 10 to 30 percent (a factor of 3) for particle densities from 1.25 to 5.0 gm/cc. When the same results are presented in Fig. 6-4 as effects of the Stokes number and the particle density Reynolds number, the results show less spread. For a Stokes number of 0.272 ($D_p = 10$ micron, $\rho_p = 2.5$ gm/cc), the variation with particle density Reynolds number is 15 to 20 percent, a ratio of 1.3. Use of the dimensionless parameters shows that the Stokes number is the dominant parameter. As will be shown in a later section, the present results are also applicable to larger and smaller turbines with the same geometry and pressure ratio if the proper scaling parameter is used. Although the dimensionless parameters collapse the results better than the dimensional parameters, the cause/effect relationships will be discussed and presented for the dimensional parameters for convenience.

Particle Impact Characteristics

Particle impact speed and impact angle strongly affect the airfoil surface erosion rate. In general, erosion rate is expected to increase with increasing impact speed. Additionally, erosion is a maximum for impact angles near 30 degrees for ductile materials and is a maximum near 90 degrees for brittle materials (see Erosion Models). The particle impact speed distributions on the baseline vane are shown in Fig. 6-5a. Note that the larger particles (25 and 100 μ) have impact speeds at the vane stagnation point which are near their initial value upstream of the vane. The impact velocity for the small particles (5 μ) are decreased to about one-fourth the inlet flow speed in the stagnation region. The impact speeds of the small particles is greater than the larger particles in the downstream section of the vane $s/Bx > 0.8$. These particle impact speed characteristics are compatible with prestudy expectations.

The particle impact speed distributions for the blade are more complex. The distributions in Figs. 6-5b & c are shown for blade inlet conditions where the particles have previously hit the vane surface ("Hit") and where the particles have passed through the vane passage without hitting a surface ("No-Hit"). The largest differences occur on the suction surfaces for the larger particles where the blade runs into the particles (e.g., Fig. 6-2).

The particle impact angle characteristics are shown in Fig. 6-6. The impact angle for the small particles is very low, except near the stagnation point, as expected. The particle impact angles of the largest particles (100 μ) on the vane (Fig. 6-6a) are near 30 degrees, where the peak erosion rates occur for ductile materials. For the blade, the medium size particles (~25 μ) impact at 20 to 30 degrees on the trailing region of the pressure side. Modest differences occur between the impact characteristics of the Hit and No Hit particles on the blade. The conclusion from this discussion of impact angle and re-examination of the particle trajectories on the blade is that the erosion distributions are influenced by complex relationships between the airfoil shapes, the airfoil operating conditions and the particle diameter and densities.

Erosion Characteristics

Ductile Material

The erosion distribution of the particles on ductile materials is shown in Fig. 6-7. The erosion distributions for the vane are greatest near the trailing edge, as expected. However,

the peak local erosion rates are less sensitive to particle size than expected for the results shown because of the counteracting effects of impact velocity and impact angle, i.e. the particles which impact at greater speed impact at shallower angles. However, the peak erosion on the vane increases with either increases in the particle size or particle density.

The erosion from the blade is more complex than that from the vane due to the large numbers of possible particle paths and multiple hits. Due to the aerodynamics of the particles leaving the vane which enter the blade airfoil row, the maximum erosion for the blade airfoil is caused by medium sized, 25 micron, particles and is not caused by the largest, 100 micron, particles. For the largest particles, the initial particle trajectories are aligned with the airfoil chordline which results in a substantially lower number of impacts on the blade airfoil surface and, therefore, lower peak erosion. Consequently, the peak erosion on the suction side of the blade occurs for the 100 μ particles due to the large number of impacts which occur due to their low speed, relative to the gas path, as the particles exit the vanes (Fig. 6-2, $St_b = 36.2$). Note that for the 100 μ particles, the peak erosion rate on the suction surface is approximately the same as the peak erosion rate on the pressure surface. In addition, the peak value of erosion on the pressure side of the blade airfoil is about a factor of 6 greater than the peak erosion predicted for the vane airfoil. The larger values of erosion on the blade airfoils are due to larger flow velocities in the airfoil blade row and to the larger amount of turning of the flow resulting in an increase in the number of impacts. In general, greater predicted erosion rates can be expected in airfoil rows with higher turning.

Brittle Material

The effects of surface material on the erosion rate is shown in Fig. 6-8. These erosion results are for the meanline baseline turbine with airfoils that have thermal barrier coatings (TBC). In general, airfoil erosion was 2 orders of magnitude greater than the erosion of the baseline airfoils with the nickel-based, super-alloy erosion model (shown as the closed symbols for $D_p = 25$ micron and $\rho_p = 2.5\text{gr/cc}$). The vane and blade airfoils with brittle coatings experienced a relative increase in erosion in the leading edge area of the airfoil because of impact angles which are closer to 90 degrees.

Although the general consensus has been that particles 5 microns or less will not cause significant erosion, the results for the erosion model used shows that the erosion rates for 5 micron particles on the TBC surface is greater than the erosion rate of 25 micron particles on a ductile surface. The conclusions are that thermal barrier coatings are very vulnerable to damage from any particles passing through the filtering system due to leaks or filter breakage and that the particle removal systems must be able to rapidly transfer the combustion products through an alternate system in the event of filter failure.

In summary, erosion is shown to be strongly dependent on particle diameter with a lesser dependence on particle density. Erosion on the baseline vane airfoil is shown to increase with increases in either the diameter or density of the particles. Erosion on the baseline blade airfoils is not as well correlated with particle diameter. Blade erosion is found to be more strongly dependent on the aerodynamic consequences of the particle behavior through the upstream vane passage. Consequently, maximum erosion on the blade is caused by the midsized particles.

Table 6-1
Dimensionless and Dimensional Particle
Variables for Baseline Vane and Blade

D_p microns	ρ_p gm/cc	<u>Vane</u>		<u>Blade</u>	
		St_v	α_v	St_b	α_b
7.1	1.25	0.068	2588	0.092	2641
5.0	2.50	↓	1294	↓	1320
3.5	5.00	↓	647	↓	660
14.0	1.25	0.272	2588	0.367	2641
10.0	2.50	↓	1294	↓	1320
7.1	5.00	↓	647	↓	660
35.4	1.25	1.70	2588	2.29	2641
25.0	2.50	↓	1294	↓	1320
17.7	5.00	↓	647	↓	660
71.0	1.25	6.8	2588	9.17	2641
500.0	2.50	↓	1294	↓	1320
35.0	5.00	↓	647	↓	660
141.0	1.25	27.2	2588	36.7	2641
100.0	2.50	↓	1294	↓	1320
71.0	5.00	↓	647	↓	660

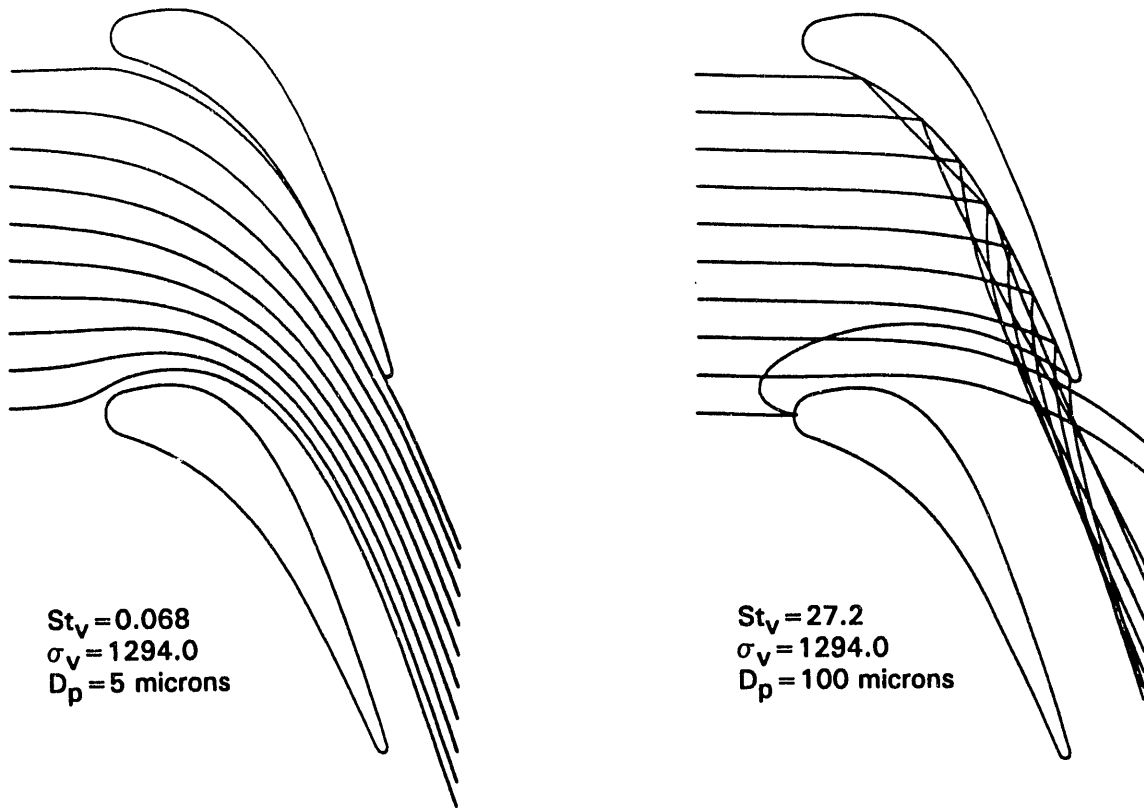


Figure 6-1 2-D Particle Trajectories Through Baseline Meanline Vane Airfoil Row

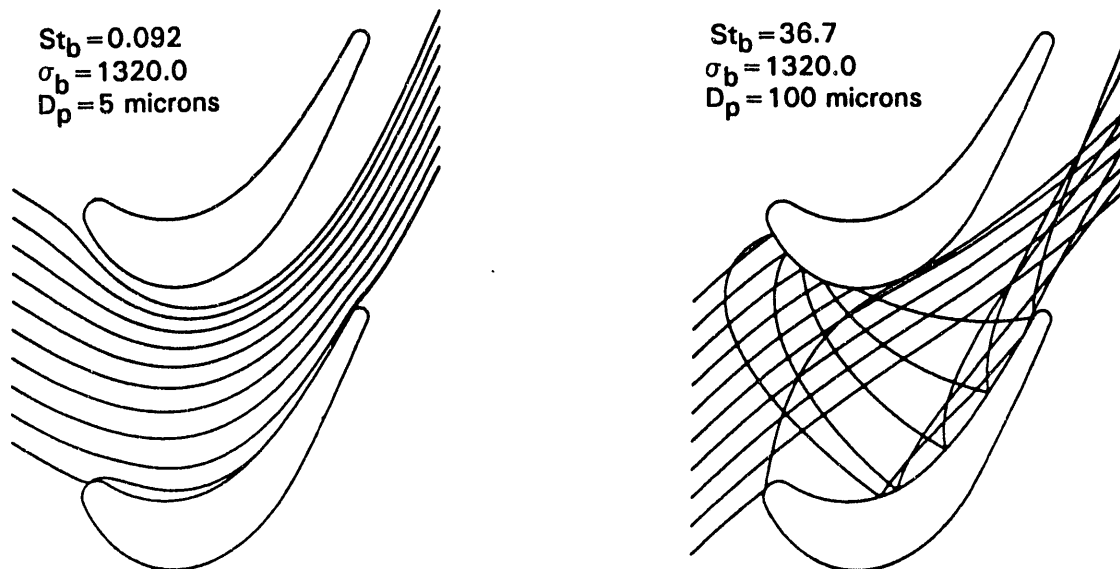


Figure 6-2 2-D Particle Trajectories Through Baseline Meanline Blade Airfoil Row

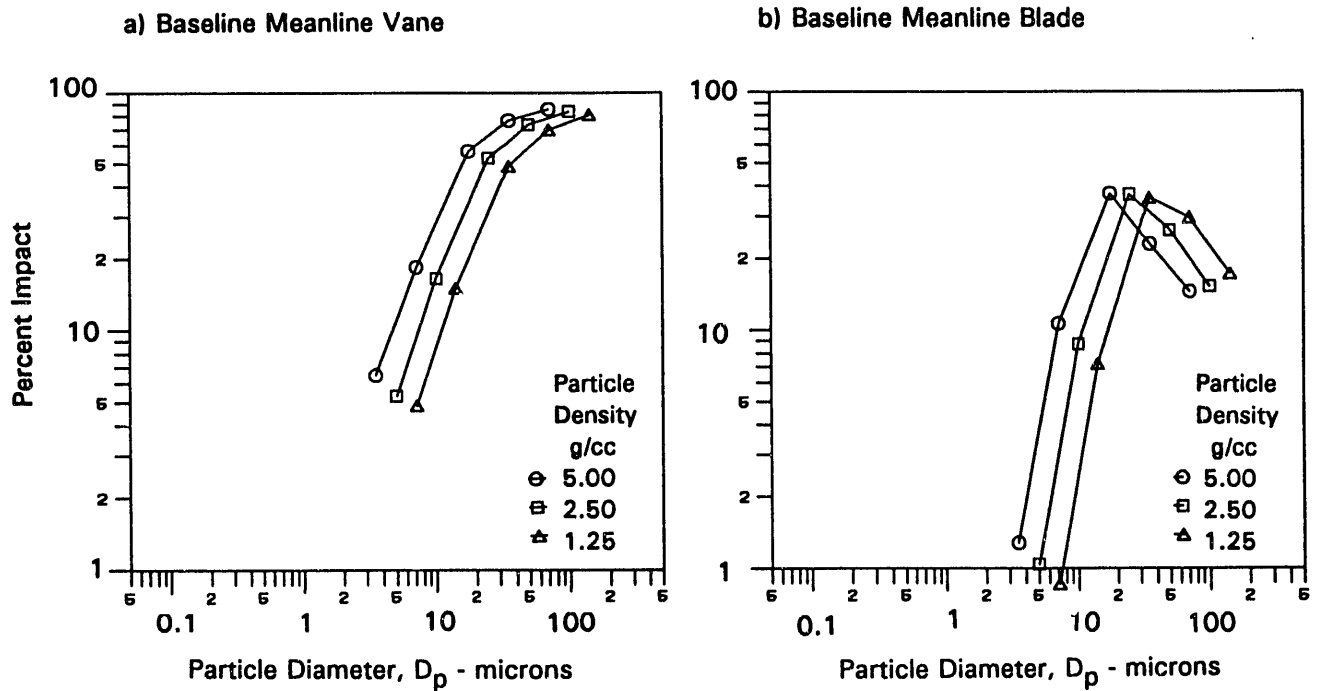


Figure 6-3 Effect of Particle Diameter and Density on Percent of Particles Hitting Vane and Blade

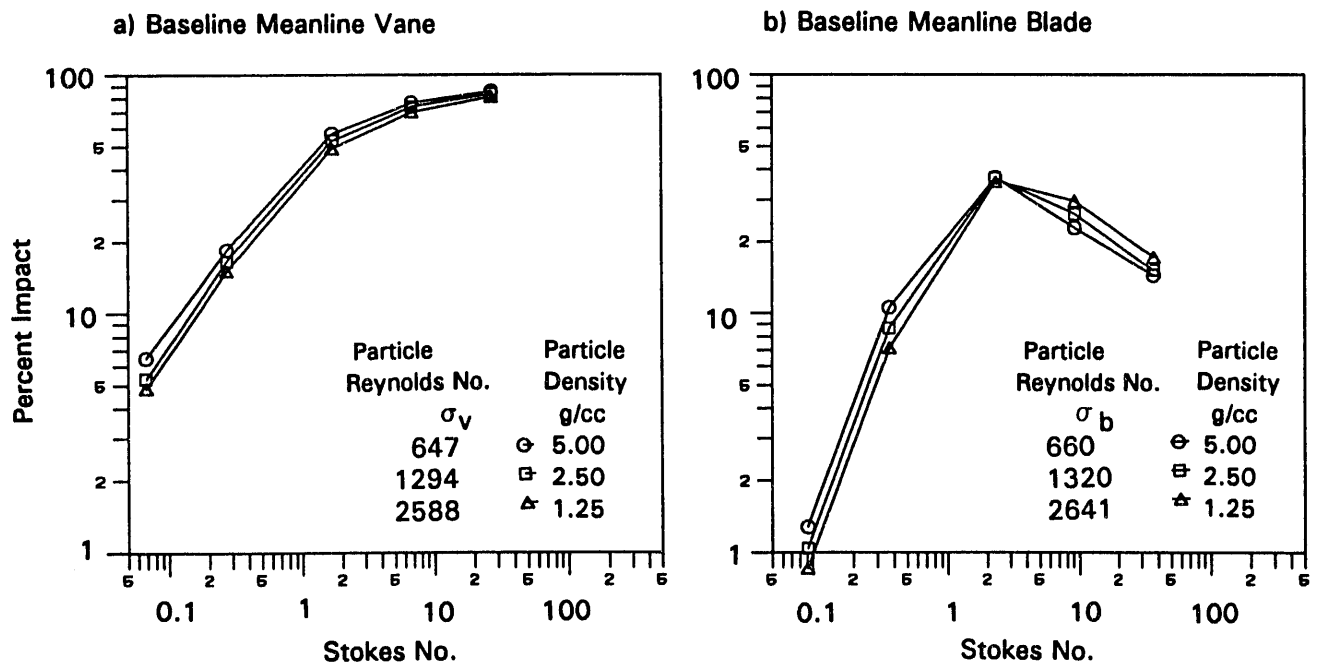


Figure 6-4 Effect of Stokes Number and Particle Reynolds Number on Percent of Particles Hitting Vane and Blade

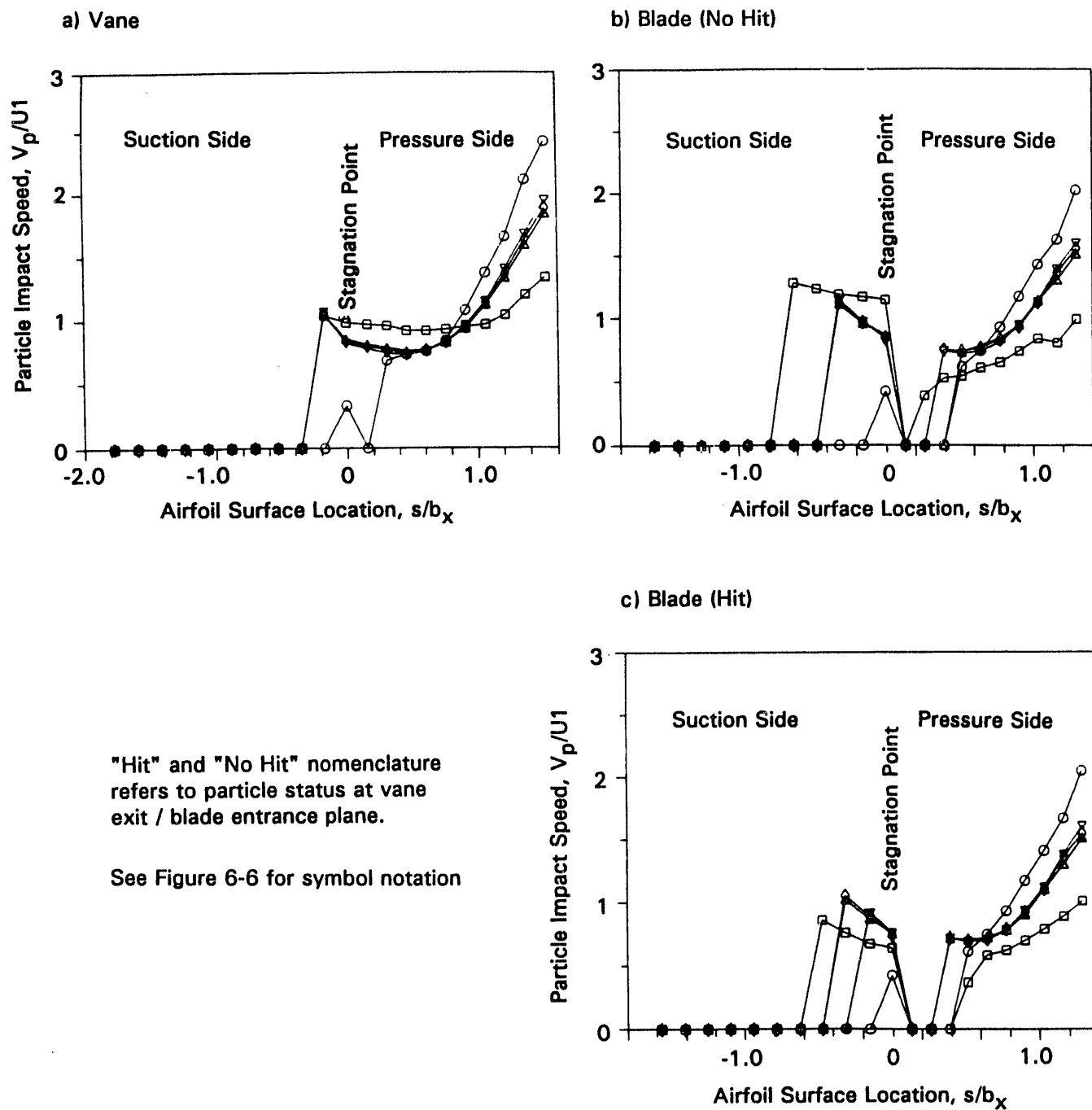


Figure 6-5 Effects of Particle Size and Density on Particle Impact Speed for Baseline Meanline Airfoils

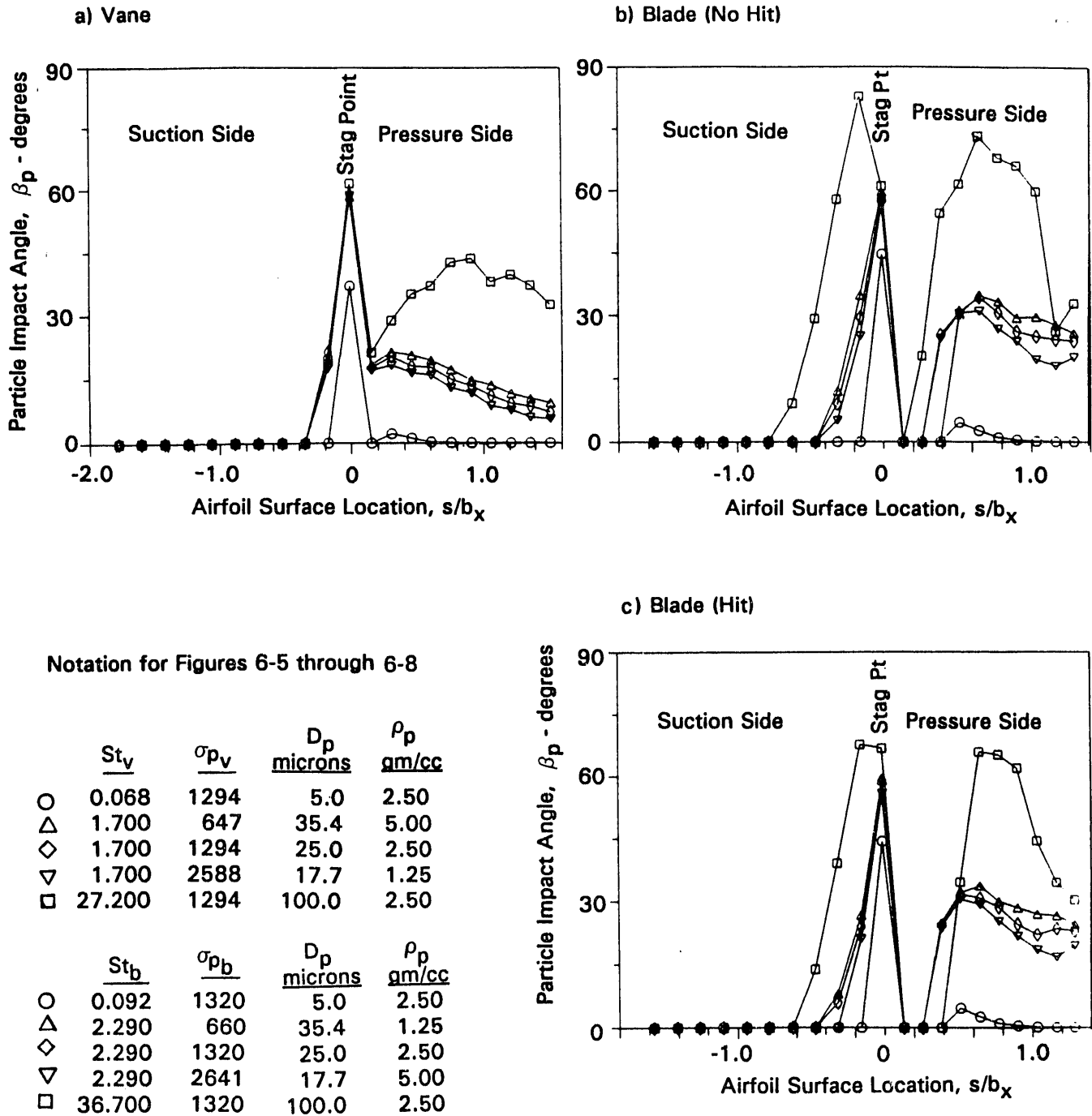


Figure 6-6 Effect of Particle Size and Density on Particle Impact Angle for Baseline Meanline Airfoils

See Figure 6-6 for symbol notation

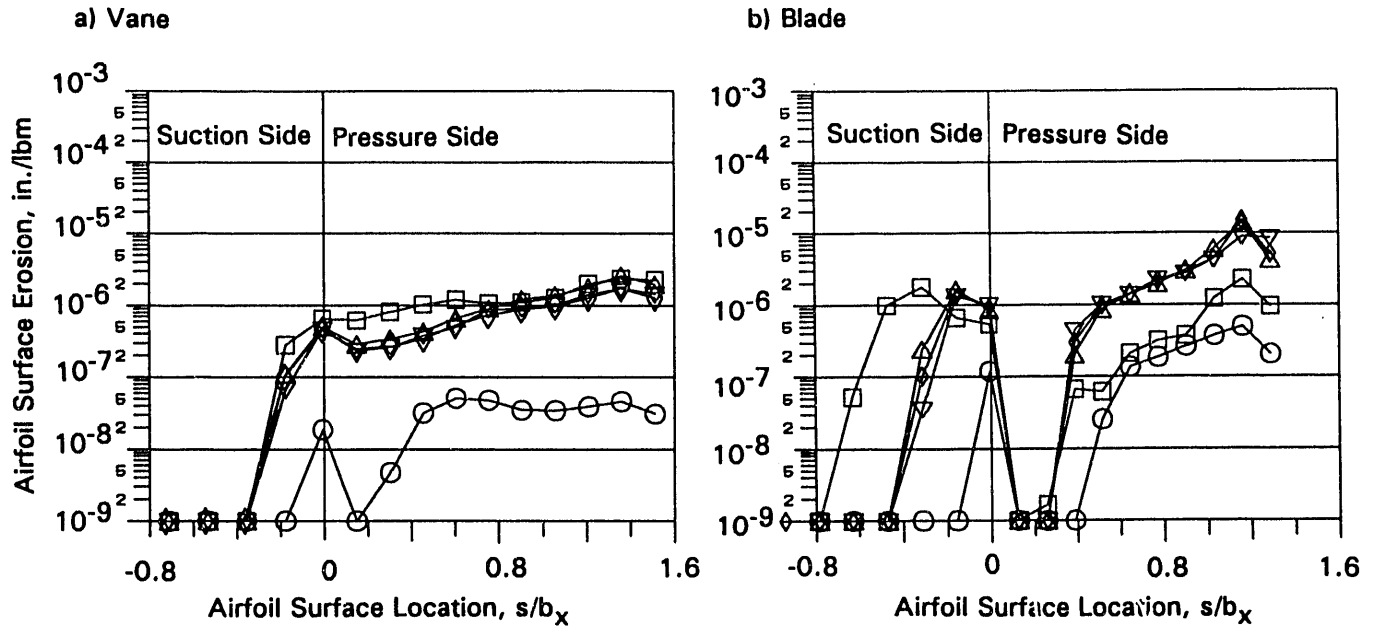


Figure 6-7 Effect of Particle Size and Density on Erosion Rate for Baseline Meanline Airfoils of Ductile Material

See Figure 6-6 for symbol notation

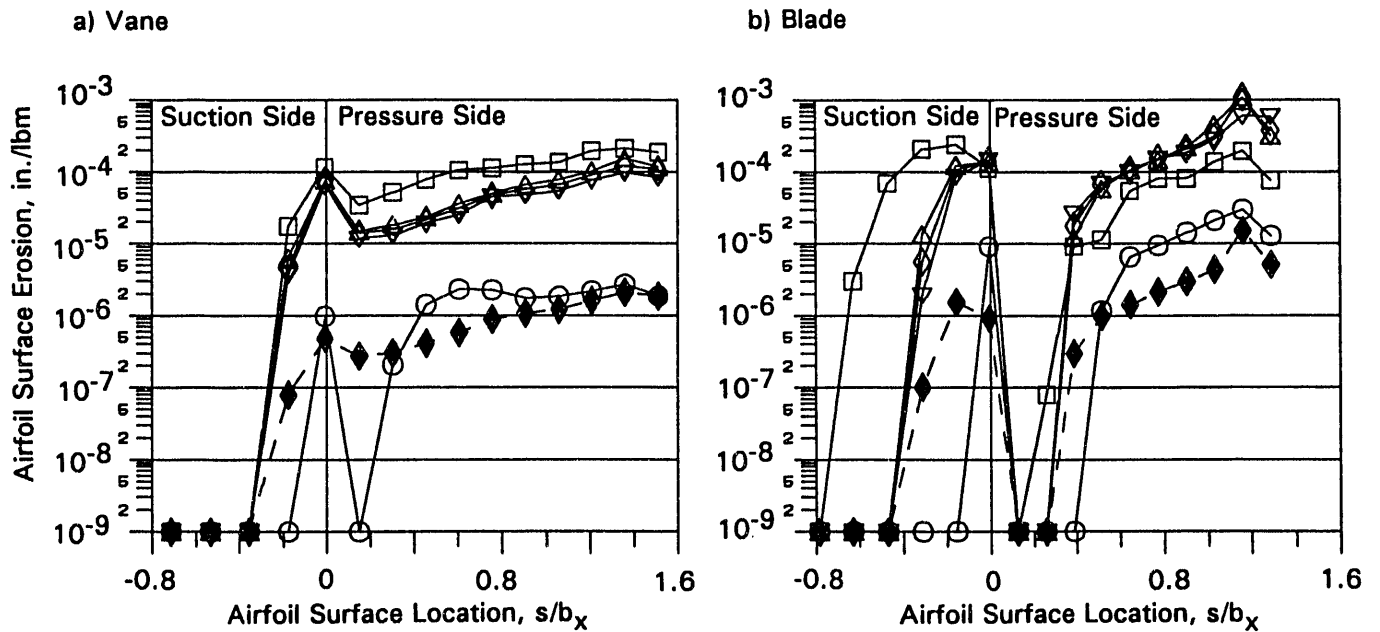


Figure 6-8 Effect of Surface Material on Erosion Rate for Baseline Meanline Airfoils.
 Open Symbols – Brittle Material (Thermal Barrier Coating);
 Shaded Symbols – Ductile Material

SECTION 7

EFFECTS OF TURBINE DESIGN ON EROSION CHARACTERISTICS

A parametric study was conducted to determine the effects of stage characteristics and blade design on the erosion characteristics. The Stokes number and the particle density Reynolds number were held at selected values for each change from the turbine meanline design. In this section the effects of turbine design on particle impact characteristics and airfoil surface erosion are discussed.

Particle Impact Speed and Angle

The particle impact speed and angle are important factors in the erosion process. For ductile materials, the erosion rate increases as the 2.25 power of the impact velocity and peaks at impact angles of 30 deg. Decreasing the impact speed and avoiding impact angles near 30 degrees will decrease the erosion rate.

The particle impact speeds on the vanes of the Four-Stage, Increased Radius and Increased Pitch designs did not vary appreciably from the values for the baseline design (Fig. 7-1a). However, the particle impact speeds on most of the pressure surface of the MOD-1 vane were 5 to 10 percent greater. The impact speeds were only noticeably smaller on the forward portion of the pressure surface. The particle impact angles (Fig. 7-1c) on the vanes of the Increased-Radius design are decreased slightly compared to the baseline and other designs on the pressure side. Impact angles on the MOD-1 vane airfoil are increased near the leading edge and decreased slightly further aft on the pressure surface. From these results, the erosion rates of the vanes except the MOD-1 vane are expected to be similar.

The impact velocity and angle are a stronger function of turbine design for the blade airfoils (Figs. 7-1b & d). Although the particle impact speeds for the Increased Radius and Four-Stage turbines are 10 to 15 percent greater than those for the baseline turbine the impact angles are decreased somewhat from the 20 to 35 degree values for the baseline blade airfoil. The MOD-1 impact speeds are greater than those for the baseline. As a result of the relatively larger variations in impact angles and impact speeds on and the blade airfoil, a larger variation in the erosion rates can be expected.

Erosion Rates

The erosion rates for these turbines are presented in several formats to show effects of particle size and density as well as turbine design. The results are presented in Figs. 7-2 through 7-7. The streamwise distribution of erosion rate on all vane and blades is shown in Fig. 7-2 for a 25 micron diameter particle with a density of 2.5 gm/cc. The effect of particle size (for 3 particle sizes and one particle density) and the effect of particle density (for 3 densities and one particle diameter) on the erosion distribution of the airfoils is shown in Figs. 7-3 and 7-6. The effects of particle size and density (for 15 combinations of 5 particle sizes and 3 particle densities) on the average airfoil erosion rate and the peak airfoil erosion rates are presented in Figs. 7-4, 7-5 and 7-7. The solid symbols in Figs. 7-3 through 7-7 represent the erosion results from the baseline turbine for comparison. The erosion characteristics for each turbine design are discussed in the following section.

Effect of Number of Stages

The effect of increasing the number of stages on vane and blade airfoil erosion distributions are shown in Figs. 7-2, -3a and -3b.. The predicted erosion on the vane airfoil was about 90 percent of that predicted for the baseline vane when the number of stages was increased from 3 to 4. Although there was a 10 percent decrease in vane exit velocity (the inlet velocity remained the same), this advantage was offset by a slight increase in required turning of about 1 degree. However, predicted erosion on the blade was reduced by a factor of 4 (Fig. 7-4b). This large reduction in the peak erosion on the blade is due to a 15 percent decrease in flow velocities combined with a 16 degree decrease in required turning. Note also that the peak erosion rate occurs for the 50 micron particle rather than the 25 micron particle as occurred for the baseline turbine.

Effect of Mean Radius

Increasing the mean radius of the turbine from 35.2 inches to 42.2 decreased the predicted erosion on the vane by approximately 30 percent (Figs. 7-2, 7-3c, -4c and -5c). This decrease is primarily associated with the decrease in the relative flow velocities in the vane airfoil row (17 percent reduction at the inlet and a 3 percent reduction at the exit). The benefit of reduced flow velocities was offset somewhat by an increase of about 3 degrees in the required turning to maintain the same stage reaction. Additional gains in erosion resistance are likely to be achieved if the stage reaction was adjusted for optimum erosion resistance. Although the decrease in vane erosion was modest for the increased-radius turbine, predicted erosion rates on the blade airfoil were reduced by a factor of 5 compared to the distribution of erosion for the baseline turbine blade (Figs. 7-2, 7-3d, -4d and -5d). This reduction is due to a decrease in inlet velocity of about 30 percent combined with a similar decrease in required turning noted above for the four-stage turbine. The peak erosion rate also occurred for the 50 micron particle rather than the 25 micron as occurred for the baseline turbine (Fig. 7-4d).

Effect of Airfoil Pitch

Erosion results for the meanline baseline turbine with a 10 percent increase in airfoil spacing (pitch) are shown in Figs. 7-2 through 7-5. In general, erosion on the vane airfoil decreased by almost 20 percent when the the airfoil pitch was increased. However, peak erosion near the trailing edge increased slightly for particle diameters of 100 micron. Most of the decrease in erosion occurred in the trailing edge area of the airfoil, even though there was some rearrangement of the erosion distributions depending on particle diameter. Peak erosion on the blade was reduced by about 50 percent when blade airfoil pitch was decreased 10 percent, however, the peak erosion occurred for particles of 50 to 75 microns rather than for particles of 25 microns for the baseline airfoil (Fig. 7-5f). The aerodynamics between airfoil rows for this turbine design were relatively unchanged from the baseline turbine. Therefore, the reductions in predicted erosion on these airfoils is entirely due to interblade flow speed reduction and to changes in the particle/airfoil interaction because the airfoils were further apart. Please note that the increased blade pitch also caused the turbine efficiency to decrease 0.5 percent (Table 3-2) compared to the baseline turbine design.

Effect of Airfoil Inlet Incidence

Erosion results for the modified baseline blade with a more conventional inlet incidence were calculated (Fig. 7-2). Airfoil peak erosion was relatively unaffected by airfoil inlet incidence. Small decreases in erosion were noted for the 25 micron particles near the leading edge region, however, the levels of erosion in this area are small and are of little consequence compared to erosion values calculated for the trailing edge region. Peak erosion values at the trailing edge are approximately 10 percent lower than the baseline blade results. This reduction is associated with a reduction in the particle impact angles which, in this case, results in reduced levels of predicted erosion.

Effect of Airfoil Shape

Erosion results for the meanline baseline turbine stage with the MOD-1 airfoils are shown in Figs. 7-2, 7-5 and 7-6. Significant increases in predicted erosion rates are noted for these airfoils especially in the trailing edge area. Peak erosion on the vane and blade airfoils (caused by the 25 micron particles) increased 60 percent and 45 percent, respectively, compared to the baseline vane and blade airfoils. However, more importantly, predicted erosion by the smallest (5 micron) particles increased by factors of 7 and 5, respectively, compared to the baseline airfoils. These results indicate that the effect of airfoil shape on erosion is strongly influenced by particle diameter. Therefore, an optimum turning vs. axial distance relationship is likely for efficient particle turning. However, due to the large difference in the predicted results for different particle diameters, an optimized airfoil shape will be "tuned" for specific particle diameter ranges.

Summary

Summary plots of erosion on the airfoil surfaces of the turbines simulated for this program were shown in Fig. 7-2 for the 25 micron particles with a density of 2.5 gm/cc. The plots show the major effects of turbine design for a specific particle. The streamwise distributions of erosion are similar in shape to those predicted by previous investigators [60]. The higher erosion levels predicted for the rotating blade compared to the stationary vane are also consistent with this earlier work. The results show that (1) erosion is strongly affected by airfoil shape and (2) substantial improvements in erosion resistance are possible with changes in turbine operating condition.

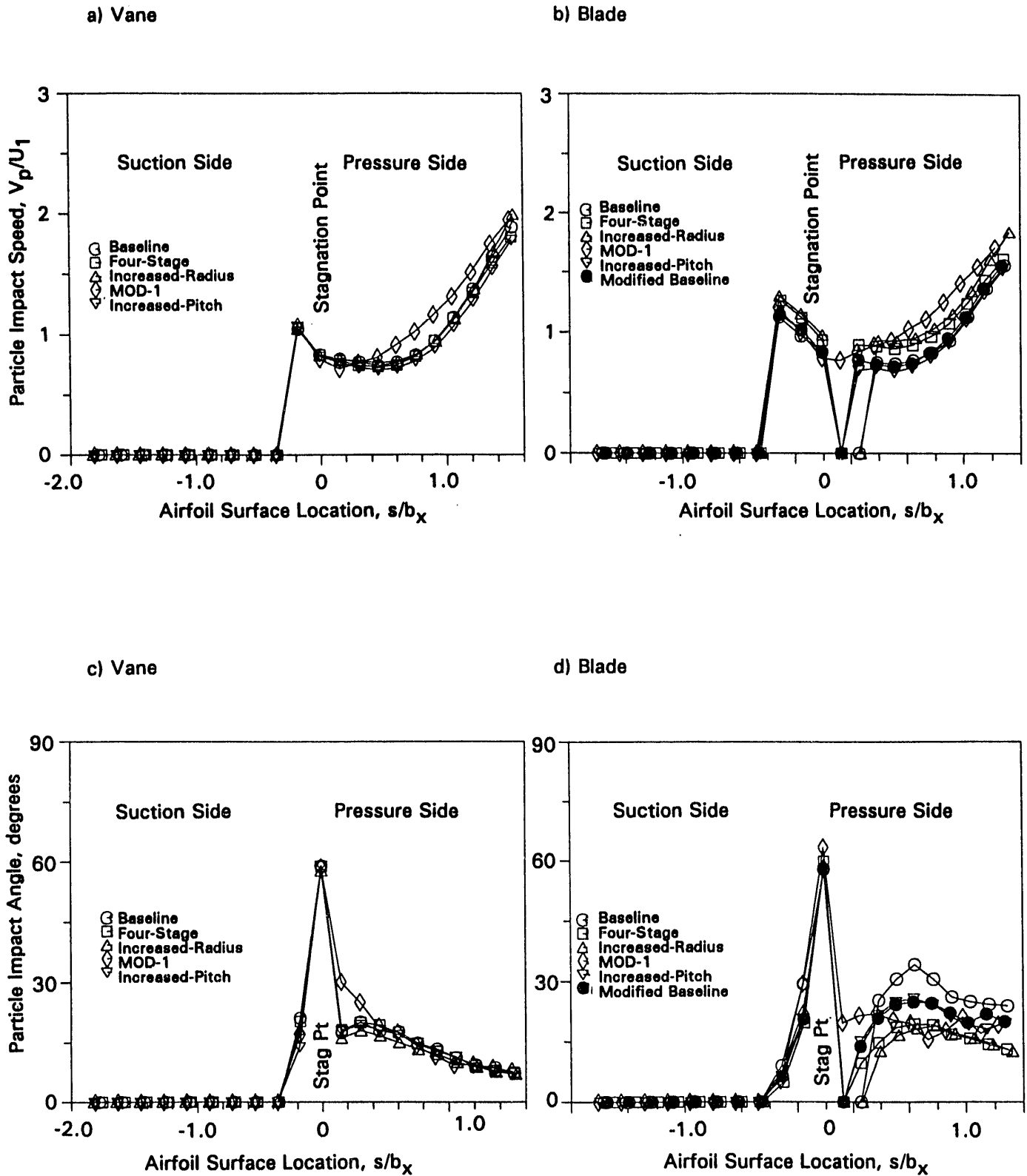


Figure 7-1 Comparison of Particle Impact Speeds and Angle Distributions on All Airfoils for 25 Micron, 2.5 gm/cc Particle

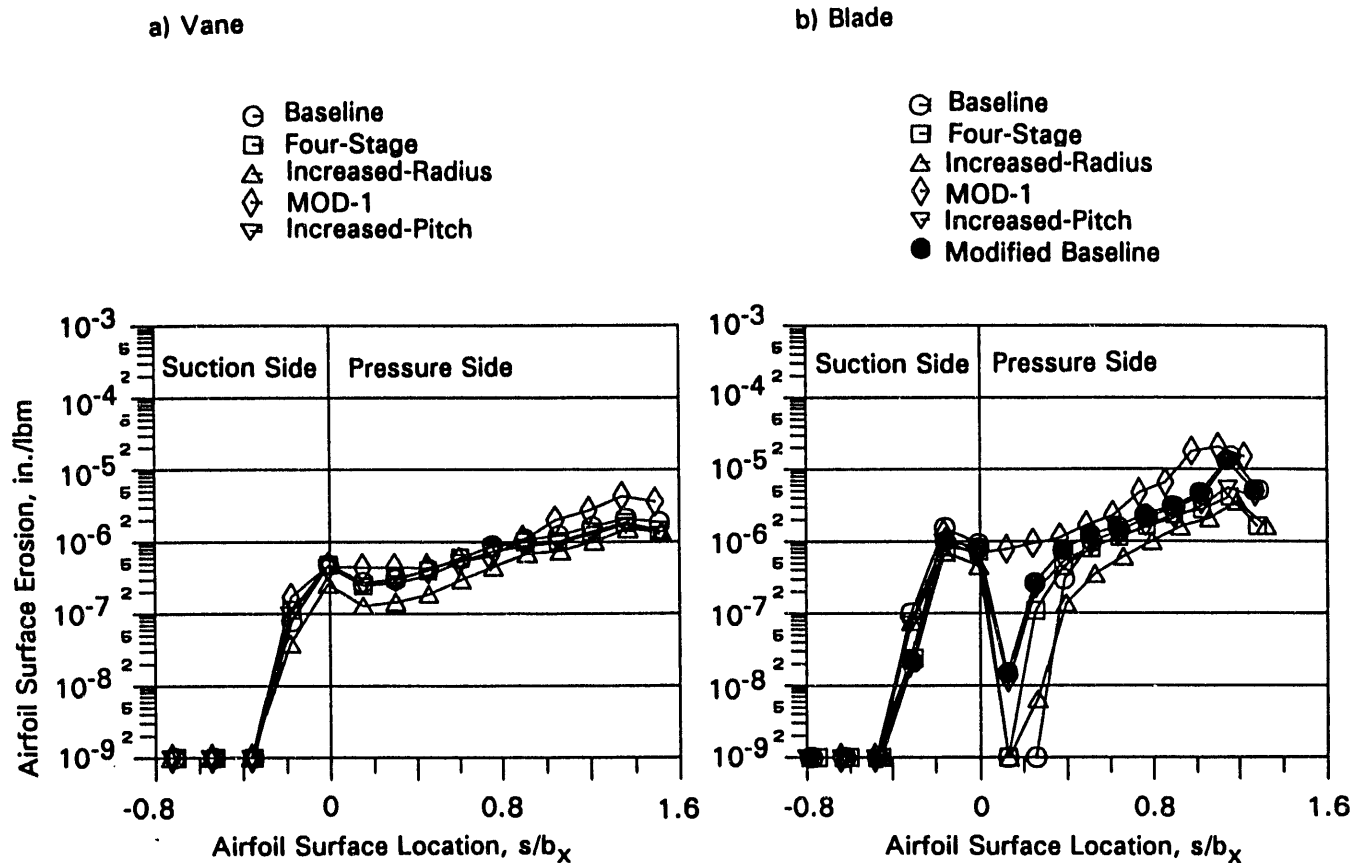


Figure 7-2 Comparison of Erosion Distributions on All Airfoils From 25 Micron 2.5 gm/cc Particles

Nomenclature for Figure 7-3

	D_p microns	ρ_p gm/cc	
○	5.0	2.50	Turbine design as noted
△	35.4	5.00	
◇	25.0	2.50	
▽	17.7	1.25	
□	100.0	2.50	
◆	25.0	2.50	Baseline design

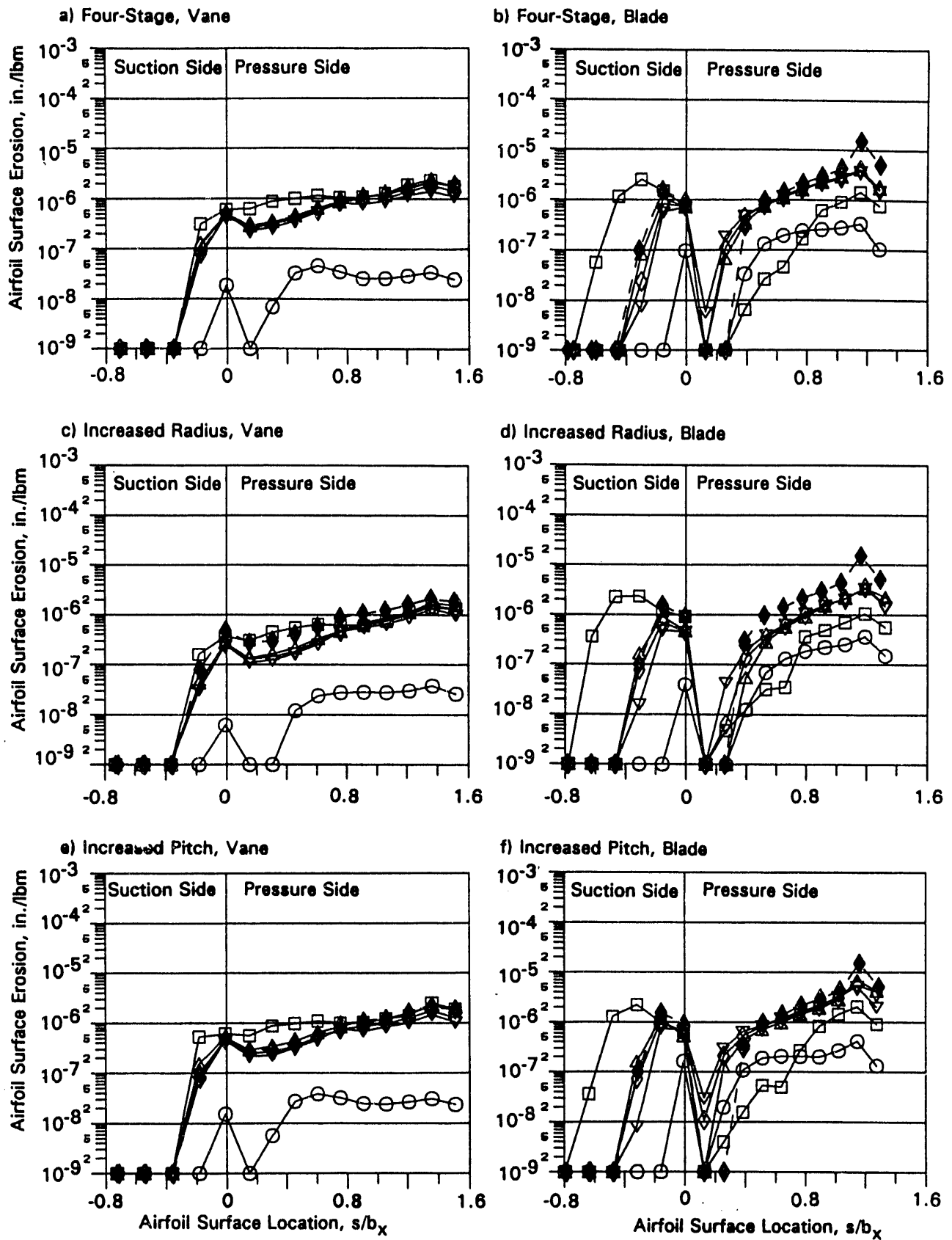
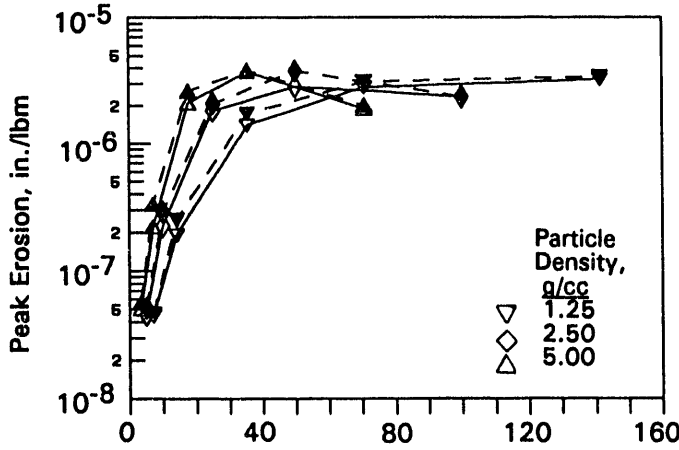
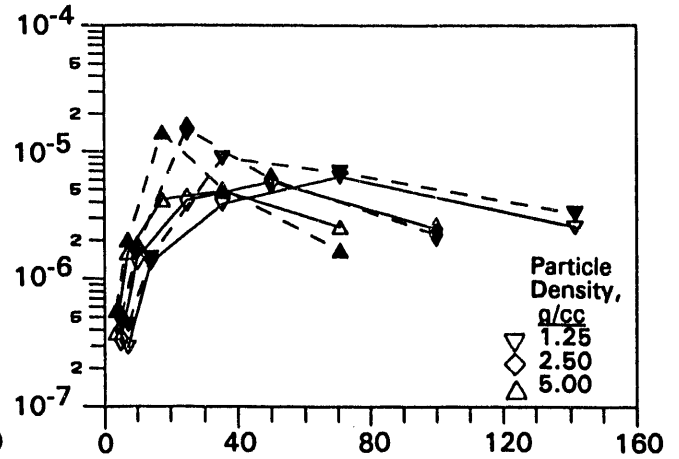


Figure 7-3 Effect of Particle Size and Density on Erosion Distribution From Four Stage, Increased Radius and Increased Pitch Airfoils

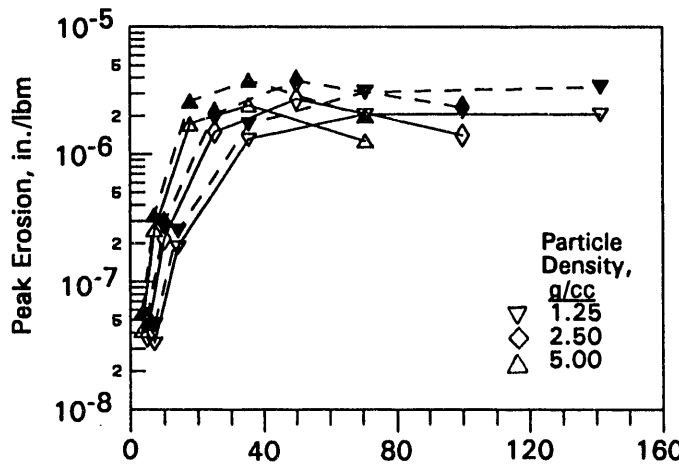
a) Four-Stage, Vane (--- Baseline)



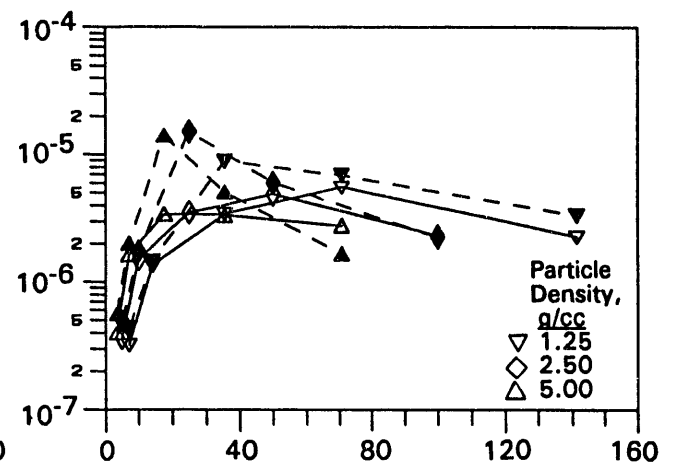
b) Four-Stage, Blade (--- Baseline)



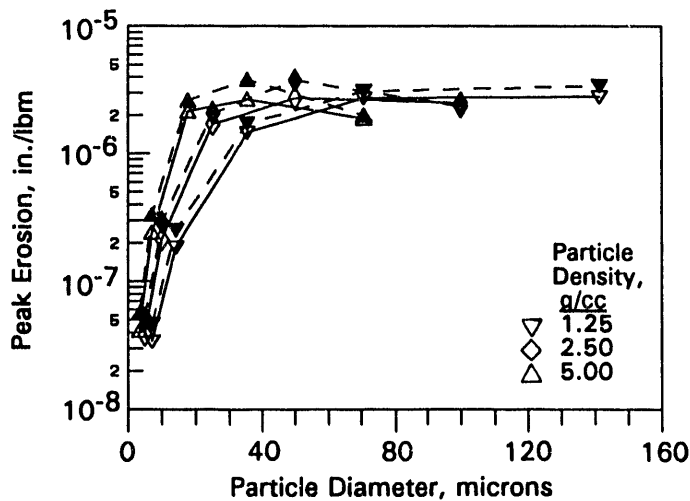
c) Increased Radius, Vane (--- Baseline)



d) Increased Radius, Blade (--- Baseline)



e) Increased Pitch, Vane (--- Baseline)



f) Increased Pitch, Blade (--- Baseline)

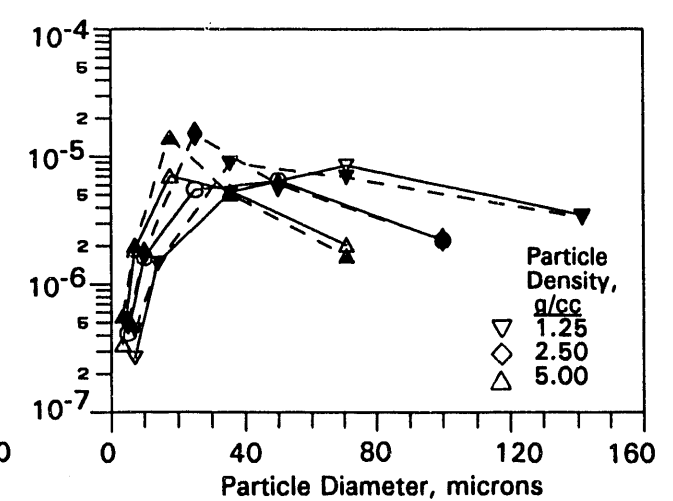


Figure 7-4 Effect of Particle Size and Density on Peak Erosion Rate From Baseline, Four Stage Increased Radius and Increased Pitch Airfoils

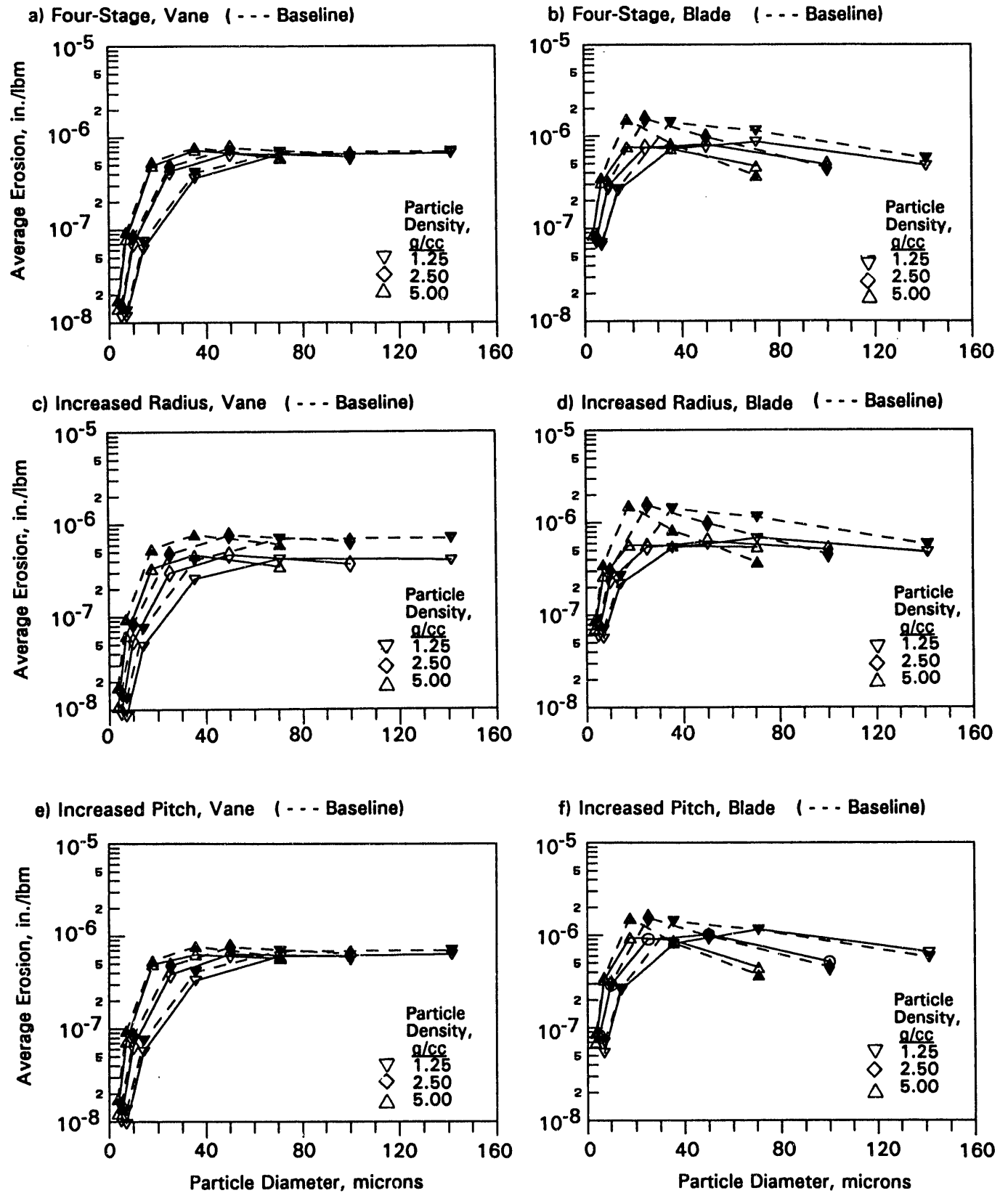


Figure 7-5 Effect of Particle Size and Density on Average Erosion Rate from Baseline. Four Stage, Increased Radius and Increased Pitch Airfoils

	St_v	σ_{p_v}	St_b	σ_{p_b}	D_p microns	p gm/cc
○	0.068	1294	0.092	1320	5.0	2.50
△	1.700	647	2.290	660	35.4	5.00
◇	1.700	1294	2.290	1320	25.0	2.50
▽	1.700	2588	2.290	2641	17.7	1.25
□	27.200	1294	36.700	1320	100.0	2.50

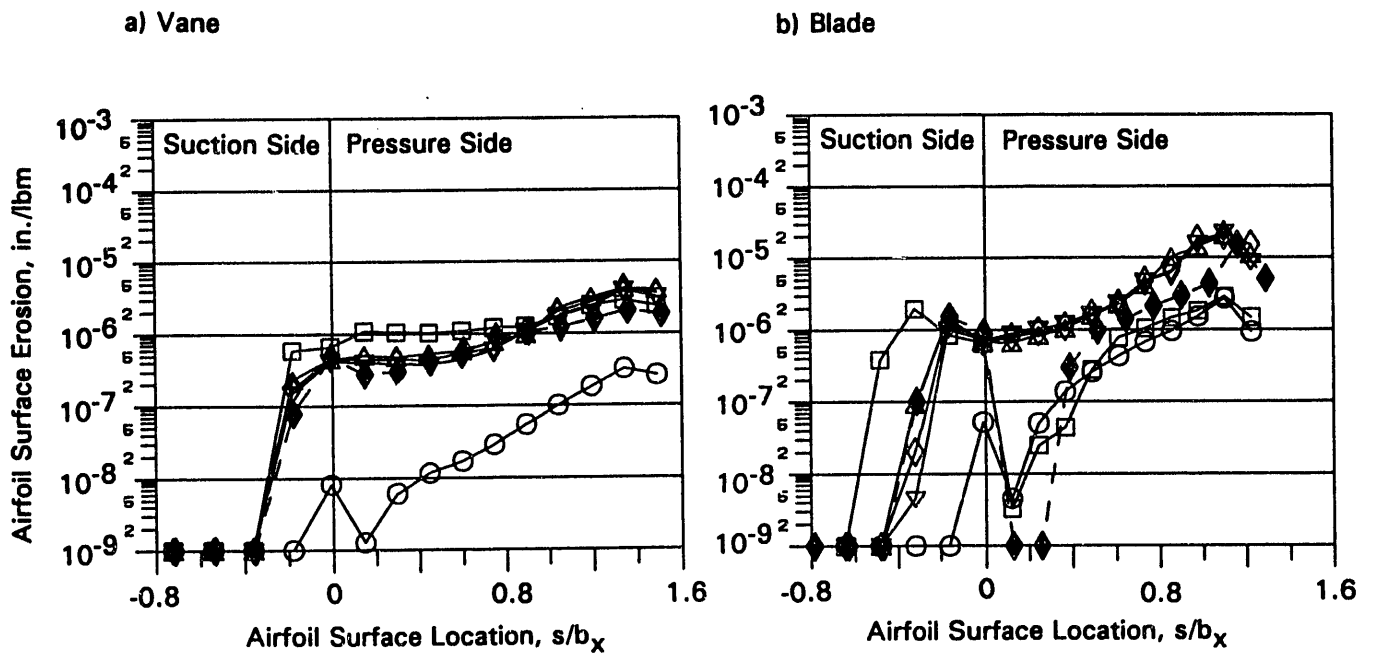
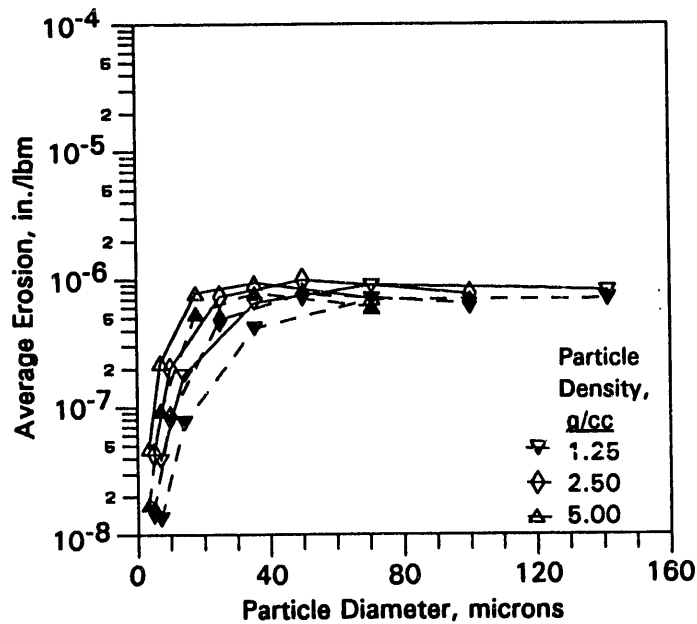
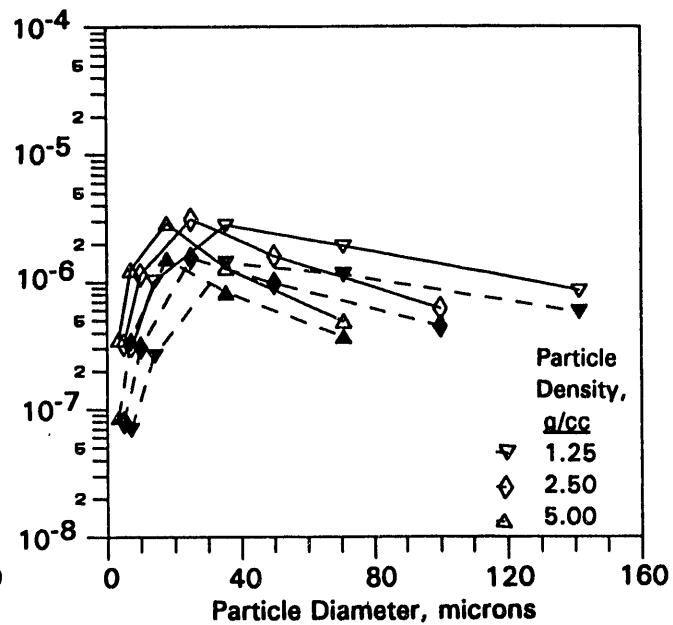


Figure 7-6 Effect of Blade Shape and Particle Size on Erosion Distribution from Airfoil.
Open Symbols: MOD-1; Shaded Symbols – Baseline

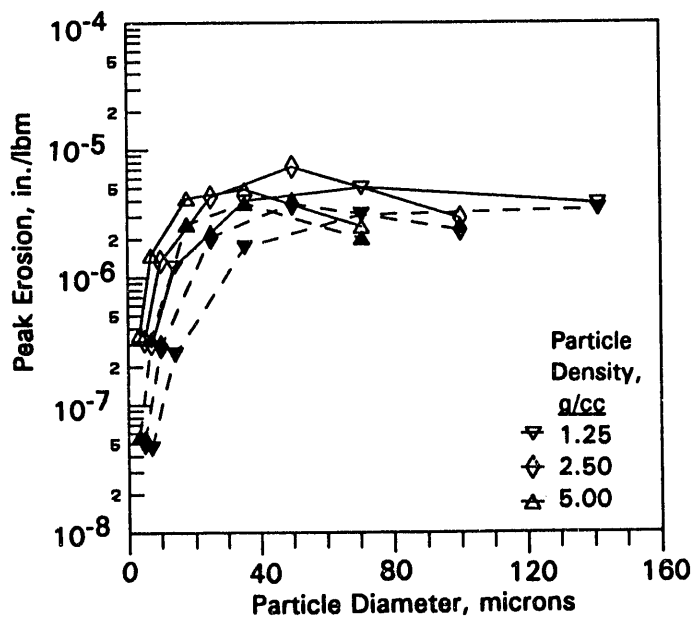
a) Average Vane Erosion Rate



b) Average Blade Erosion Rate



c) Peak Vane Erosion Rate



d) Peak Blade Erosion Rate

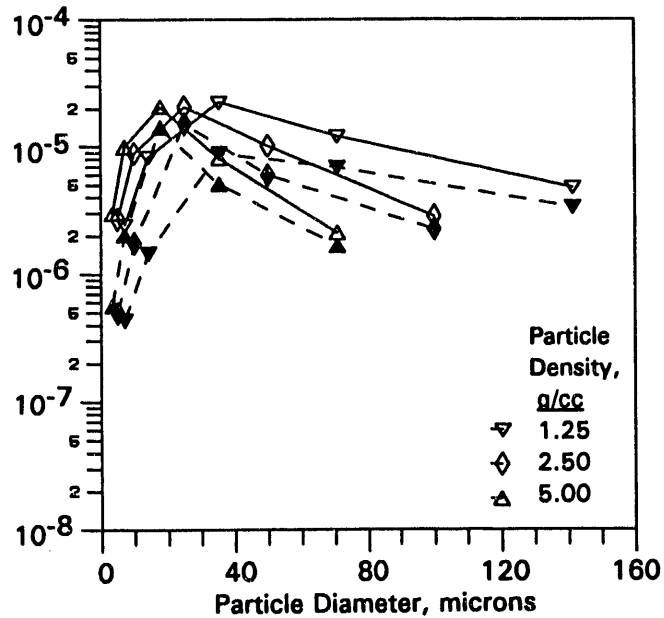


Figure 7-7 Effect of Blade Shape, Particle Size and Particle Density on Average and Peak Erosion Rates. Open Symbols MOD-1; Shaded Symbols - Baseline

SECTION 8

PARTICLE TRAJECTORY AND EROSION CHARACTERISTICS FOR 3-D BASELINE TURBINE

Single and multistage turbine manufacturers and users are aware of the three-dimensional characteristic of erosion on airfoils and outer airseals. The radial variation in erosion is more pronounced on blades than on vanes. This spatial variation in erosion is attributed to the radial migration of large particles to the outer radii of the blades and the outer air seal and to the convection of small particles by the secondary flow in the turbine airfoil passages.

Particle Trajectories

The present calculation of erosion from the baseline turbine first stage airfoils and outer airseal uses 3-D aerodynamic results which include secondary flows due to inlet velocity profiles and viscous losses through the turbine stage. Previous studies have demonstrated that airfoil erosion is most dependent on particle diameter (the Stokes number in the present study). The effect of particle density and initial velocity have lesser effects on the resultant erosion patterns [32]. Therefore, only the particle diameter (i.e., Stokes number) was varied to determine the effect of secondary flows on airfoil and case erosion.

Particle trajectories of three particle diameters were calculated for the full-span, 3-D baseline turbine first stage for a particle density of 2.5 gm/cc. The flow analysis was for a blade without a tip shroud.

Typical particle trajectories through the baseline blade airfoil row are shown in Fig. 8-1 for two particle diameters. The trajectories of the 5 micron particle (Fig. 8-1a) generally tend to follow the flow in and around the blade airfoils. Some of the particle traces shown are entrained in the strong secondary flows which occur between airfoils with high turning. Aside from the entrainment in the secondary flow cells, there is little migration of the 5 micron particles to the outer case due to particle centrifuging. For the small number of particles shown, none of the particles are shown to come in contact with the outer case. The 25 micron particle trajectories (Fig. 8-1b) are less affected by the secondary flows and are strongly influenced by the centrifugal forces as shown by the radially outward migration of the particles toward the outer case. The radial migration is especially strong immediately following a particle rebound where particle momentum is lost to the surface by way of the rebound model. In general, particle trajectories are directed radially outward away from the hub resulting in a large number of the particles rebounding off the outer case. The absence of particle impacts in the hub region are consistent with previous 3-D erosion studies [10]. Therefore, erosion is not expected to be significant on the hub and on the airfoil surfaces near the hub.

Erosion Characteristics

A surface impact analysis code was used to analyze trajectory results from the particle trajectory calculations from the meanline turbines and from the fully 3-D turbine baseline vane and blade. Erosion results were obtained by dividing the pressure and suction sides of

the airfoil into surface elements. Surface impact statistics for each surface element were generated from the trajectory results. Surface erosion rate was determined from the sum of the erosion values predicted for each impacting particle on each surface element as described in the section describing the erosion models. The formulations derived in Section 5 were used to calculate the airfoil surface erosion. These results may be used with the particle loading factor (i.e. particle flow rate/turbine inlet airflow rate) and the total turbine inlet flowrate to estimate the recession rate per unit time. In this manner turbine airfoil life may be estimated as discussed in Section 9.

Vane Results

Contours of the particle impact speed on the vane airfoil are shown in Fig. 8-2. The results show that as particle diameter increases from 5 to 100 microns, the particle impact speeds on the pressure surface generally increase in the leading edge region and decrease near the trailing edge. However, for the 5 micron particles the impact angles are typically below 5 degrees over most of the vane airfoil surface (Fig. 8-3) resulting in small values of predicted erosion. Contours of particle impact speed on the outer case between the 3-D vane airfoils (not shown) show that as particle diameter increases from 5 to 100 micron, the location where the particles impact on to the casing becomes closer to the leading edge of the airfoil row. This migration of particles is due to the centrifugal forces on the particles as the swirl (i.e. tangential velocity) increases from the leading edge to the trailing edge.

Contours of erosion on the stationary vane row surfaces are shown in Fig. 8-4. Negligible erosion is predicted for the suction side of the vane airfoil, regardless of particle diameter. Peak erosion on the pressure side of the vane airfoil for the three particle diameters analyzed is located at the trailing edge of the airfoil near the root. These results are consistent with observed phenomena discussed by Smith et al. [57]. Smith's discussion of the Bureau of Mines Coal Burning Gas Turbine indicated that the bases of the stators experienced wear due to particulate erosion. The increase in erosion in this area is due to an increased number of particle impacts (because of the three dimensionality of the airfoil) combined with impact angles which are relatively more erosive than impact angles on other regions of the airfoil surface.

Blade Results

Contours of the particle impact speed on the blade airfoil are shown in Fig. 8-5. The results show that as particle diameter increases from 5 to 100 micron the particle impact speeds on the blade airfoil decreases. But more importantly, the affected blade areas change markedly as the particle diameter is varied. The 5 micron particles generally come in contact with most of the pressure surface of the airfoil and is relatively independent of spanwise location. The suction surface is affected in the aft portion of the airfoil near the hub and outer case regions due to secondary flow effects and particle/case rebounds, respectively. As particle diameter is increased to 100 micron, less of the pressure surface is affected while the level of particle/airfoil interaction on the suction surface increases. Note that the smaller particles impact most of the airfoil surface at shallow angles (Fig. 8-6), typically below 5 degrees, resulting in small values of predicted erosion.

Contours of erosion on the rotating blade row surfaces are shown in Fig. 8-7. Predicted peak erosion is located on the suction side of the blade near the tip, regardless of particle

diameter. Erosion is highest on the suction surface because of the particle rebounds from the stationary outer case. Particles which normally would pass through a shrouded blade airfoil row are drawn to the suction surface, thereby, increasing the frequency of impacts in this area. The effect is further compounded in that particles which subsequently rebound from the suction surface may again hit the outer case and be drawn to the suction surface a number of times before passing through the airfoil row. This phenomena is generally unique to unshrouded airfoils. Erosion on the pressure surface of the blade airfoil is strongly dependent on the particle diameter. Peak erosion on the pressure surface, caused by the 5 micron particles, is located in the trailing edge root area while regions of peak erosion for the larger, 25 and 100 micron, particles are located at progressively larger spanwise locations. As was predicted in the 2-D flow analyses, maximum erosion on the blade airfoils is caused by the midsized, 25 micron, particles. The effect of secondary flow on erosion due to these particles is clearly seen in Fig. 8-7d where two regions of locally high levels of erosion are predicted near the trailing edge. The local erosion peaks at about 40 and 80 percent radial span are attributed to secondary centrifuging effects of particles entrained in the two, counter-rotating secondary flow cells due to high airfoil turning. The lower peak is slightly greater because (1) entrained particle energy is enhanced when the particle direction is coincident with the centrifugal force and (2) the particles in the upper cell are moving counter to the centrifugal force.

In summary, erosion patterns on the blade airfoil are highly dependent on the particle diameter which results in large variations of initial particle directions and, therefore, results in large variations in the location of the affected areas of erosion.

Vane Shroud and Blade Outer Airseal Results

The erosion patterns on the outer vane case are strongly dependent on particle diameter. The erosion contours on the case for the 5 micron particles (Fig. 8-8a) indicate that slightly more erosion occurs along the suction side of the vane airfoil. However, the maximum erosion for the midsized and large particles occurs near the pressure side and between the airfoils, respectively. The location on the suction side is more susceptible to erosion by the smaller particles because of the larger velocities near the suction side (which contribute to erosion because of increased impact speed as well as increased number of impacts because of centrifuging effects). The location of the high erosion areas on the tip caused by the midsized and larger particles is governed by the combined effects of particle rebounds from the pressure side of the airfoil and particle centrifuging.

The erosion contours on the blade outer case (air seal) are also shown in Fig. 8-8. The axisymmetric contours were determined from area averaged erosion predictions in the circumferential direction. The erosion patterns on the outer case of the rotating blade are also strongly dependent on particle diameter. The distributions of erosion on the blade outer case is more easily seen in Fig. 8-9 where the circumferentially averaged results are shown vs. axial location. These results show that a single region of peak erosion caused by the 5 micron particles occurs in the leading edge region followed by a fairly rapid decline in erosion from the leading to the trailing edge. However, the erosion distributions for the 25 and 100 micron particles indicate regions of local peak erosion at about the 25 percent axial chord location with another set of local peaks at about 75 and 90 percent axial chord, respectively. The peaks near the 25 percent chord location are attributed to particles which become "trapped" in a

sequence of rebounds from the outer case to the suction surface to the outer case because of the convex shape of the suction surface in this region. The secondary, and some what lower, peaks in the aft region of the outer case are also attributed to multiple rebounds, however, the “trapping” of the particles should be minimal at these locations. In general, outer case erosion is strongly dependent on the particle diameter but should also be strongly affected by airfoil shape, especially in the leading edge region.

The erosion distribution due to 25 micron particles on the vane and blade surfaces, the vane outer shroud and the blade outer air seal are shown in Fig. 8-10. Note the locations of peak erosion on the blade are more than 10 times the peak erosion on the vane. Note also that erosion on the blade outer air seal is relatively low for this ductile material. If an abradable outer air seal surface were employed, the blade outer air seal erosion rate would be increased by approximately 100.

Comparison Between 3-D and 2-D Erosion Results

Comparisons of peak and average vane airfoil erosion results calculated using 2-D and 3-D flowfields are shown in Fig. 8-11. For the vane, peak and average erosion results for the two flowfields increases with increases in the particle diameter. However, the predicted erosion results for the 3-D flowfield are consistently higher than those from the 2-D calculations. (These results are not consistent with those of Hamed [28] where vane erosion was reduced when secondary flow effects were included. The difference in the predicted results between the present analysis and Hamed may be attributed to differing characterizations of the flowfields and particle diameters analysed.) The variance in 2-D and 3-D predicted erosion is also shown to increase as particle diameter decreases. Because the variance increases for the smaller particles (which are influenced more by secondary flow effects) the results suggest that the particles in fully 3-D flow fields are more erosive than particles in 2-D flows due to the increased secondary flow activity.

Comparisons of peak and average blade airfoil erosion results calculated using 2-D and 3-D flowfields are also shown in Fig. 8-11. The averaged erosion from both the 2-D and 3-D flowfields indicated that the maximum erosion on the blade airfoil is caused by the midsized, 25 micron, particles. However, the predicted peak and average erosion results for the 3-D flowfield are again consistently higher than those from the 2-D calculations. The variations in the predicted peak erosion results using the 3-D flowfield vs. the 2-D flowfield is due to the effect of the moving blade tip relative to the stationary outer case. The 2-D analysis was incapable of determining this kind of effect. The variations between the 2-D and 3-D averaged erosion results is attributed to secondary flow effects combined with high erosion tip effects because of the stationary outer case.

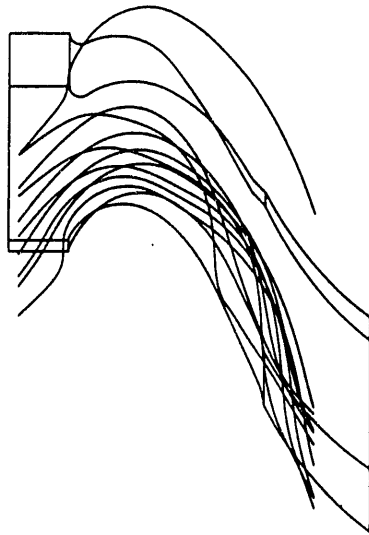
In summary, erosion patterns on the vane airfoil are governed by the three dimensionality of the vane airfoil while the erosion patterns on the outer case are highly dependent on the particle diameter. In addition, erosion patterns on the blade airfoil are governed by the particle diameter which results in large variations in initial particle directions and by the moving outer case which results in an increase in the number of particle/airfoil interactions.

Particle Size 5μ

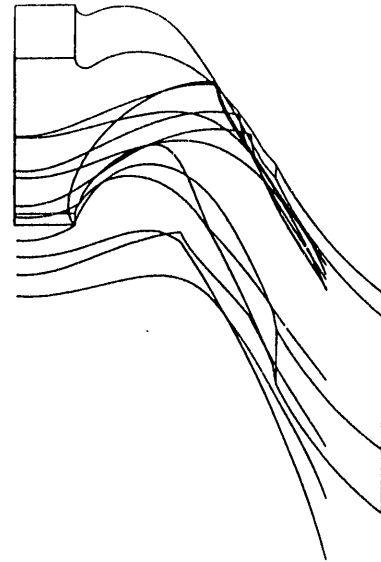
25μ

a)

b)

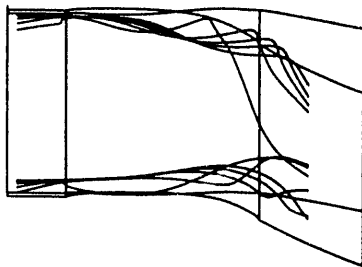


Theta-Z Plane

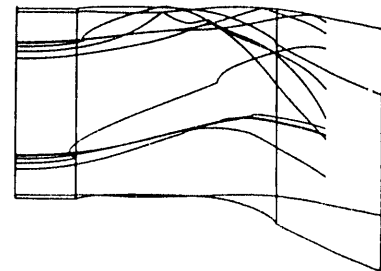


c)

d)

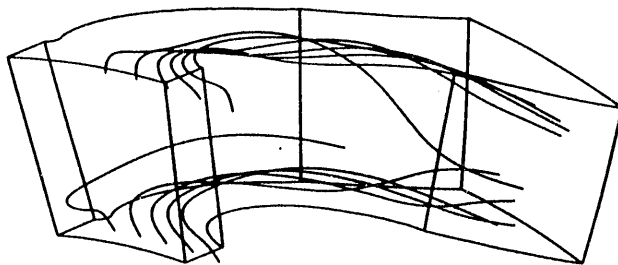


R-Z Plane



e)

f)



Isometric View

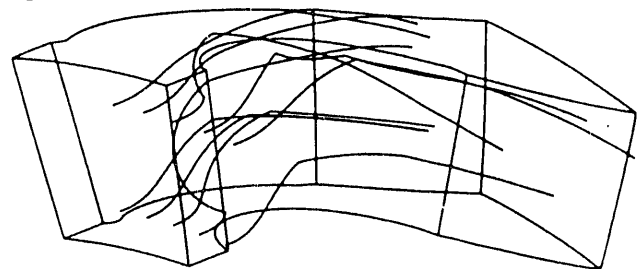
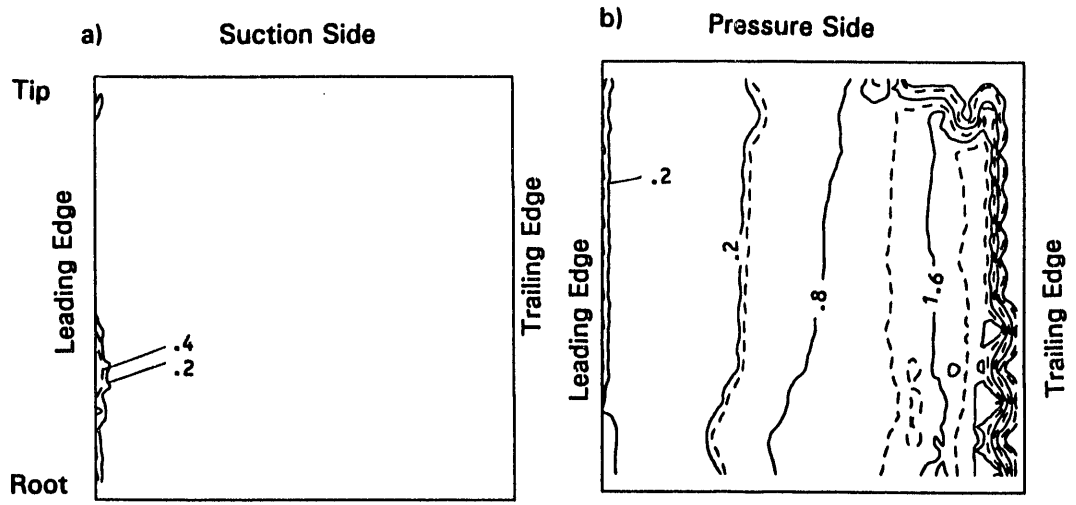


Figure 8-1 Typical 3-D Particle Trajectories in Baseline Blade Passage

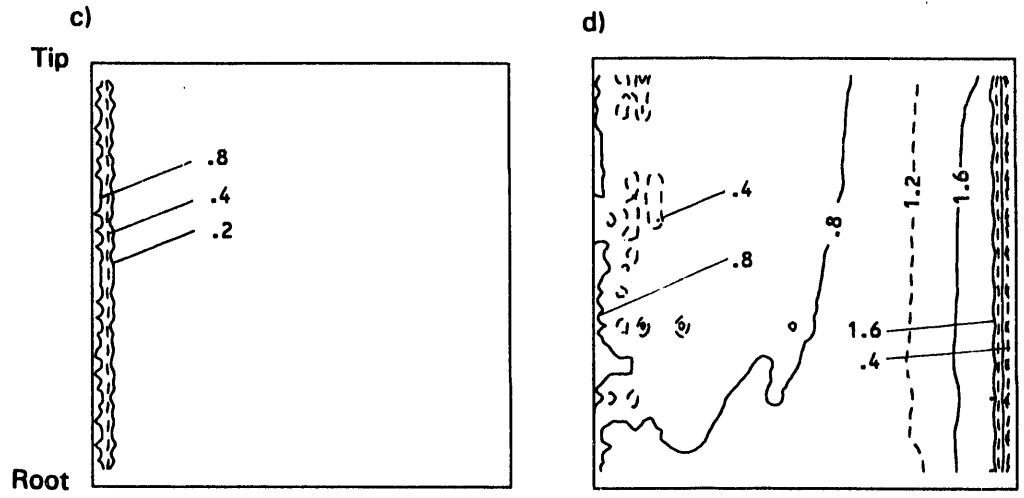
Chosen Contours	
—	0.2
- - -	0.4
—	0.8
- - -	1.2
—	1.6
- - -	2.0
- - -	2.4
- - -	2.8
—	3.2

See Figure 4-1 for particle impact notation

$D = 5\mu$



$D = 25\mu$



$D = 100\mu$

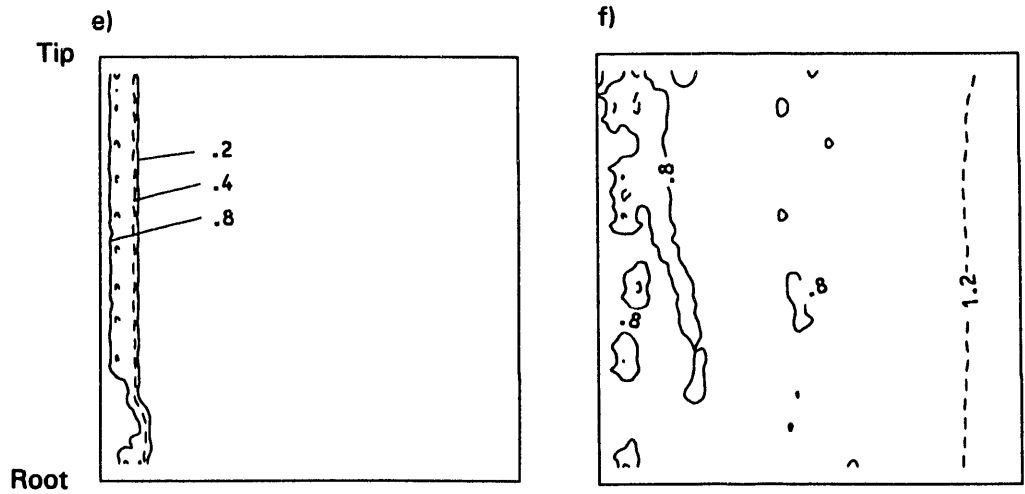


Figure 8-2 Contours of Particle Impact Speeds, V/U_1 , in 3-D Baseline Vane Airfoil Row

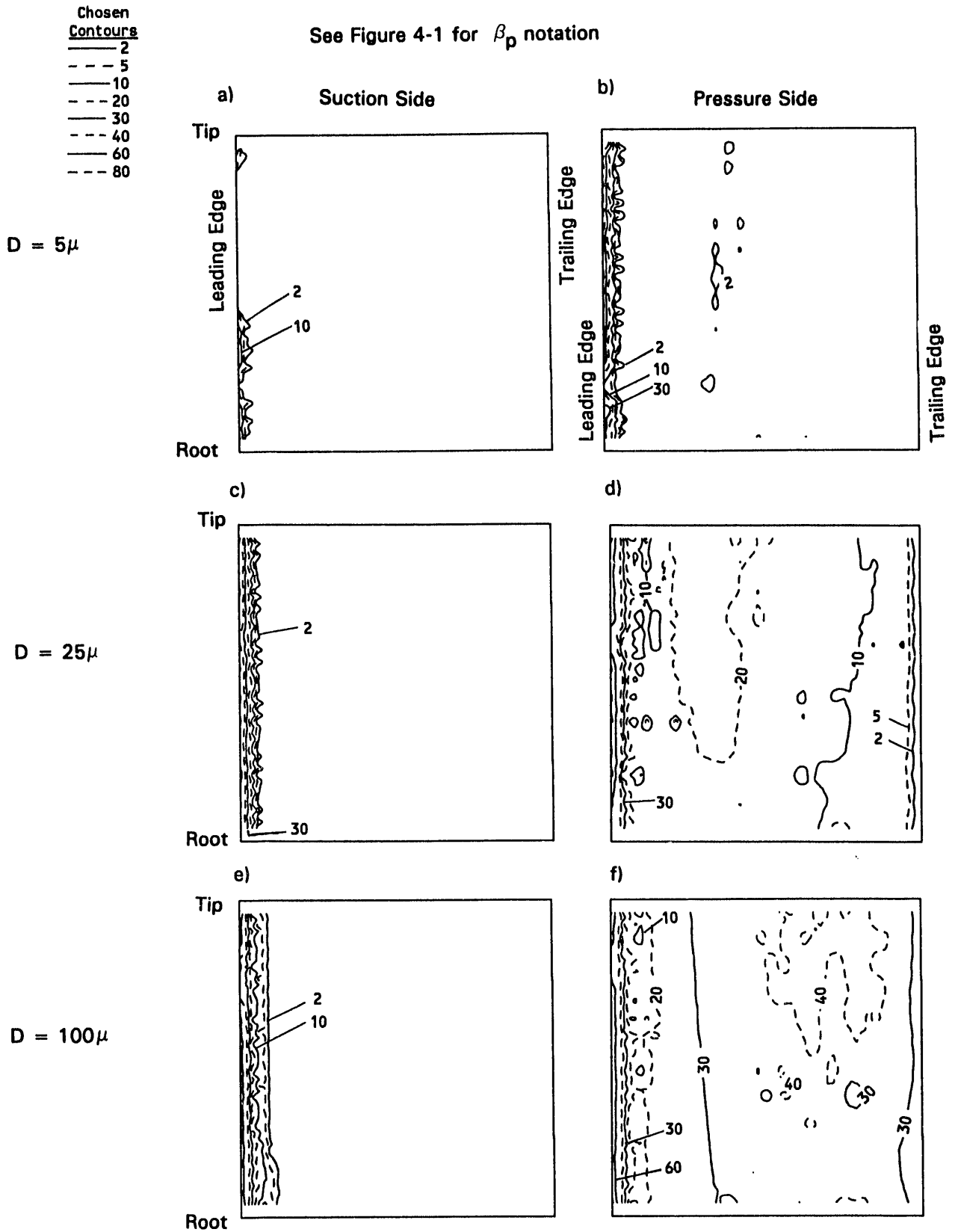


Figure 8-3 Contours of Particle Impact Angles, β_p , in 3-D Baseline Vane Airfoil Row

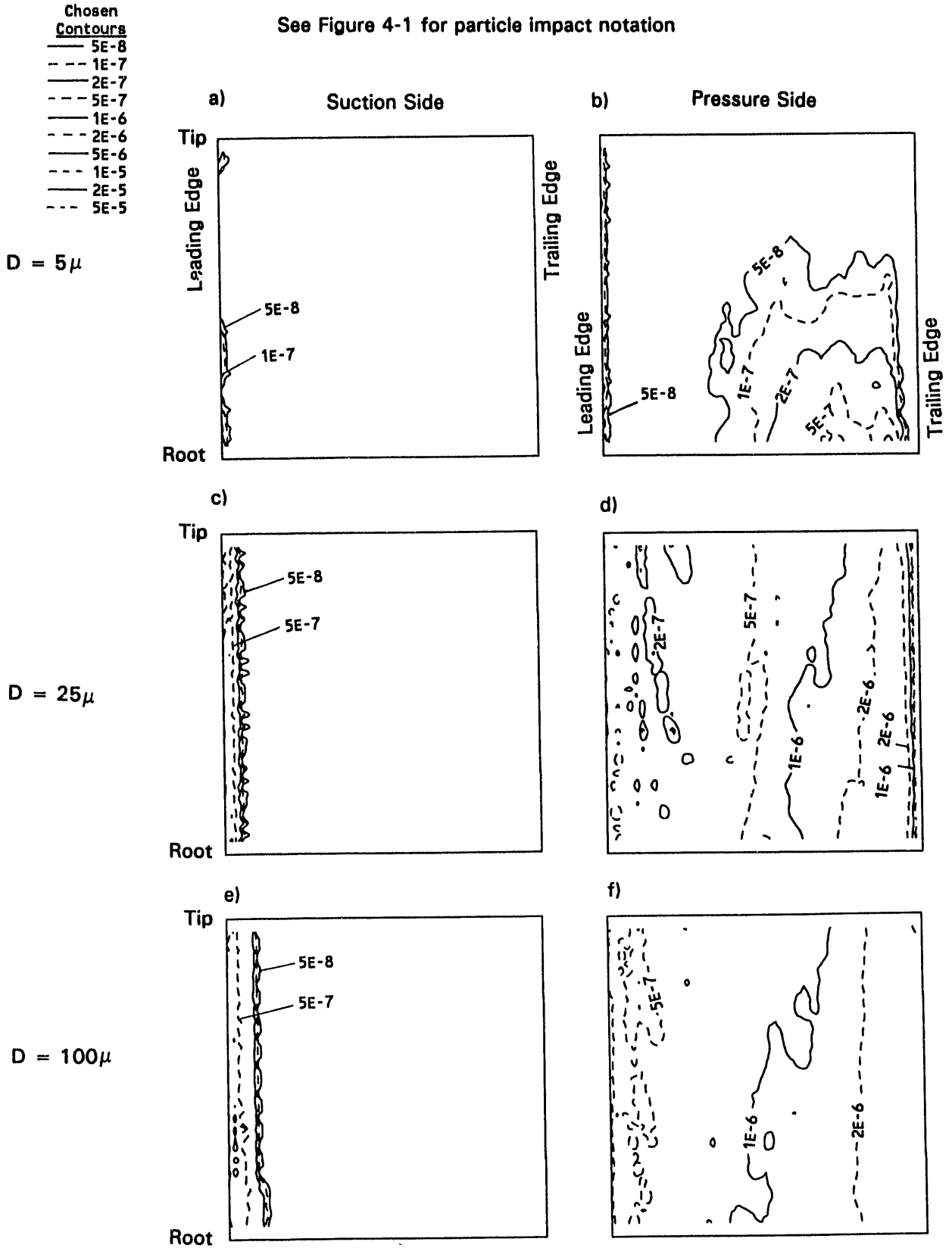


Figure 8-4 Effect of Particle Diameter on the Erosion Distribution, e (in./lbm), From Vane Airfoils

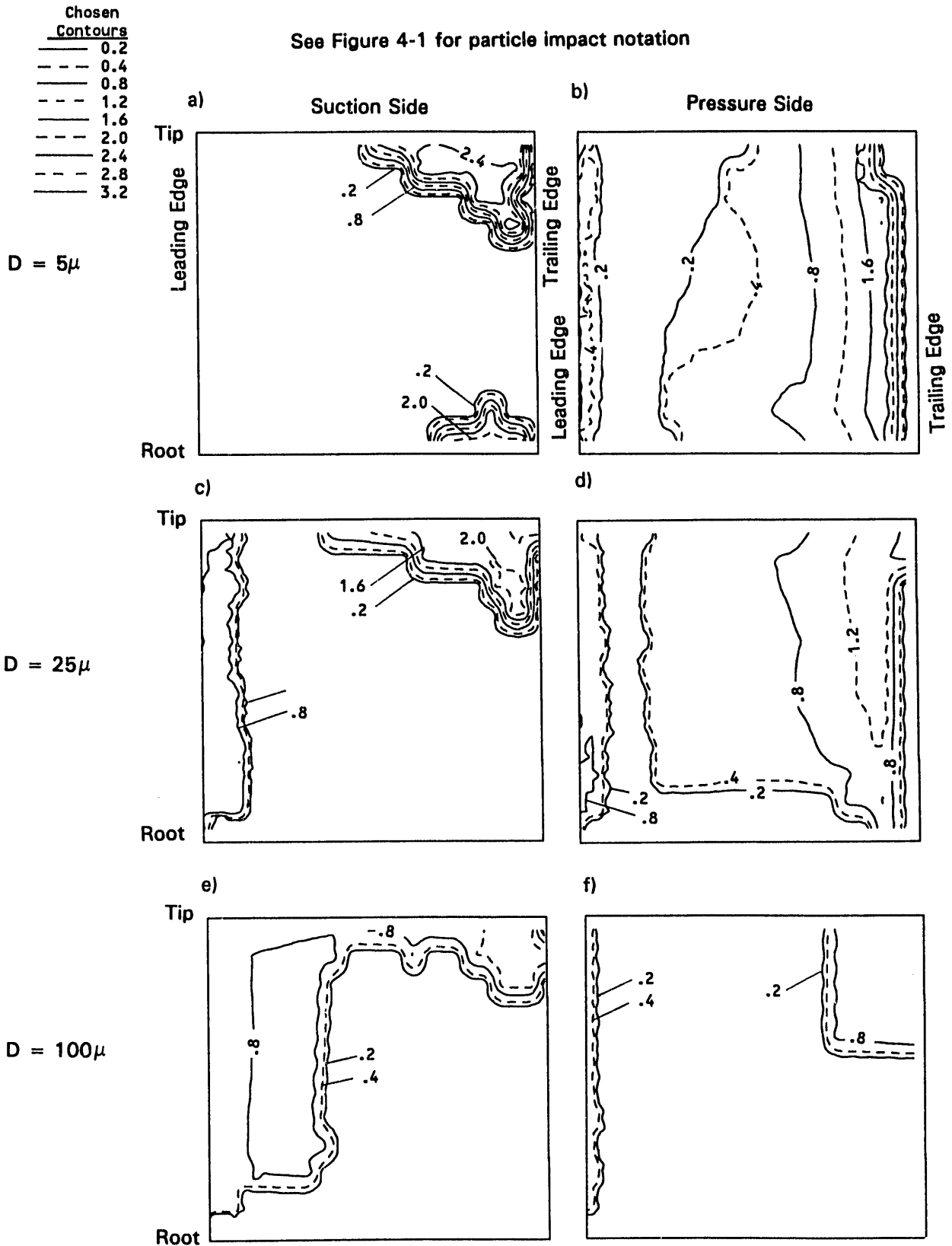


Figure 8-5 Contours of Particle Impact Speeds, V/U_1 , in 3-D Baseline Blade Airfoil Row

Chosen
Contours

- 2
- - - 5
- 10
- - - 20
- 30
- - - 40
- 60
- - - 80

See Figure 4-1 for β_p notation

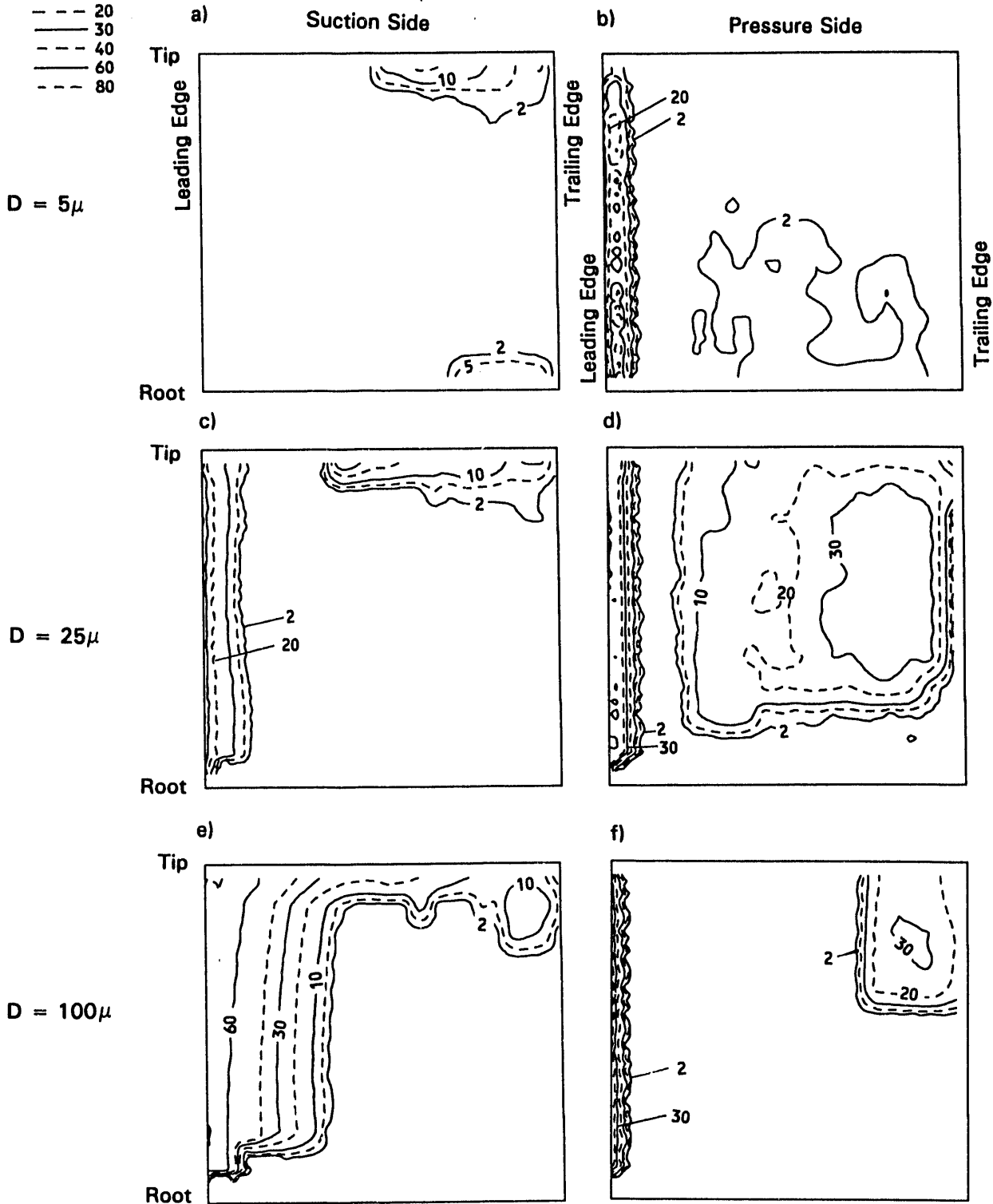


Figure 8-6 Contours of Particle Impact Angles, β_p , in 3-D Baseline Blade Airfoil Row

Chosen Contours	
—	5E-8
- - -	1E-7
—	2E-7
- - -	5E-7
—	1E-6
- - -	2E-6
—	5E-6
- - -	1E-5
—	2E-5
- - -	5E-5

See Figure 4-1 for particle impact notation

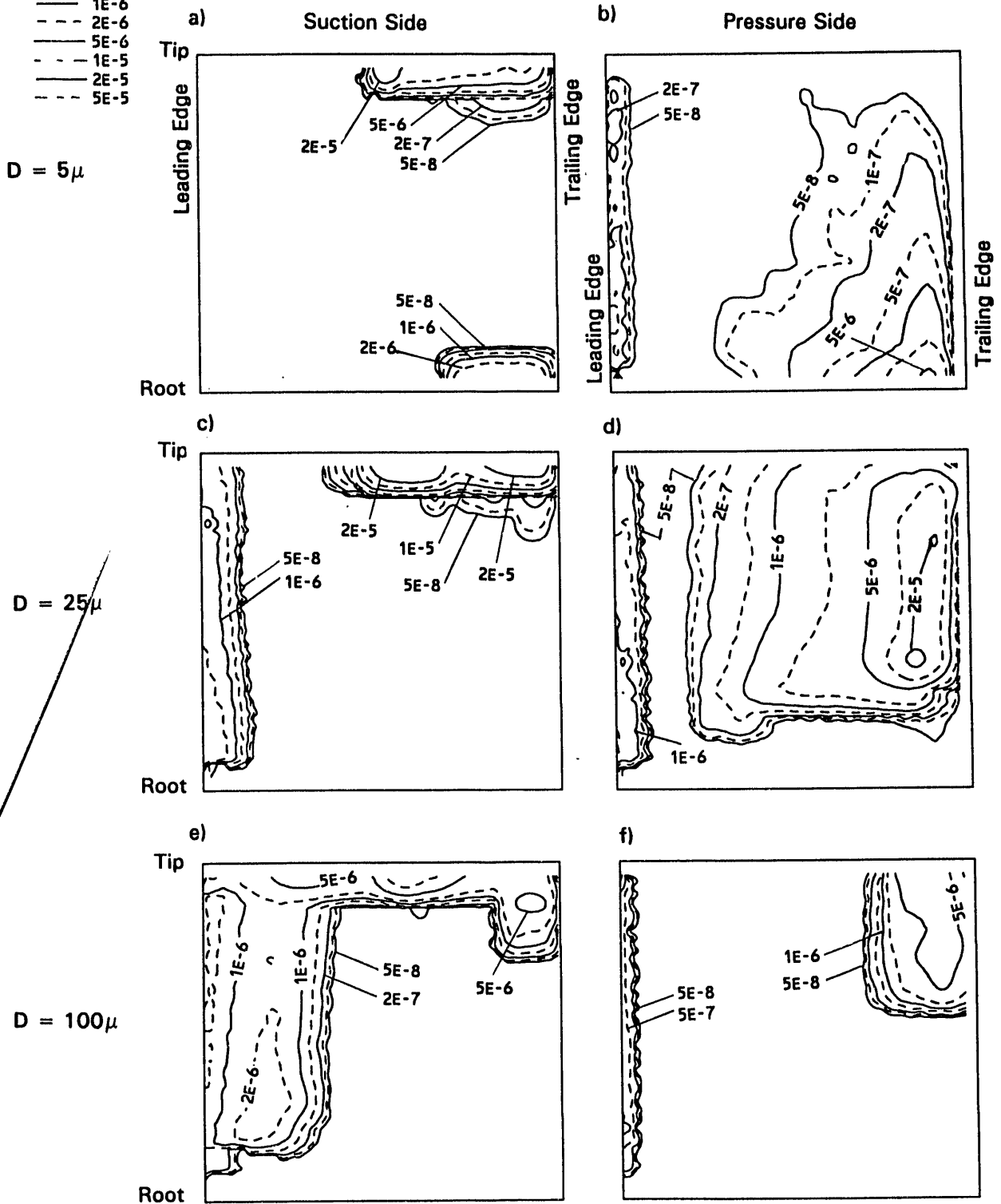


Figure 8-7 Effect of Particle Diameter on the Erosion Distribution, e(in./lbm), From Blade Airfoils

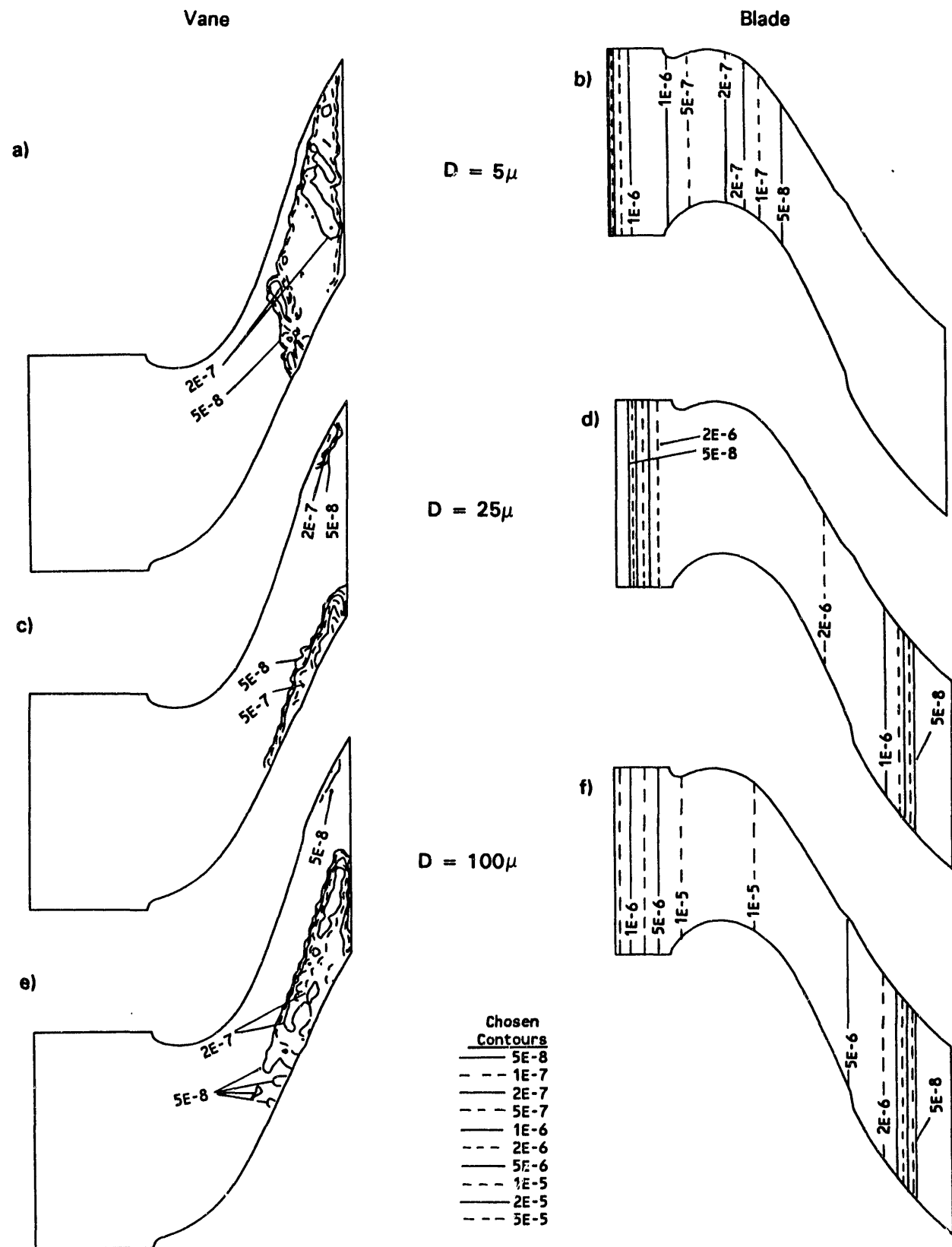


Figure 8-8 Effect of Particle Diameter on the Erosion Distribution, e (in./lbm), From Vane and Blade Outer Case

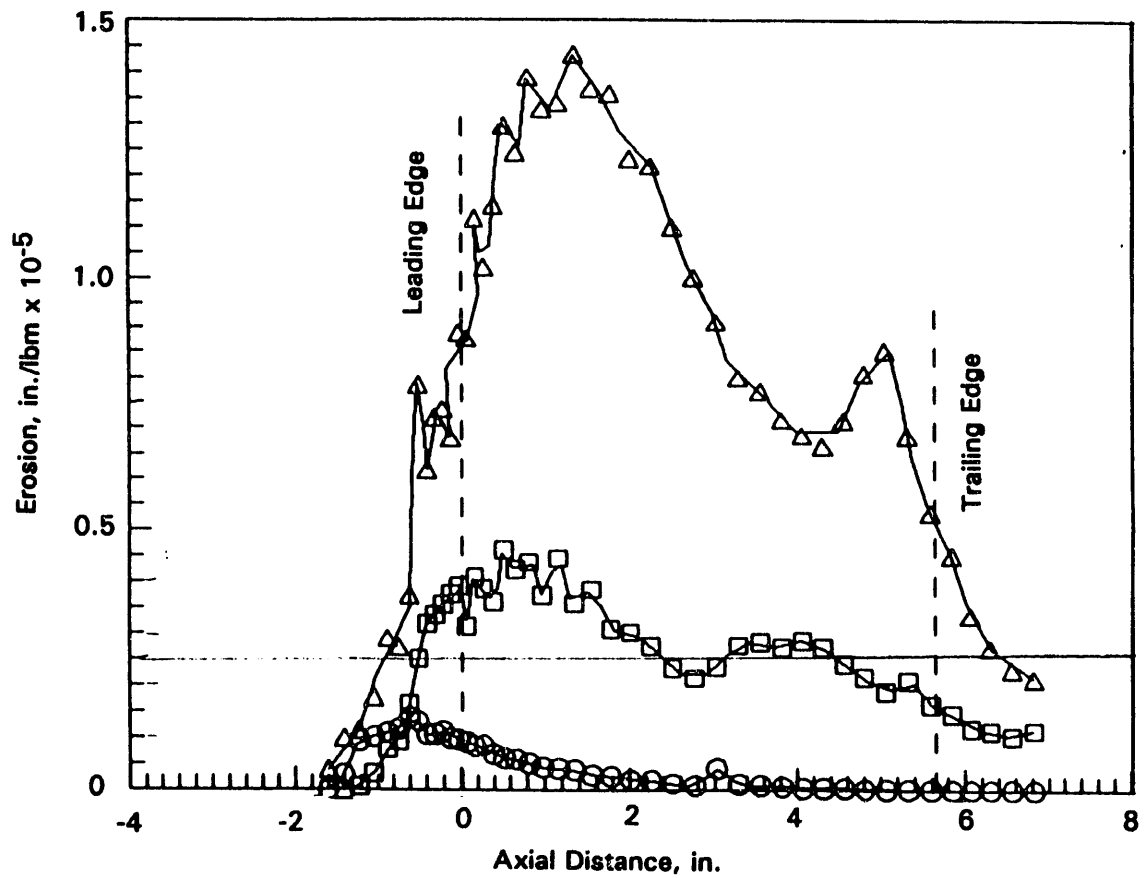


Figure 8-9 Streamwise Distribution of Erosion on Outer Airfoil for Baseline Airfoils and Sphere Particle Diameters: ○ - 5; □ - 25; △ - 100 microns

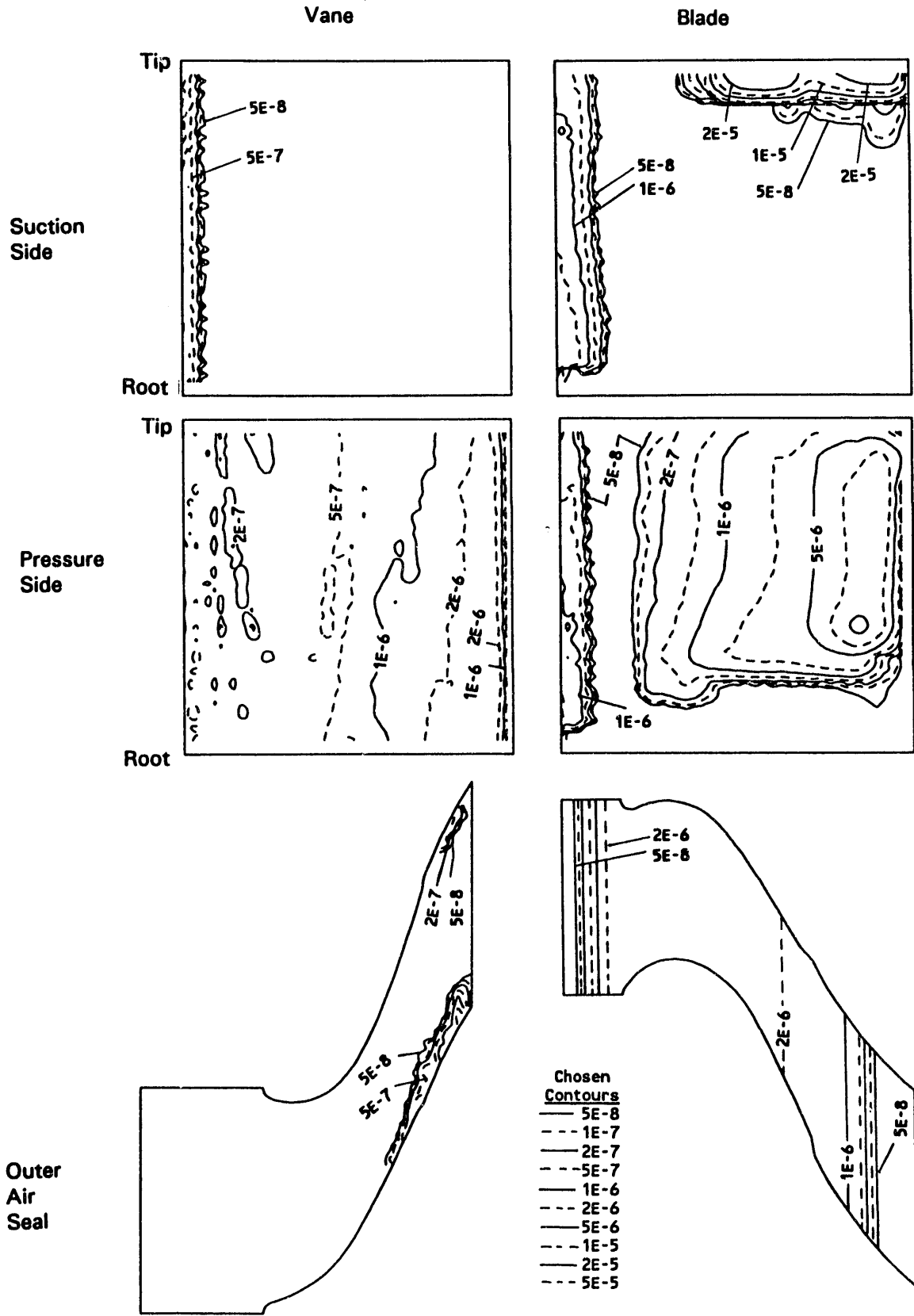


Figure 8-10 Erosion Distribution, $e(\text{in./lbm})$, Due to 25 Micron Particles on Baseline Airfoils

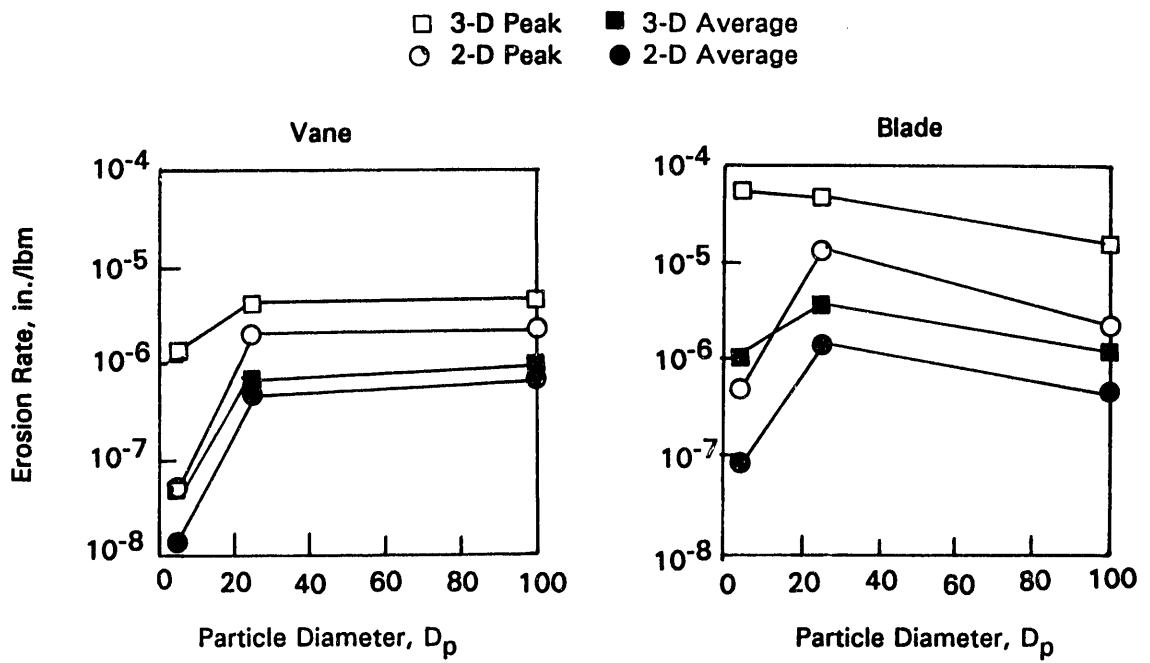


Figure 8-11 Effects of Particle Diameter on Peak and Average Erosion Rates From 2-D and 3-D Baseline Airfoils

SECTION 9

ANALYSIS

Predictions of Turbine Life

This section presents the implications of the results on erosion in coal-fueled, direct-fired gas turbines. The results presented thus far show the effects of various turbine design parameters and secondary flow/3-D effects on turbine erosion. In this section, the results of this study will be used to estimate useful blade life for a given particle loading, allowable loading for a required airfoil life and the implications of a hot gas cleanup system failure. Although the results presented could be combined to give overall erosion results from an anticipated distribution of particles at the turbine inlet, as discussed by Kotwal and Tabakoff [35], the following analysis will assume that all of the particles are of the same size and uniformly distributed at the turbine inlet.

Recent test results [Ref.77] indicate that without particulate filtration, the particulate loading can be as great as 580 ppm as shown in Fig. 9-1a. Particle loadings of this magnitude require some hot gas cleanup to achieve acceptable turbine life. Barrier filters have been shown to remove 99.9 percent of all particles greater than 0.1 micron and 99.99 percent of all particles greater than 1.0 micron (e.g. Fig. 9-2b from Ref. [54]). Therefore, erosion downstream of intact filtration systems of this efficiency will be negligible. However, this section will address the effects of a hot gas filter failure, as well as, what level of filtration is required for an acceptable turbine life. A typical distribution of particle diameters entering a gas turbine without barrier filters is shown in Fig. 9-1b from Ref. [36]. Roughly 75 percent of the particles have diameters less than 25 microns. Therefore, for the following sample calculation, particles with a diameter of 10 microns will be used to represent the average particulate at the turbine inlet.

Sample Calculation (10 Micron Particle, 2-D Baseline Blade)

The assumptions used to estimate erosion rate are listed below. The peak predicted erosion result for the baseline turbine blade airfoil was chosen as the basis for this sample calculation. A material removal allowance was chosen based on an estimated physical wall thickness of the airfoil at the location of peak erosion (i.e. trailing edge). The material removal allowance chosen was based on an airfoil cooling system compromise due to coolant system failure. Several values of particle loading at the turbine inlet were chosen. The values listed were chosen to (A & E) reflect anticipated maximum loading for acceptable turbine life, (B) simulate the NSPS allowable standard, (C) simulate recent combustion test results without filtering and (D) anticipated dust loading at the turbine inlet of a second generation PFB baseline plant with no filtering (see Figure 9-2). The assumptions listed are for the turbines simulated in this program.

Assumptions for Erosion Analysis of 2-d Baseline Blade:

Particle Diameter	10 microns
Particle Density	2.5 gm/cc
Airfoil Material	Nickel-Based Super Alloy

Peak Blade Airfoil Erosion 1.75E-06 in/lbm (Figure 7-4)
 Turbine Mass Flowrate 670 lbm/sec
 Material Removal Allowance 0.1 inches
 Acceptable Airfoil Life (where required) 25000 hours
 Particulate Loading (where required):

- (A) Particle Separation - On 5 ppm (by weight)
- (B) Particle Separation - On (NSPS) 30 ppm (by weight)
- (C) Particle Separation - Off 350 ppm (by weight)
- (D) Particle Separation - Off (PFBC) 2000 ppm (by weight)

The relationship between airfoil life and particulate loading is determined by dividing the material removal allowance by the rate of erosion as shown below.

$$\text{Airfoil Life} = \frac{\text{Material Removal Allowance}}{\text{Erosion} * \text{Particulate Loading} * \text{Turbine Mass Flowrate}}$$

$$\text{Airfoil Life (hrs)} = \frac{0.1}{1.75E - 6 * \text{Particulate Loading (ppm)} * 670 * 3600 * E - 6}$$

$$\text{Airfoil Life (hrs)} = \frac{23700}{\text{Particle Loading (ppm)}}$$

The resulting particulate loading for an acceptable life of 25000 hrs is on the order of 1 ppm (by weight), location E. Fig. 9-3. Using the particle loadings in the table above, the following airfoil life expectancies are determined for the 2-D Baseline Blade with a 10 micron diameter particle.

Particle Loading (ppm)	5	30	350	2000	1
Predicted Airfoil Life (hrs)	4740	790	68	12	23700
	A	B	C	D	E

The calculation outlined in the preceding paragraphs is easily adapted for other combinations of particle diameter and airfoil configuration, substituting the erosion rate (in/lbm) results from Sections 7 and 8 for the value of $1.75 * 10^{-6}$ in/lbm (10 micron particle, 2-D baseline blade). The parametric relationships for peak erosion rates from $1.0 * 10^{-6}$ to $5 * 10^{-5}$ in/lbm are shown in Fig. 9-3.

Consequences of Hot Gas Filter Failure

The consequences of hot gas filter failure are severe. Corrosion resistant coatings are typically extremely thin relative to the wall thickness of a cooled turbine airfoil, i.e. 0.005 to

0.030 inch. The results presented in the previous paragraph indicate that the airfoil life (0.1 inch of recession) is on the order of 1 to 10 hours in a unfiltered PFB combustion environment. The life of the corrosion resistant coating (0.005 to 0.030 inch) could be a factor of three to 20 less than for the airfoil base material (i.e, 3 minutes to 3 hours). Therefore, an unnoticed filter failure would have serious consequences in that the material removal rate would be altered by the enhancement of erosion by corrosion.

Utilization of Results for Larger or Smaller Turbines

The particle trajectory analysis used to determine the aerodynamic response of coal and ash particles in the turbine stage was developed with dimensionless parameters as described in Section 4 and by Dring [20]. One important benefit of this formulation is that results from this study for an 80 MW turbine also can be utilized for larger or smaller turbines, provided the gas path aerodynamic shapes and pressure ratios are similar. The two parameters needed to describe the particles are the effective diameter and the density. However, the dimensionless parameters developed by Dring are used to describe the particles and make results from the calculation applicable to turbines of different scale but with the same airfoil passage shape and pressure ratio. An analysis of the equations of motion for particles showed that two parameters, the Stokes number, St , and a particle density Reynolds number, σ , govern the trajectories of particles (Equations 9-1 and 2). Thus, for a given flowfield, only two parameters were needed to do a parametric particle trajectory analysis for a given set of particle initial conditions (i.e. initial location, speed and direction).

$$St = (\rho_p U_1 D_p^2) / (18 \mu_i b_x) \quad (9-1)$$

$$\sigma = (Re_{bx}) / (\rho_p / \rho_1) \quad (9-2)$$

Assuming similar aerodynamic properties (i.e. velocity, density and temperature), the results in this report are applicable to turbines of different scale. Corresponding particle diameters and densities can be determined for geometrically similar turbines of different scales and operating conditions by using the Stokes and particle density Reynolds numbers provided in Tables 9-1 and 9-2 and the particular aerodynamic and airfoil size information of the turbine to be analyzed. The turbine aerodynamic and scale parameters used to calculate the dimensionless parameters for size scale = 1.0 and velocity scale = 1.0 are provided in Table 3-3. Simulated particle diameters and densities applicable to two turbines of different scale are also provided in the tables. One case suggests a turbine of 1/4 the scale of the turbine analyzed in this program with identical scaled geometry and identical aerodynamics. The second case is for a turbine 1/2 the size of the present scale with a 20% increase in flow velocities (i.e. mass flow). Therefore, use of dimensionless variables in the analysis of turbine erosion makes the results more easily applied to other turbines of different size and operating condition.

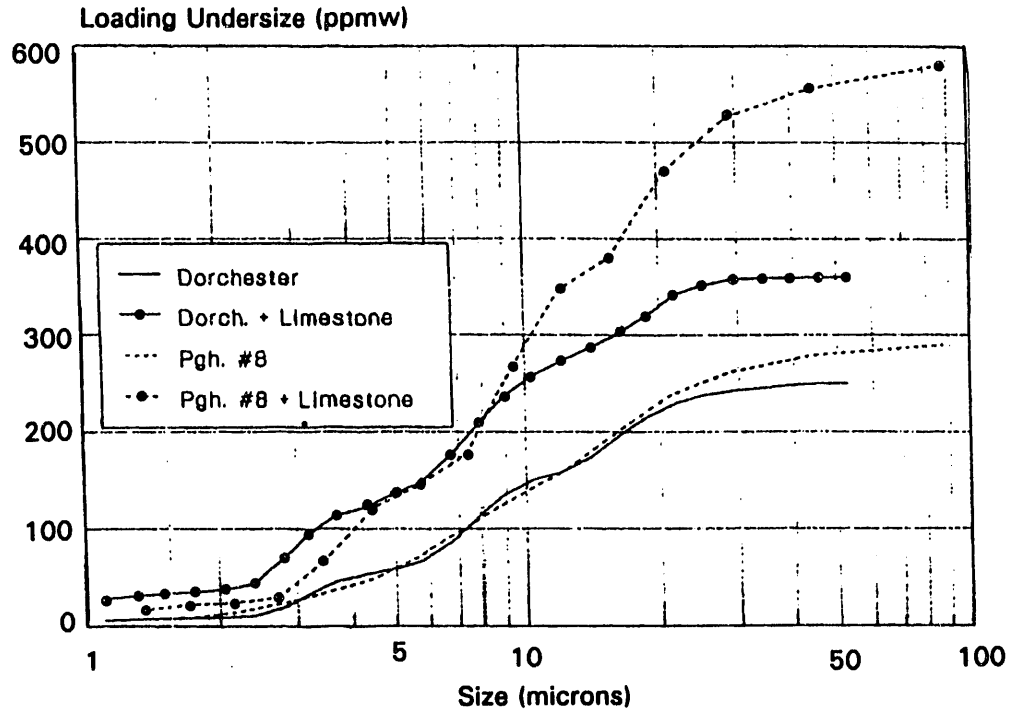
Table 9-1
Simulated Particle Diameters and Densities for Three Turbines
for Selected Stokes Numbers, St
(using central value of σ)

Size Scale	Vel. Ratio	ρ_p gm/cc	D_p microns	Baseline		Four-Stage		Increased-Radius	
				Vane	Blade	Vane	Blade	Vane	Blade
1	1.0	2.500	5	0.068	0.092	0.068	0.078	0.056	0.067
1/4	1.0	0.625	5	↓	↓	↓	↓	↓	↓
1/2	1.2	1.500	4.2	↓	↓	↓	↓	↓	↓
1	1.0	2.500	10	0.272	0.367	0.272	0.310	0.226	0.267
1/4	1.0	0.625	10	↓	↓	↓	↓	↓	↓
1/2	1.2	1.500	8.3	↓	↓	↓	↓	↓	↓
1	1.0	2.500	25	1.70	2.29	1.70	1.94	1.41	1.67
1/4	1.0	0.625	25	↓	↓	↓	↓	↓	↓
1/2	1.2	1.500	20.8	↓	↓	↓	↓	↓	↓
1	1.0	2.500	50	6.80	9.17	6.80	7.76	5.64	6.66
1/4	1.0	0.625	50	↓	↓	↓	↓	↓	↓
1/2	1.2	1.500	41.7	↓	↓	↓	↓	↓	↓
1	1.0	2.500	100	27.2	36.7	27.2	31.0	22.6	26.6
1/4	1.0	0.625	100	↓	↓	↓	↓	↓	↓
1/2	1.2	1.500	83.3	↓	↓	↓	↓	↓	↓

Table 9-2
Simulated Particle Diameters and Densities for Three Turbines
for Selected Particle Density Reynolds Numbers, σ
(using central value of St)

Size Scale	Vel. Ratio	ρ_p gm/cc	D_p microns	Baseline		Four-Stage		Increased-Radius	
				Vane	Blade	Vane	Blade	Vane	Blade
1	1.0	1.25	35.4	2588	2641	2588	2473	2172	1977
1/4	1.0	0.313	35.4	↓	↓	↓	↓	↓	↓
1/2	1.2	0.75	29.5	↓	↓	↓	↓	↓	↓
1	1.0	2.50	25.0	1294	1320	1294	1237	1086	988
1/4	1.0	0.625	25.0	↓	↓	↓	↓	↓	↓
1/2	1.2	1.50	20.8	↓	↓	↓	↓	↓	↓
1	1.0	5.00	17.7	647	660	647	618	543	494
1/4	1.0	1.25	17.7	↓	↓	↓	↓	↓	↓
1/2	1.2	3.00	14.75	↓	↓	↓	↓	↓	↓

a)



b)

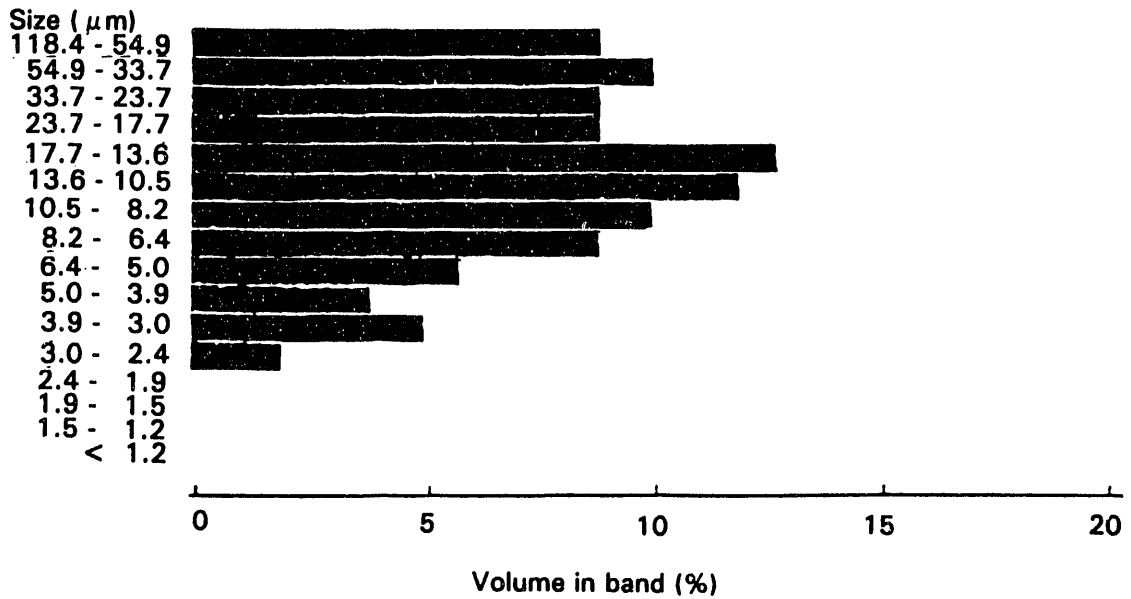


Figure 9-1 Particle Size Distributions From Selected Coal-Fired Combustion Tests

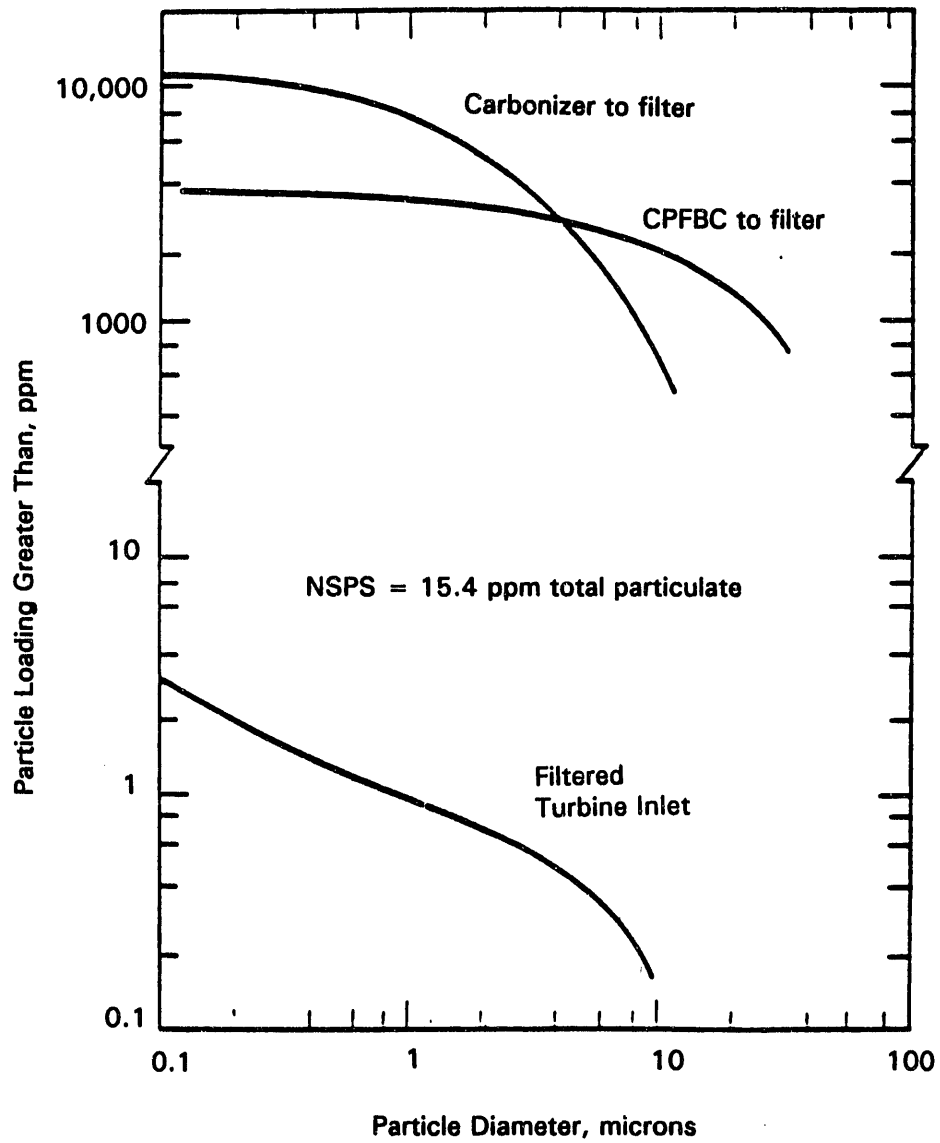


Figure 9-2 Dust Loading and Size Distribution at Turbine Inlet of Second-Generation PFB Baseline Plant (Fig. D-4 of Ref. 54)

- - Westinghouse 501 Turbine estimates
- △ - GE Turbine Tolerance estimates
- (with wavy line) - Westinghouse estimate
- A through E ● - Sample calculations from present study discussed in text
- (solid) - Peak erosion rates (in./lbm) used to estimate turbine life (0.1 in. erosion, 670 lb/sec turbine flow rate)

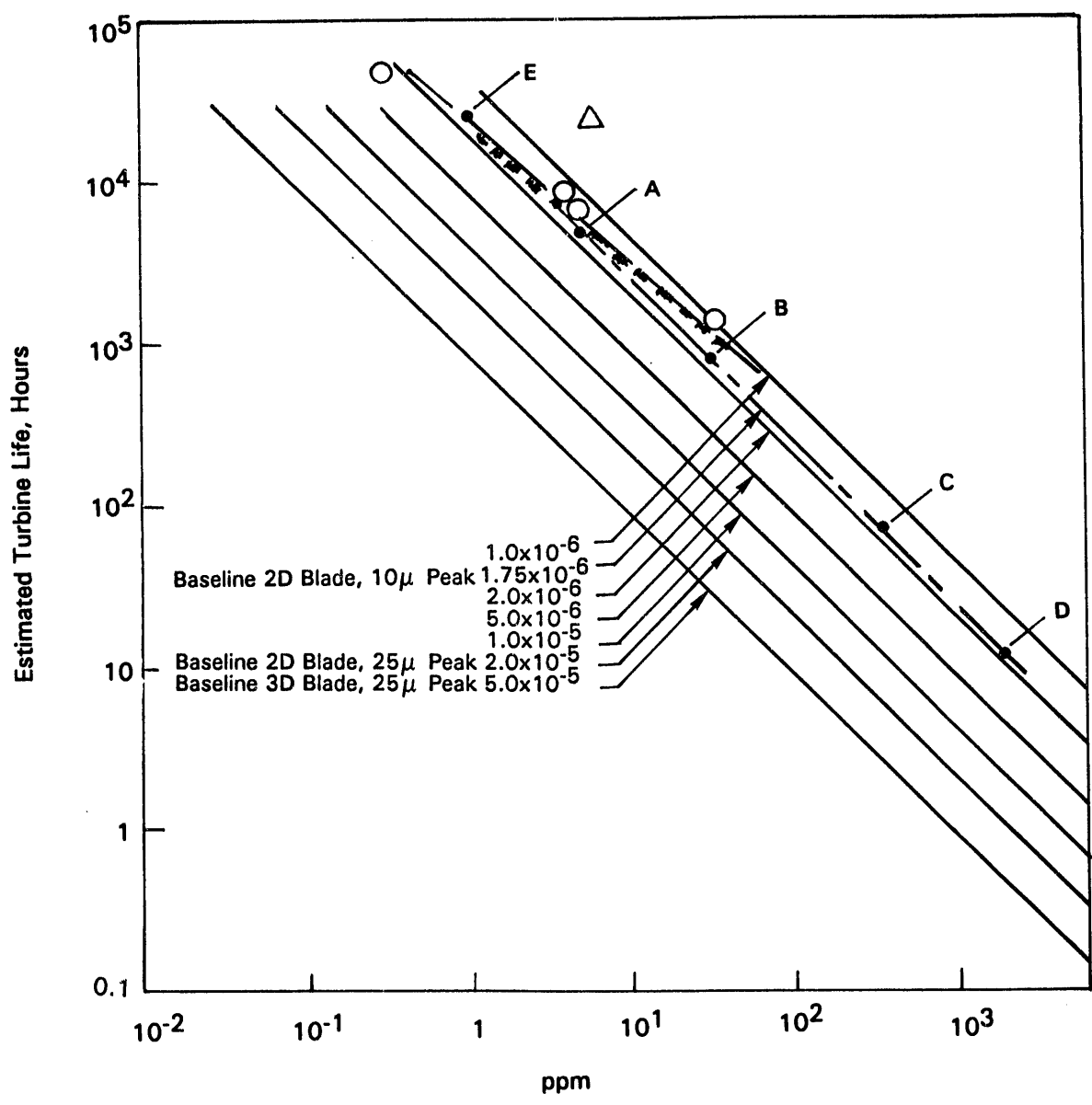


Figure 9-3 Effect of Particle Loading and Peak Erosion Rates on Estimated Turbine Life (Westinghouse & GE life estimates from [54])

SECTION 10

CONCLUSIONS

This report summarizes an analytical effort studying the effect of turbine design on turbine component erosion. The study resulted in 2-D airfoil surface erosion predictions for a number of feasible turbine designs which could be utilized in a medium scale (i.e. ~80MW) power generation system. The results for a baseline turbine were obtained with and without 3-D flow effects to estimate the effects of secondary flows. The results were applied to estimate airfoil life based on assumed levels of particulate loading. These results provide insight into the requirements for hot-gas clean up systems and auxiliary/backup clean up systems. Following is a list of the major conclusions of this study.

1. Turbine erosion resistance was shown to be improved by a factor of 5 by varying the turbine design. Increasing the number of stages and increasing the mean radius reduces the peak predicted erosion rates for 2-D flows on the blade airfoil from values which are 6 times those of the vane to values of erosion which are comparable to those of the vane airfoils.

2. Turbine erosion was a strong function of airfoil shape depending on particle diameter. Different airfoil shapes for the same turbine operating condition resulted in a factor of 7 change in airfoil erosion for the smallest particles studied (5 micron).

3. Predicted erosion for the various turbines analyzed was a strong function of particle diameter and weaker function of particle density.

4. Three dimensional secondary flows were shown to cause increases in peak and average erosion on the vane and blade airfoils. Additionally, the interblade secondary flows and stationary outer case caused unique erosion patterns which were not obtainable with 2-D analyses.

5. Analysis of the results indicate that hot gas cleanup systems are necessary to achieve acceptable turbine life in direct-fired, coal-fueled systems. In addition, serious consequences arise when hot gas filter systems fail for even short time periods measure in hours. For a complete failure of the filter system, a 0.030 inch thick, corrosion-resistant protective coating could be eroded at some locations within eight minutes.

REFERENCES

1. Abamowitz, M. and Stegun, I. A.: Handbook of Mathematical Functions. Dover Publications, Inc., New York, 1965.
2. Abbott, M .F., Conn, R. E. and Austin, L. G.: Studies on Slag Deposit Formation in Pulverized-Coal Combustors. Fuel, Vol. 64, pp. 827-831, June 1985.
3. Anderson, R .J., Romanowski, C .J. and France, J. E.: The Adherence of Ash Particles from Combustion of Micronized Coal. Report DE85-008600 (DOE/METC--85/2007).
4. Austin, L. G., Abbott, M .F., Conn, R. E., Kinneman, W. P. and Tangsathit-kulchai, M.: Studies of the Mineral Matter Distribution in Pulverized Coal with Respect to Slag Deposit Formation in Boiler Furnaces. DOE/PC/30199-T1 Report (DE 84015849), May 1984.
5. Banniser, R. L., Pillsbury, P. W. and Diehl, R. C., 1990, "Recent Test Results in the Direct Coal-Fueled 80 MW Combustion Turbine Program," presented at the Gas Turbine and Aeroengine Congress and Exposition, Brussels, Belgium, ASME Paper 90-GT-58.
6. Barkalow, R. H.: Erosion-Corrosion by High-Velocity Particles in Fluidized-Bed Combustion Systems. EPRI CS-3396 Report, February 1984.
7. Barkalow, R .H., Goebel, J. A. and Pettit, F. S.: Erosion-Corrosion of Coatings and Super-Alloys in High Velocity Hot Gases. Erosion: Prevention and Useful Applications. Edited by W.F. Adler, ASTM STP664, pp. 163-190, October 1977.
8. Beacher, B., Tabakoff, W. and Hamed, A., January 1982, "Improved Particle Trajectory Calculations Through Turbomachinery Affected by Coal Ash Particles." Journal of Engr. for Power, Vol. 104, pp. 64-68.
9. Beacher, B. and Tabakoff, W., 1984, "Trajectories of Ash Particles Through a Coal-Burning Gas Turbine," ASME Paper 84-GT-122.
10. Beacher, B. F. and Mansour, M. L.: Erosion of a Coal-Burning Gas Turbine by Ash Particles. Turbomachinery Performance Deterioration. Edited by W. Tabakoff. ASME FED-Vol. 37, pp. 81-93, May 1986.
11. Benford, S. M. and Kutina, F. J.: The Erosion/Corrosion of Super-Alloy Test Coupons Exposed to PFB Coal Combustor Effluent. Proceedings -Corrosion-Erosion-Wear of Materials in Energy Fossil-Energy Systems. Edited by A.V. Levy, DE83-009716 CONF-820144--, pp. 881-909, January 1982.
12. Blair, M. F., Dring, R. P. and Joslyn, H. D.: The Effects of Turbulence and Stator/Rotor Interactions on Turbine Heat Transfer, Part-II, Effects of Reynolds Number and Incidence.
13. Brandt, D. E.: Heavy Duty Turbopower. Mechanical Engineering, July 1987.
14. Brown, R. and Edington, J. W.: Material Loss and Ripple Formation During Solid Particle Erosion at 30 Degree Impact Angles. Proceedings -Corrosion-Erosion-Wear of Materials in Energy Fossil-Energy Systems. Edited by A.V. Levy, DE83-009716 CONF-820144--, pp. 911-932, January 1982.

15. Butler, T. L., Sharma, O. P., Joslyn, H. D. and Dring, R. P.: Redistribution of an Inlet Temperature Distortion in an Axial Flow Turbine Stage. AIAA Paper 86-1468.
16. Caspar, J. R., Hobbs, D. E. and Davis, R. L.: Calculation of Two-Dimensional Potential Cascade Flow Using Finite Area Method. AIAA Paper 79-0077.
17. Cowell, L. H. and LeCren, R. T., June 1989, "Development of a Coal-Fueled Gas Turbine Slagging Combustor," presented at the Gas Turbine and Aeroengine Congress and Exposition, Toronto, Canada. ASME Paper 89-GT-115.
18. Dring, R. P.: Sizing Criteria for Laser Anemometry Particles. Journal of Fluids Engineering, Vol. 104, pp. 15, March 1982.
19. Dring, R. P., Joslyn, H. D., Hardin, L. W. and Wagner, J. H.: Turbine Rotor-Stator Interaction. Trans. ASME Journal of Engineering for Power, Vol. 106, No. 4, pp. 729-742, October 1981.
20. Dring, R. P., Caspar, J. R. and Suo, M.: Particle Trajectories in Turbine Cascades. AIAA Journal of Energy, Vol. 3, No. 3, pp. 161, May 1979.
21. Dring, R. P. and Suo, M.: Particle Trajectories in Swirling Flows. Journal of Energy, Vol. 2, pp. 232, July 1978.
22. Eaton, H. E. and Novak, R. C.: Erosion of Plasma Sprayed Porous Zirconia Under Differing Conditions. Corrosion & Particle Erosion at High Temperatures. Edited by V. Srinivasan and K. Vedula, The Minerals, Metals & Materials Society, 1989.
23. Eroglu, H. and Tabakoff, W.: Effect of Inlet Flow Angle on the Erosion of Radial Guide Vanes. ASME Paper 89-GT-208.
24. Federal Register, Wednesday, September 12, 1990, Part II, Environmental Protection Agency, 40 CFR Part 60, "Standards of Performance for New Stationary Sources; Small Industrial-Commercial-Institutional Steam Generating Units; Final Rule."
25. Finnie, I., Levy, A. and McFadden, D. H.: Fundamental Mechanisms of the Erosive Wear of Ductile Metals by Solid Particles. Erosion: Prevention and Useful Applications. Edited by W.F. Adler, ASTM STP664, pp. 36-58, October 1977.
26. France, J. E., Grimm, U., Anderson, R. J. and Kovach, J. J.: Deposition and Corrosion in Gas Turbines Utilizing Coal or Coal-Derived Fuel. DOE/METC/84-17 Report (DE 84009290), April 1984.
27. Grey, D. A. and McCarron, R. L., August 1980, "Materials Problems in Fluidized-Bed Combustion Systems, Review of the Information on Gas Turbine Materials in Coal Combustion Turbines - Interim Report (RP 1337-1)," EPRICS-1469, Palo Alto, CA. Electric Power Research Institute.
28. Hamed, A.: Influence of Secondary Flow on Turbine Erosion. ASME Paper 88-GT-264.
29. Horner, M. W., Sabla, P. E. and Kimura, S. G.: Coal Fueled Aero-Derivative Gas Turbine: Design Approach. ASME Paper 88-GT-119.
30. Humphrey, J. A. C., Pourahmadi, F. and Levy, A.: Prediction of Erosive Wear by Solid Particles In a Turbulent Curved-Channel Flow. Presented at the 7th Annual Conference on Materials for Coal Conversion and Utilization, Gaithersburg, MD, November 1987.

31. Humphrey, J. A. C., September 1990, "Fundamentals of Fluid Motion in Erosion by Solid Particle Impact," *Int. J. of Heat and Fluid Flow*, Vol. 11, No. 3, pp. 170-195.
32. Hussein, M. F. and Tabakoff, W.: Three Dimensional Dynamic Characteristics of Solid Particles Suspended by Polluted Air Flow in a Turbine Stage. AIAA Paper No. 73-140, 1973.
33. Joslyn, H. D. and Dring, R. P., 1989, "Three Dimensional Flow and Temperature Profile Attenuation in an Axial Flow Turbine," AFOSR Final Report for Contract F39620-86-C-0020.
34. Kosel, T. H. and Sriram, T. S.: A Study of Erosive Particle Rebound Parameters. Fossil Energy Materials Program Conference Proceedings. US DOE/METC ORNL/FMP-87/4, pp. 492-516, August 1987.
35. Kotwal, R. and Tabakoff, W.: A New Approach for Erosion Prediction Due to Fly Ash. *Journal of Engineering for Power*, Vol. 103, pp. 265-270, April 1981.
36. LeCren, R. T. and Smith, K. D.: Advanced Coal-Fueled Industrial Cogeneration Gas Turbine System - Semi-Annual Progress Report for the Period June 2 to December 1, 1987, Solar Report No. SR87-R-5278-33, Fig. 7, December 1987.
37. Levy, A. V.: The Erosion of Metal Alloys and Their Scales. Proceedings - Corrosion-Erosion-Wear of Materials in Energy Fossil-Energy Systems. Edited by A.V. Levy, DE83-009716 CONF-820144--, pp. 298-376, January 1982.
38. Levy, A.V.: Studies of Material Erosion in Coal Conversion. Fossil Energy Materials Program Conference Proceedings. US DOE/METC ORNL/FMP-87/4, pp. 467-491, August 1987.
39. Levy, A. and Hickey, G.: Erosion of Corrosion-Resistant Surface Treatments on Alloy Steels. *Wear*, Vol. 108, pp. 61-79, 1986.
40. Levy, A.V., Yan, J. and Patterson J.: Elevated Temperature Erosion of Steels. *Wear*, Vol. 108, pp. 43-60, 1986.
41. Liu, H. and Ma, C.: Dilute Gas-Particle Flow in a Centrifugal Impeller. Turbomachinery Performance Deterioration. Edited by W. Tabakoff, ASME FED-Vol. 37, pp. 67-73, May 1986.
42. Maji, J. and Sheldon, G. L.: Mechanisms of Erosion of a Ductile Material by Solid Particles. Erosion: Prevention and Useful Applications. Edited by W.F. Adler, ASTM STP664, October 1977.
43. McCarron, R. L. and Brobst, R. P.: Erosion/Corrosion of Turbine Blades in Coal Combustion. Proceedings - Corrosion-Erosion-Wear of Materials in Energy Fossil-Energy Systems. Edited by A.V. Levy, DE83-009716 CONF-820144--, January 1982.
44. Menguturk, M., Gunes, D., Erten, M. and Sverdrup, E. F.: Multistage Turbine Erosion. ASME Paper 86-GT-238.
45. Menguturk, M. and Sverdrup, E. F.: Calculated Tolerance of a Large Electric Utility Gas Turbine to Erosion Damage by Coal Ash Particles. Erosion: Prevention and Useful Applications. Edited by W.F. Adler, ASTM STP664, pp. 193-224, October 1977.

46. Mills, K. C. and Rhine, J. M.: The Measurement and Estimation of the Physical Properties of Slags Formed During Coal Gasification. *Fuel*, Vol. 68, pp. 193–200, February 1989.
47. Moza, A. K., Shoji, K. J. and Austin, L. G.: The Sticking Temperature and Adhesion Force of Slag Droplets from Coals on Oxidized Mild Steel. *Journal of Institute of Energy*, Vol. 53, pp. 17–19, 1980.
48. Nagarajan, R. and Anderson, R. J.: Effect of Coal Constituents on the Liquid-Assisted Capture of Impacting Ash Particles in Direct Coal Fired Gas Turbines. ASME Paper 88-GT-192.
49. Oates, G. C. (editor): *The Aerothermodynamics of Aircraft Gas Turbine Engines*. AFAPL-TR-78-52 Air Force Report, p. 18–4, July 1978.
50. Parsons, E. L., Jr. and Byam, J. W., Jr., June 1989, “Overview of Gas Turbine Coal-Fired Combustor Concepts,” presented at the Gas Turbine and Aeroengine Congress and Exposition, Toronto, Canada. ASME Paper 89-GT-252.
51. Parsons, E. L., Jr., Webb, H. A. and Zeh, C. M., June 1990, “Assessment of Hot Gas Cleanup Technologies in Coal-Fueled Gas Turbines,” presented at the Gas Turbine and Aeroengine Congress and Exposition, Brussels, Belgium. ASME Paper 90-GT-111.
52. Rai, M. M. and Madavan, N. K.: Multi-Airfoil Navier-Stokes Simulations of Turbine Rotor-Stator Interaction. AIAA Paper 88-0361.
53. Ramezan, M., Ross, J. S., Anderson, R. J. and Nagarajan, R.: A Theoretical and Experimental Investigation of Deposition Rates and Heat Transfer Properties of Deposits Formed in a Direct Coal-Fired Combustion Environment. Fourth Annual Pittsburgh Coal Conference, September 1987.
54. Robertson, A., et al.: Second-Generation Pressurized Fluidized Bed Combustion Plant; Conceptual Design and Optimization of a Second-Generation PFB Combustion Plant, Phase 1, Task I, Volume III. DOE Report DOE/MC/21023-2825, Vol. 3 (DE90000493), September 1989.
55. Rosfjord, T. J.: Coal-Water Mixture Combustion Technology Development. Final Technical Report, DE-AC21-83MC-20404, May 1986.
56. Scalzo, A. J., Holden, P. C. and Howard, G. S.: The Westinghouse 501D Combustion Engine. ASME Paper 81-GT-32, December 1980.
57. Smith, J., Strimbeck, D. C., Coates, N. H. and McGee, J. P.: Bureau of Mines Progress in Developing Open and Closed-Cycle Coal-Burning Gas Turbine Power Plants. ASME Paper 66-GT/CLC-7.
58. Spengler, C. J., Lee, S. Y., Mulik, P. R., Whitlow, G. A. and Cohn, A.: Corrosion and Deposition in Coal-Derived Liquid Fueled Combustion Turbines: Turbine Simulator Tests. Proceedings -Corrosion-Erosion-Wear of Materials in Energy Fossil-Energy Systems. Edited by A.V. Levy, DE83-009716 CONF-820144--, pp. 601–641, January 1982.
59. Spriggs, D. R. and Brobst, R. P.: The Effect of PFBC Particulate on High Velocity Erosion-Corrosion of Gas Turbine Materials. Proceedings -Corrosion-Erosion-Wear of Materials in Energy Fossil-Energy Systems. Edited by A.V. Levy, DE83-009716 CONF-820144--, pp. 799–831, January 1982.

60. Stringer, J. and Drenker, S., 1981, "Turbine Erosion and Hot Gas Cleanup Requirements for PFB Combustion Systems," Proceedings of the American Power Conference, Vol. 43, pp. 943-949.
61. Strong, R. E. and Levan, G. N.: Advanced Cooling Full-Scale Engine Demonstration Program. Westinghouse Electric Corporation, EPRI AP-1933, Final Report, July 1981.
62. Suo, M., Patrick, W. P. and Johnson, B. V.: Particle Trajectories Near an Airfoil with a Film-Cooled Leading Edge. AIAA Journal of Energy, Vol. 3, No. 3, pp. 156-160, May 1979.
63. Tabakoff, W.: Erosion Behavior of Materials in Multiphase Flows. Proceedings - Corrosion-Erosion-Wear of Materials in Energy Fossil-Energy Systems. Edited by A.V. Levy, DE83-009716 CONF-820144--, pp. 642-676, January 1982.
64. Tabakoff, W.: Study of Particle Rebound Characteristics and Material Erosion at High Temperatures. Fossil Energy Materials Program Conference Proceedings. US DOE/METC ORNL/FMP-87/4, pp. 492-516, August 1987.
65. Tabakoff, W., Hamed, A. and Eroglu, H.: Study of Particle Rebound Characteristics and Material Erosion at High Temperature. Final Report ORNL/Sub/84-89628/01, December 1987.
66. Tabakoff, W., Hamed, A. and Ramachandran, J.: Study of Metals Erosion in High Temperature Coal Gas Streams. Transactions of ASME, Vol. 102, pp. 148-152, January 1980.
67. Tabakoff, W., Kotwal, R. and Hamed, A.: Erosion Study of Different Materials Affected by Coal Ash Particles. Wear, pp. 161-173, 1979.
68. Tabakoff, W. and Malak, M. F.: Laser Measurements of Fly Ash Rebound Parameters for Use in Trajectory Calculations. Journal of Turbomachinery, Vol. 109, pp. 535-540, October 1987.
69. Tabakoff, W. and Sugiyama, Y.: Experimental Methods of Determining Particle Restitution Coefficients. Polyphase Flow and Transport Technology. Edited by R.A. Bajura, ASME 1980.
70. Tabakoff, W. and Vittal, B. V. R.: High Temperature Erosion of Inco 600 Metal. Wear, Vol. 86, pp. 89-99, 1983.
71. Tabakoff, W. and Wakeman, T.: Test Facility for Material Erosion at High Temperature. Erosion: Prevention and Useful Applications. Edited by W.F. Adler, ASTM STP664, pp. 123-135, October 1977.
72. Ulke, A. and Rouleau, W. T., 1976, "The Effects of Secondary Flows on Turbine Blade Erosion." ASME Paper 76-GT-74.
73. University of Cincinnati: Erosion Study in Turbomachinery Affected by Coal Ash Particles. Final Report FE-2465-13, Contract DE-AC01-76ET1020 (DOE/ET/10620-13), October 1981.
74. Wakeman, T. and Tabakoff, W.: Measured Particle Rebound Characteristics Useful for Erosion Prediction. ASME Paper 82-GT-170.
75. Wakeman, T. and Tabakoff, W.: Effect of Particle Rebound Characteristics on Erosion of Turbomachinery Components. ASME Paper 83-GT-169.

76. Wenglarz, R. A. and Menguturk, M., 1981, "Use of Cascade and Small Turbine Tests to Determine Erosion of Utility Turbines," ASME Paper 81-GT-52.
77. Westinghouse Electric Corporation: Advanced Coal-Fueled Gas Turbine Systems, Annual Technical Progress Report, July 1988 - June 1989, DOE Report No. DOE/MC/23167-2836 (DE9000 0669), pp. 6-7, July 1989.

APPENDIX

Derivation of Particle Trajectory Equations

The following derivation of particle trajectory equations used in this study is taken from previous work at UTRC [20]. For simple particle motion influenced by only aerodynamic drag forces, the resulting fundamental expression to be solved was obtained.

$$\vec{\ddot{X}} = \frac{\rho_f a}{2\rho_p v} C_d |\vec{V}| \vec{V} \quad (A1)$$

where

- $\vec{\ddot{X}}$ = particle acceleration vector
- a = projected area of particle
- C_d = drag coefficient, $f(Re_p)$
- \vec{V} = particle velocity vector relative to the fluid
- v = particle volume

For spherical particles, a/v can be replaced by $3/2D_p$. Additionally, the equation is made dimensionless by normalizing with the inlet axial flow speed of the airfoil row, U_1 , and the axial chord, b_x . The use of dimensionless, rather than dimensional, parameters in the calculations provide an easy method of scaling the results to larger or smaller turbines with similar aerodynamic characteristics. The normalization of the governing equation is outlined below:

For

$$\ddot{X} = \frac{d^2X}{dT^2}$$

where X = particle position
 T = time

$$\text{let } x = \frac{X}{b_x} \text{ and } t = \frac{U_1 T}{b_x}$$

which represent dimensionless distance and time, respectively.

Taking derivatives yields dimensionless forms of acceleration and velocity,

$$\dot{X} = \frac{dX}{dT} = \frac{dx}{dt} U_1$$

and

$$\ddot{X} = \frac{d^2X}{dT^2} = \frac{d^2x}{dt^2} \frac{U_1^2}{b_x}$$

Substitution of the equations above into Eqn. (A1) yields the following relationship:

$$\frac{\vec{x}}{b_x} U_1^2 = \frac{3\rho_f C_d}{4\rho_p D_p} |\vec{u} - \vec{x}| (\vec{u} - \vec{x}) U_1^2$$

where \vec{u} is the dimensionless flowfield velocity vector and C_d is a function of $|\vec{u} - \vec{x}| U_1$.

Simplification of the expression above and substitution of Reynolds numbers based on particle diameter and axial chord (Re_p and Re_{bx}), Stokes number (St) and the particle density Reynolds number (σ), defined below, yield the final expression to be solved to calculate particle trajectories using dimensionless flow and particle parameters.

$$Re_{bx} = \frac{\rho_{f,1} U_1 b_x}{\mu_1}$$

$$Re_p = Re_{bx} \left(\frac{D_p}{b_x} \right) \left(\frac{\rho_f}{\rho_{f,1}} \right) \left(\frac{\mu_1}{\mu} \right) |\vec{u} - \vec{x}|$$

where Re_{bx} is based on inlet conditions and Re_p is based on local conditions for the determination of particle drag. Following are the definitions for the Stokes number (St) and the particle density Reynolds number (σ).

$$St = \frac{\rho_p U_1 D_p^2}{18\mu_1 b_x} \quad (A2)$$

and

$$\sigma = \frac{Re_{bx}}{(\rho_p/\rho_{f,1})} \quad (A3)$$

Substitution of above yields.

$$\vec{x} = \frac{3}{4} \sqrt{\frac{\sigma}{18 St}} \left(\frac{\rho_f}{\rho_{f,1}} \right) C_d |\vec{u} - \vec{x}| (\vec{u} - \vec{x}) \quad (A4)$$

where C_d is a function of Re_p which can be rewritten with St and σ as

$$Re_p = \sqrt{18\sigma} St \left(\frac{\rho_f}{\rho_{f,l}} \right)^{1 - 0.684 (\gamma - 1)} \frac{\vec{u} \cdot \vec{x}}{|\vec{u} - \dot{\vec{x}}|}$$

for $\gamma =$ ratio of specific heats

The vector forms of Eq. A4 were used to develop the 2-D and 3-D particle trajectory codes for the prediction of 2-D or 3-D, particle trajectories in stationary and rotating cascade coordinate system.

END

**DATE
FILMED**

6 / 18 / 93

